NASA TECHNICAL MEMORANDUM

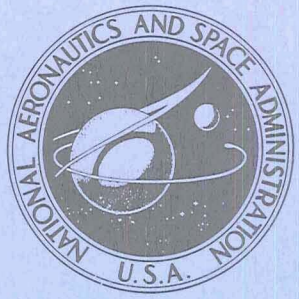

NASA TM X-3324

NASA TM X-3324

AN INVESTIGATION OF SEVERAL NACA 1-SERIES INLETS AT MACH NUMBERS FROM 0.4 TO 1.29 FOR MASS-FLOW RATIOS NEAR 1.0

Richard J. Re

Langley Research Center
Hampton, Va. 23665

NATIONAL AERONAUTICS AND SPACE ADMINISTRATION • WASHINGTON, D. C. • DECEMBER 1975

1. Report No.	2. Government Accession No.	3. Recipient's Catalog No.
NASA TM X-3324		

4. Title and Subtitle	5. Report Date
AN INVESTIGATION OF SEVERAL NACA 1-SERIES INLETS AT MACH NUMBERS FROM 0.4 TO 1.29 FOR MASS-FLOW RATIOS NEAR 1.0	December 1975
	6. Performing Organization Code
7. Author(s)	8. Performing Organization Report No.
Richard J. Re	L-10497
	10. Work Unit No.
9. Performing Organization Name and Address	505-04-11-01-00
NASA Langley Research Center Hampton, Va. 23665	11. Contract or Grant No.
	13. Type of Report and Period Covered
12. Sponsoring Agency Name and Address	Technical Memorandum
National Aeronautics and Space Administration Washington, D.C. 20546	14. Sponsoring Agency Code

15. Supplementary Notes

16. Abstract

An investigation to determine the performance of eight NACA 1-series inlets at mass-flow ratios near 1.0 was conducted in the Langley 16-foot transonic tunnel. The inlet diameter ratios (ratio of inlet diameter to maximum diameter) were 0.85 and 0.89 for an inlet length ratio (ratio of inlet length to maximum diameter) of 1.0. Inlet lip radius varied from 0.061 cm to 0.251 cm, and internal contraction area ratio (ratio of inlet area to throat area) varied from 1.006 to 1.201. Reynolds number based on model maximum diameter ranged from 3.6×10^6 at a Mach number of 0.4 to 5.9×10^6 at a Mach number of 1.29.

The results indicate that nearly uniform pressure distributions on a given inlet were obtained over a limited range of mass-flow ratios and Mach numbers. When inlet lip thickness was increased by means of lip radius or contraction ratio, the inlet critical Mach number decreased. Drag-divergence Mach number inferred from forebody pressure integrations was above 0.94 for most of the inlets tested.

17. Key Words (Suggested by Author(s))	18. Distribution Statement
Inlet NACA 1-series inlets Inlet performance	Unclassified – Unlimited Subject Category 02

19. Security Classif. (of this report)	20. Security Classif. (of this page)	21. No. of Pages	22. Price*
Unclassified	Unclassified	109	$5.25

*For sale by the National Technical Information Service, Springfield, Virginia 22161

AN INVESTIGATION OF SEVERAL NACA 1-SERIES INLETS AT MACH NUMBERS FROM 0.4 TO 1.29 FOR MASS-FLOW RATIOS NEAR 1.0

Richard J. Re
Langley Research Center

SUMMARY

An investigation to determine the performance of eight NACA 1-series inlets at mass-flow ratios near 1.0 was conducted in the Langley 16-foot transonic tunnel. The inlet diameter ratios (ratio of inlet diameter to maximum diameter) were 0.85 and 0.89 for an inlet length ratio (ratio of inlet length to maximum diameter) of 1.0. Inlet lip radius varied from 0.061 cm to 0.251 cm, and internal contraction area ratio (ratio of inlet area to throat area) varied from 1.006 to 1.201. Reynolds number based on model maximum diameter ranged from 3.6×10^6 at a Mach number of 0.4 to 5.9×10^6 at a Mach number of 1.29.

The results indicate that nearly uniform pressure distributions on a given inlet were obtained over a limited range of mass-flow ratios and Mach numbers. When inlet lip thickness was increased by means of lip radius or contraction ratio, the inlet critical Mach number decreased. Drag-divergence Mach number inferred from forebody pressure integrations was above 0.94 for most of the inlets tested.

INTRODUCTION

The development of airfoil sections which delay the formation of strong shocks until high supercritical local Mach numbers are reached has opened the way for the design of lifting surfaces for efficient transport aircraft in the high subsonic speed range. Section characteristics of a supercritical airfoil determined in a wind tunnel are presented in references 1 to 5. Flight verification of wind-tunnel airfoil section characteristics for unswept and sweptback wings of finite span are contained in references 6 to 10.

The development of turbofan engines of various sizes and bypass ratios and the advent of the supercritical airfoil section provide the airplane designer with sufficient tools to design a wide variety of cruise-efficient subsonic transport airplanes. No one airplane configuration would satisfy the variety of performance requirements possible in this speed range. However, many configurations would probably incorporate turbofan

engines with air induction systems using axisymmetric or pitot-type inlets. These inlets, because of the high mass flows of turbofan engines, would have large diameter ratios (ratio of inlet diameter to maximum diameter). In addition, some configurations with high subsonic cruise speeds require these inlets to operate at supercritical speeds; little high-speed inlet data exists, however, to aid in nacelle design for advanced subsonic transports. The most comprehensive data on axisymmetric inlets (NACA 1-series) (reported in refs. 11 and 12) were obtained at low speeds. Investigations in the transonic speed range (refs. 13 to 18) were conducted on inlets which, in comparison with inlets required for most turbofan engines, had small diameter ratios. To complement the data just mentioned, several NACA 1-series inlets of large diameter ratio were investigated over a range of mass flows in the Langley 16-foot transonic tunnel at Mach numbers from 0.4 to 1.29. These data are reported in reference 19.

This investigation extends the external pressure-distribution results for four of the inlets discussed in reference 19 to higher inlet mass-flow ratios and includes external pressure distributions for four additional inlets. Mass-flow ratios near 1.0 were obtained using a model afterbody with a larger throttleable exit area than was used in the previous investigation. All of the inlets investigated here had a length ratio (ratio of inlet length to maximum diameter) of 1.0 and diameter ratios of 0.85 to 0.89. Inlet lip radius varied from 0.061 cm to 0.251 cm and internal contraction ratio (ratio of inlet area to throat area) varied from 1.006 to 1.201.

The investigation was conducted in the Langley 16-foot transonic tunnel at a 0° angle of attack over a range of mass-flow ratios and at small angles of attack for mass-flow ratios near 1.0. Reynolds number based on model maximum diameter ranged from 3.6×10^6 at a Mach number of 0.4 to 5.9×10^6 at a Mach number of 1.29.

SYMBOLS

A area normal to inlet center line

$C_{A,F}$ integrated forebody axial-force coefficient (positive downstream), $\frac{1}{A_{max}} \int_{A_{sp}}^{A_{max}} C_p dA$

C_p pressure coefficient, $\frac{p_\ell - p_\infty}{q_\infty}$

d intake diameter of NACA 1-series inlet (difference between D_h and twice inlet lip radius)

D	diameter
M	Mach number
$\dot{m}/\dot{m}_\infty$	inlet mass-flow ratio, $\frac{1}{\rho_\infty A_h V_\infty}\int \rho_r V_r dA$
p	static pressure
q	dynamic pressure
R	radius measured from model center line
R_∞	free-stream Reynolds number based on maximum diameter of model
r	lip radius
T_t	stagnation temperature
V	velocity
X	length of inlet from lip to start of cylindrical part of model, X = 45.72 cm
x	distance from lip of inlet measured longitudinally
Y	maximum ordinate measured perpendicular to reference line at maximum diameter station for NACA 1-series inlets
y	local ordinate measured perpendicular to reference line for NACA 1-series inlet
α	angle of attack with respect to model center line, deg
ρ	density
ϕ	meridian angle, measured from top of model in clockwise direction when looking upstream, deg

Subscripts:

cr	critical condition corresponding to local sonic flow
d	duct
D	point at which external axial-force coefficient reaches 1.1 times its low Mach number level (from force-balance data of ref. 19)
h	most forward point on inlet lip
ℓ	local
max	maximum
min	minimum
P	point at which $C_{A,F}$ reaches peak (negative) value
r	mass-flow rake station in duct
sp	stagnation point on inlet lip
w	duct wall at mass-flow rake station
∞	free-stream condition

MODEL

The model consisted of an inlet and afterbody and had a maximum diameter of 45.72 cm. The model was mounted in the wind-tunnel test section by a rear sting. A simplified cross-sectional sketch of the model assembly with an NACA 1-85-100 inlet is shown in figure 1.

Eight NACA 1-series inlets (45.72 cm in length) were used for this investigation. Four of the inlets were used in the investigation described in reference 19 and four additional inlets were constructed for the present investigation. The variations in inlet geometry include inlet diameter ratio, inlet lip radius, and inlet internal area contraction ratio. The nondimensional NACA 1-series outer profile ordinates, as presented for a given lip radius in reference 11, are reproduced in table I. Figure 2 contains a

summary of the important geometric parameters for each of the inlets. Nondimensionalized internal ordinates for each inlet are shown in table II. The inlets with internal contraction ratios of 1.046 or greater are elliptical between the lip and the minimum duct-area station (throat). From the throat to the 25-percent station (x/X = 0.25), the internal contour of all the inlets consisted of a 1° semicone expansion. A faired curve made up the remainder of the internal contour. The proportional rate of area growth (based on the difference between maximum duct area and throat area) as a function of distance in the faired section was identical for all inlets. Diffuser area ratios (ratio of maximum duct internal area to inlet throat area) for each inlet are shown in table II.

Static-pressure orifices were drilled into tubing placed in grooves in the model surface and which had been covered with a filler material. The locations of the orifices on each inlet outer profile are presented in table III. The four struts which connected the inlets to the centerbody were used to route the inlet static-pressure tubes to differential pressure-scanning units mounted in the nose of the centerbody. Three of the struts were instrumented with the pressure probes necessary to measure duct mass flow (see fig. 3). The inlets and afterbody were made from aluminum; parts of the primary structure, the sting, for example, were made of steel.

The afterbody had a cylindrical external shape $\left(2.89D_{max} \text{ in length}\right)$ and was 45.72 cm in diameter. The afterbody had a constant internal diameter back to station 111.76 where the duct changes to a conical shape, and thereafter increased in diameter to the exit. External orifice locations for the afterbody are presented in table IV; the locations are based on inlet length (where inlet length X = 45.72 cm). The afterbody was attached directly to the sting by four struts (see fig. 1).

The mass-flow throttle plug was driven by an internally housed remote-control electric motor and had a travel of about 25.4 cm. The open area at the exit of the model (normal to the free-stream flow direction) could be varied from 1022.42 cm^2 to 1573.46 cm^2 with the plug in either of its two extreme positions.

WIND TUNNEL

The investigation was conducted in the Langley 16-foot transonic tunnel, a single-return atmospheric wind tunnel with continuous air exchange. The test section is octagonal in shape measuring 4.724 m between opposite walls (an area equivalent to a circle 4.85 m in diameter). The test section has axial slots at the wall vertices; the total width of the eight slots in the vicinity of the model is approximately 3.7 percent of the test section perimeter. At Mach numbers from 1.2 to 1.3, the divergence angle of the test section walls was adjusted (based on calibration data) as a function of airstream dewpoint temperature; the adjustment eliminated longitudinal static-pressure gradients that would

have occurred on the center line because of condensation of atmospheric moisture. A complete description of the wind tunnel and its airflow characteristics is contained in reference 20. The solid blockage of the model in the test section is between 0.88 percent (no flow through model) and 0.33 percent (throttle plug area only). The tunnel sting-support system pivots in such a manner that the model remains on or near the test-section center line through the angle-of-attack range.

TESTS AND METHODS

Each inlet was tested at Mach numbers from 0.40 to 1.01 at an angle of attack of 0°. The NACA 1-89-100 inlet with a contraction ratio of 1.006 was also tested at Mach numbers of 1.20 and 1.29. Most of the inlets were also tested at a nominal angle of attack between 1° and 2° with a high mass-flow ratio at several subsonic Mach numbers. Sketches showing the variations in inlet geometry included in this investigation are presented in figure 2.

The variations of free-stream stagnation temperature and Reynolds number (based on maximum model diameter) with Mach number are shown in figure 4. All the data presented here are for free boundary-layer transition on the model since the tunnel stream conditions and the large scale of the model result in a Reynolds number approaching one-half that of a nacelle 2.13 m in diameter at operating altitude.

Inlet angle of attack was obtained by correcting the angle of the model support system for deflection of the sting under aerodynamic loads and for test-section stream angularity. No corrections were made to the pressure data for test-section wall-interference effects or for local condensation effects that may have occurred in the model flow field. The presence of the mass-flow throttle plug at the base of the afterbody affects the afterbody pressure field; therefore, the small amount of afterbody pressure data presented should be considered qualitative.

PRESENTATION OF RESULTS

The results of this investigation are presented in graphic form as model external surface-pressure coefficients in figures 5 to 21. External and internal pressure coefficients were machine plotted as a function of nondimensionalized inlet length for each mass-flow ratio and were faired by connecting adjacent readings with straight line segments. Critical pressure coefficients are shown in figures 6 to 13 for reference purposes. The pressure-coefficient data for each inlet are presented in the figures as follows:

Inlet designation	Lip radius, cm	Internal contraction ratio, A_h/A_{min}	Figures showing pressure coefficients for –	
			$\alpha = 0^o$	α (range)
NACA 1-85-100	0.084	1.009	6	14
↓	.168	1.017	7	15
	.251	1.026	8	16
	.084	1.046	9	17
	↓	1.093	10	18
↓	↓	1.201	11	---
NACA 1-89-100	.061	1.006	12	19
NACA 1-89-100	.061	1.195	13	20

Figure 22 presents the variation of forebody axial-force coefficient (numerical integration in axial direction of external surface-pressure force coefficients from the stagnation point on the lip, as determined from the pressure distributions, to the maximum diameter) with Mach number. This figure includes the appropriate data from reference 19 at lower mass-flow ratios. Figure 23 shows inlet lower critical Mach number as obtained from cross plotting peak negative pressure coefficient against mass-flow ratio and Mach number. Peak pressure coefficients of the present investigation were combined with those of reference 19 to refine and extend the lower critical Mach number variation with mass-flow ratio. An indication of the breakdown of the inlet lip suction force as a function of Mach number was obtained from the peaks of the forebody axial-force coefficient $C_{A,F}$ curves of figure 22. A comparison of the Mach number M_P where this breakdown occurred with the force-balance derived drag-divergence Mach number M_D of reference 19 is presented in figure 24.

RESULTS AND DISCUSSION

It is obvious from this and many previous inlet investigations that a given inlet of fixed geometry can be efficient over a limited range of operation and perform poorly or unacceptably at off-design conditions. Acceptable inlet operation over the complete flight envelope of an aircraft, including zero flight speed, can only be achieved by careful consideration of many factors. An aircraft with a wide performance envelope is likely to require an inlet with some variable-geometry feature or some means to satisfy extreme off-design engine requirements.

The intent of this investigation and that of reference 19 was to obtain inlet pressure distributions under isolated conditions. To this end the model for the investigation of reference 19 was designed with a cylindrical section between the inlet and boattailed afterbody. The results indicated that the inlet was successfully isolated from the boattail at Mach numbers up to 0.98 for the range of mass flows studied in that investigation. To increase mass flow for this investigation, the boattailed afterbody of reference 19 was replaced by a cylindrical section. In this way the model aft of the inlet was made cylindrical to the base. Pressure distributions over the model with the different afterbody shapes in the range of mass-flow ratio overlap (fig. 5) indicate no effects on the inlet pressure distributions. This result substantiates the conclusion of reference 21 that development of inlets for nacelles to be used at high subsonic speeds need not be conducted in conjunction with specific afterbodies for nacelles of moderate fineness ratios. However, the reverse is not necessarily true.

Additional pressure distributions over the complete model with the cylindrical afterbody are shown in figure 21 for various Mach numbers and mass-flow ratios. In general, the inlet appears to be isolated from the varying exit conditions by the cylindrical afterbody up to a Mach number of 0.98 for the mass-flow range of this investigation. At Mach numbers of 0.96 and above, changes in mass flow shifted the pressure distributions on the cylindrical portion of the model downstream of the inlet. This shift may be the influence of the inlet flow field or an effect of changing tunnel blockage by varying inlet mass flow; it is not necessarily the result of the exit flow conditions.

Inlet Pressure-Coefficient Distributions at $\alpha = 0^{\circ}$

The following sections of this discussion are not intended to imply the superiority of one inlet over another; they merely point out comparative differences in external performance on the basis of uniformity of pressure distributions over the length of each inlet. A uniform pressure distribution is desirable so that the formation of shocks, resulting from local supercritical flow conditions, is delayed to the highest free-stream Mach number possible. At the same time, extensive positive external pressure coefficients near the lip are undesirable because of pressure drag considerations.

The internal pressure-coefficient distributions between the lip and throat presented in figures 6 to 13 indicate that supercritical flow conditions occurred at the throat as choking conditions were approached at high mass-flow ratios. At choking conditions, the suction peak at the throat apparently developed into a shock wave and caused flow separation in the diffuser.

Effect of lip radius (NACA 1-85-100 inlet).- Comparison of the external pressure distributions on three NACA 1-85-100 inlets having different lip radii (figs. 6, 7, and 8) indicates that the inlet with the largest lip radius ($r = 0.251$ cm, fig. 8) had the flattest

pressure distributions at mass-flow ratios near 1.0. However, at the lower mass-flow ratios, this inlet had higher negative pressure-coefficient peaks while the inlet with the smallest lip radius (r = 0.084 cm, fig. 6) had the more uniform pressure distributions.

In general, the effects of changes in inlet lip radius on the external pressure distributions were confined to the forward 20 percent of the inlet at the lowest mass-flow ratios and to the forward 30 percent at the highest mass-flow ratios.

Effect of contraction ratio (NACA 1-85-100 inlet).- Comparison of the pressure distributions of figures 6, 9, 10, and 11 shows the effect of contraction ratio on an inlet of given external contour. Except at Mach numbers of 0.40 and 0.60, inlet choking limited the range of mass-flow ratios obtainable for the inlet with the largest contraction ratio (1.201, fig. 11). However, at Mach numbers of 0.40 and 0.60, this inlet had the most uniform pressure distributions at mass-flow ratios close to 1.0. At a mass-flow ratio of 0.90, the inlet with a contraction ratio of 1.046 (fig. 9) had the most nearly uniform pressure distribution at most Mach numbers. At the lower mass-flow ratios of reference 19, contraction ratio (in the range 1.009 to 1.093) had little effect on the external pressure distributions at any Mach number.

In general, for the mass-flow range of this investigation, negative pressure peaks at the inlet lip became more severe with increasing inlet contraction ratio and increasing Mach number. The effects of changes in inlet contraction ratio on the external pressure distributions were largely confined to the forward 20 percent of the inlet.

Effect of contraction ratio (NACA 1-89-100 inlet).- Comparison of the pressure distributions of figures 12 and 13 shows the effect of a large change in contraction ratio on an NACA 1-89-100 inlet. Inlet choking limited the range of mass-flow ratios obtainable at the higher free-stream Mach numbers for the inlet with the large contraction ratio (1.195, fig. 13). At a Mach number of 0.40, however, where the mass-flow ratio ranged from 0.84 to 1.05, a nearly uniform pressure distribution was obtained at a mass-flow ratio of 1.01. The inlet with the 1.006 contraction ratio (fig. 12) had considerable rounding-off of the pressure distribution near the lip for similar conditions. The effects of the change in inlet contraction ratio on the pressure distributions of the NACA 1-89-100 inlet was confined to the forward 20 percent of the inlet.

Effect of inlet diameter ratio.- Comparison of the data of figures 6 (NACA 1-85-100, contraction ratio 1.009) and 12 (NACA 1-89-100, contraction ratio 1.006) indicates that the inlet with the smaller diameter ratio (NACA 1-85-100) generally has the more uniform pressure distributions at mass-flow ratios below about 0.93. At these mass-flow ratios, the NACA 1-89-100 inlet had high negative pressure-coefficient peaks at the lip. At the lower mass-flow range of reference 19, this inlet (NACA 1-89-100) could not sustain the high negative pressure peaks, and separation occurred over as much as 30 percent of the inlet at Mach numbers 0.40 through 0.80 for mass-flow ratios up to about 0.6.

Depending on Mach number, the most nearly uniform pressure distributions occurred in the mass-flow ratio range from 0.83 to 0.88 for the NACA 1-85-100 inlet and in the range from 0.92 to 0.94 for the NACA 1-89-100 inlet.

Inlet critical and drag-divergence Mach numbers.- The variation of inlet lower critical Mach number with mass-flow ratio as determined from the pressure distributions of this investigation and from those of reference 19 is shown in figure 23. In general, the data indicate that for a given inlet, in the absence of separation, increasing thickness near the lip by either lip radius or internal contraction decreased inlet lower critical Mach number.

An indication of the drag-divergence Mach number can be obtained from the integrated forebody pressure coefficients $C_{A,F}$ of figure 22 since peak values of $C_{A,F}$ should occur at the start of the breakdown of lip suction. The Mach number M_P at which peak values of $C_{A,F}$ occurred is plotted in figure 24; for comparison, the drag-divergence Mach numbers M_D from reference 19 for four of the inlets are included. The drag-divergence Mach number from the force-balance data of reference 19 is defined as the Mach number at which the external axial-force coefficient reaches 1.1 times its subsonic level. As indicated in the figure, M_D is generally greater than M_P. From these data the conclusion can be drawn that seven of the inlets investigated have drag-divergence Mach numbers of 0.94 or greater for mass-flow ratios above 0.74. The limited mass-flow range for the inlets with large contraction ratios (1.201 and 1.195) is insufficient to show trends in drag-divergence Mach number. However, the NACA 1-89-100 inlet with a contraction ratio of 1.195 had a drag-divergence Mach number of about 0.96 at the one mass-flow ratio at which a peak value of $C_{A,F}$ could be obtained. The NACA 1-85-100 inlet with a contraction ratio of 1.201 had a drag-divergence Mach number of about 0.91 at mass-flow ratios from 0.82 to 0.84.

Pressure Distributions at Small Angles of Attack

Pressure-coefficient distributions at an angle of attack of 1.2° and maximum mass-flow ratio were obtained for several of the inlets at a Mach number of 0.40. In addition, distributions were obtained for the NACA 1-85-100 inlet (contraction ratio 1.009) and the NACA 1-89-100 inlet (contraction ratio 1.006) at an angle of attack of about 2° at several higher Mach numbers. (See figs. 14 to 20.) The inlets had rows of pressure orifices on the top ($\phi = 0^{\circ}$) and bottom ($\phi = 180^{\circ}$). Therefore, for a given model attitude setting, data from the top row are for positive angles of attack; data from the bottom row can be considered for negative angles of attack.

As expected, increasing angle of attack resulted in a higher level of pressure coefficient near the lip. The data at higher Mach numbers for the NACA 1-89-100 (contraction ratio 1.006) inlet (figs. 19(b) and 19(c)) indicate that the effect of angle of attack on the

pressure distribution extends back over half the inlet length as it did for the lower mass-flow ratio range of reference 19.

CONCLUDING REMARKS

An investigation was conducted in the Langley 16-foot transonic tunnel to determine the external performance of eight NACA 1-series inlets at mass-flow ratios near 1.0. The inlet diameter ratios (ratio of inlet diameter to maximum diameter) were 0.85 and 0.89 for an inlet length ratio (ratio of inlet length to maximum diameter) of 1.0. Inlet lip radius varied from 0.061 cm to 0.251 cm and internal contraction area ratio (ratio of inlet area to throat area) varied from 1.006 to 1.201.

The results indicate that nearly uniform pressure distributions on a given inlet were obtained over a limited range of mass-flow ratios and Mach numbers. When inlet lip thickness was increased by means of lip radius or contraction ratio, the inlet critical Mach number decreased. However, drag-divergence Mach number inferred from forebody pressure integrations was above 0.94 for most of the inlets tested.

Langley Research Center
National Aeronautics and Space Administration
Hampton, Va. 23665
November 26, 1975

REFERENCES

1. Whitcomb, Richard T.; and Clark, Larry R.: An Airfoil Shape for Efficient Flight at Supercritical Mach Numbers. NASA TM X-1109, 1965.

2. Blackwell, James A., Jr.: Aerodynamic Characteristics of an 11-Percent-Thick Symmetrical Supercritical Airfoil at Mach Numbers Between 0.30 and 0.85. NASA TM X-1831, 1969.

3. Harris, Charles D.: Wind-Tunnel Investigation of Effects of Trailing-Edge Geometry on a NASA Supercritical Airfoil Section. NASA TM X-2336, 1971.

4. Harris, Charles D.; and Blackwell, James A., Jr.: Wind-Tunnel Investigation of Effects of Rear Upper Surface Modification on an NASA Supercritical Airfoil. NASA TM X-2454, 1972.

5. Whitcomb, Richard T.; and Blackwell, James A., Jr.: Status of Research on a Supercritical Wing. Conference on Aircraft Aerodynamics, NASA SP-124, 1966, pp. 367-381.

6. Ferris, James C.: Static Aerodynamic Characteristics of a Model With a 17-Percent-Thick Supercritical Wing. NASA TM X-2551, 1972.

7. Palmer, William E.; and Elliott, Donald W.: Summary of T-2C Supercritical Wing Program. Supercritical Wing Technology – A Progress Report on Flight Evaluations. NASA SP-301, 1972, pp. 13-34.

8. Harris, Charles D.: Wind-Tunnel Measurements of Aerodynamic Load Distribution on an NASA Supercritical-Wing Research Airplane Configuration. NASA TM X-2469, 1972.

9. Bartlett, Dennis W.; and Re, Richard J.: Wind-Tunnel Investigation of the Basic Aerodynamic Characteristics of a Supercritical-Wing Research Airplane Configuration. NASA TM X-2470, 1972.

10. Supercritical Wing Technology – A Progress Report on Flight Evaluations. NASA SP-301, 1972.

11. Baals, Donald D.; Smith, Norman F.; and Wright, John B.: The Development and Application of High-Critical-Speed Nose Inlets. NACA Rep. 920, 1948. (Supersedes NACA ACR L5F30a.)

12. Nichols, Mark R.; and Keith, Arvid L., Jr.: Investigation of a Systematic Group of NACA 1-Series Cowlings With and Without Spinners. NACA Rep. 950, 1949. (Supersedes NACA RM L8A15.)

13. Pendley, Robert E.; and Robinson, Harold L.: An Investigation of Several NACA 1-Series Nose Inlets With and Without Protruding Central Bodies at High-Subsonic Mach Numbers and at a Mach Number of 1.2. NACA TN 3436, 1955. (Supersedes NACA RM L9L23a.)

14. Pendley, Robert E.; Robinson, Harold L.; and Williams, Claude V.: An Investigation of Three Transonic Fuselage Air Inlets at Mach Numbers From 0.4 to 0.94 and at a Mach Number of 1.19. NACA RM L50H24, 1950.

15. Nichols, Mark R.; and Pendley, Robert E.: Performance of Air Inlets at Transonic and Low Supersonic Speeds. NACA RM L52A07, 1952.

16. Pendley, Robert E.; Milillo, Joseph R.; and Fleming, Frank F.: An Investigation of Three NACA 1-Series Nose Inlets at Subsonic and Transonic Speeds. NACA RM L52J23, 1953.

17. Pendley, Robert E.; and Smith, Norman F.: An Investigation of the Characteristics of Three NACA 1-Series Nose Inlets at Subcritical and Supercritical Mach Numbers. NACA RM L8L06, 1949.

18. Pendley, Robert E.; Milillo, Joseph R.; Fleming, Frank F.; and Bryan, Carroll R.: An Experimental Study of Five Annular-Air-Inlet Configurations at Subsonic and Transonic Speeds. NACA RM L53F18a, 1953.

19. Re, Richard J.: An Investigation of Several NACA 1-Series Axisymmetric Inlets at Mach Numbers From 0.4 to 1.29. NASA TM X-2917, 1974.

20. Corson, Blake W., Jr.; Runckel, Jack F.; and Igoe, William B.: Calibration of the Langley 16-Foot Transonic Tunnel With Test Section Air Removal. NASA TR R-423, 1974.

21. Leynaert, J.: Transonic Testing of the Engine Nacelle Air Intake and Afterbody. NASA TT F-14,154, 1972.

TABLE I.- NACA 1-SERIES ORDINATES

[Ordinates in percent]

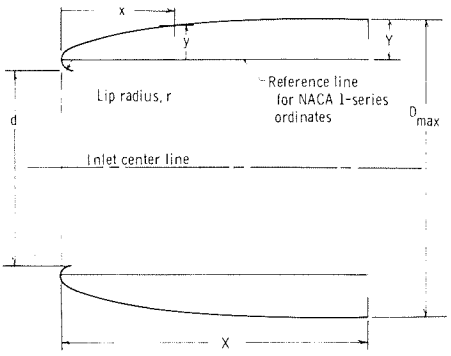

$$x = \left(\frac{X}{D_{max}}\right) D_{max} \qquad Y = \frac{D_{max} - d}{2} + r$$

Sample NACA 1-series designation: NACA 1 - 81 - 100 (Series; $\frac{d}{D_{max}}$ (in percent); $\frac{X}{D_{max}}$ (in percent))

x/X	y/Y	x/X	y/Y	x/X	y/Y
0	0	20.0	52.70	48.0	81.25
.2	4.80	21.0	54.05	49.0	81.99
.4	6.63	22.0	55.37	50.0	82.69
.6	8.12	23.0	56.66	52.0	84.10
.8	9.33	24.0	57.92	54.0	85.45
1.0	10.38	25.0	59.15	56.0	86.73
1.5	12.72	26.0	60.35	58.0	87.95
2.0	14.72	27.0	61.52	60.0	89.11
2.5	16.57	28.0	62.67	62.0	90.20
3.0	18.31	29.0	63.79	64.0	91.23
3.5	19.94	30.0	64.89	66.0	92.20
4.0	21.48	31.0	65.97	68.0	93.11
4.5	22.96	32.0	67.03	70.0	93.95
5.0	24.36	33.0	68.07	72.0	94.75
6.0	27.01	34.0	69.08	74.0	95.48
7.0	29.47	35.0	70.08	76.0	96.16
8.0	31.81	36.0	71.05	78.0	96.79
9.0	34.03	37.0	72.00	80.0	97.35
10.0	36.13	38.0	72.94	82.0	97.87
11.0	38.15	39.0	73.85	84.0	98.33
12.0	40.09	40.0	74.75	86.0	98.74
13.0	41.94	41.0	75.63	88.0	99.09
14.0	43.66	42.0	76.48	90.0	99.40
15.0	45.30	43.0	77.32	92.0	99.65
16.0	46.88	44.0	78.15	94.0	99.85
17.0	48.40	45.0	78.95	96.0	99.93
18.0	49.88	46.0	79.74	98.0	99.98
19.0	51.31	47.0	80.50	100.0	100.00
Lip radius: 0.025Y					

TABLE II.- INTERNAL ORDINATES OF INLETS

[Ordinates in percent]

NACA 1-85-100;
Lip radius, 0.084 cm;
Contraction ratio, 1.009;
Diffuser area ratio, 1.154

x/X	y/Y
0	0
.2	-2.4
12.5	.5
25.0	3.5
35.0	5.9
45.0	9.3
60.0	17.9
80.0	37.8
90.0	48.0
100.0	54.5

NACA 1-85-100;
Lip radius, 0.168 cm;
Contraction ratio, 1.017;
Diffuser area ratio, 1.164

x/X	y/Y
0	0
.4	-5.1
12.5	-2.1
25.0	.9
35.0	3.5
45.0	7.2
60.0	16.5
80.0	37.9
90.0	48.9
100.0	55.9

NACA 1-85-100;
Lip radius, 0.251 cm;
Contraction ratio, 1.026;
Diffuser area ratio, 1.174

x/X	y/Y
0	0
.6	-7.9
12.5	-4.9
25.0	-1.8
35.0	1.0
45.0	5.0
60.0	15.0
80.0	38.0
90.0	49.8
100.0	57.4

NACA 1-85-100;
Lip radius, 0.084 cm;
Contraction ratio, 1.046;
Diffuser area ratio, 1.197

x/X	y/Y
0	0
.1	-2.8
.2	-4.2
.3	-4.9
.5	-6.1
.6	-7.1
1.1	-9.0
2.1	-11.5
3.0	-12.6
4.1	-13.1
4.4	-13.1
13.9	-10.8
25.0	-8.1
35.0	-5.2
45.0	-1.0
60.0	9.7
80.0	34.1
90.0	46.5
100.0	54.5

NACA 1-85-100;
Lip radius, 0.084 cm;
Contraction ratio, 1.093;
Diffuser area ratio, 1.250

x/X	y/Y
0	0
.1	-5.5
.2	-8.0
.3	-9.6
.5	-11.8
.6	-13.7
1.1	-17.3
2.1	-22.3
3.0	-24.4
4.1	-25.3
4.4	-25.3
13.9	-23.1
25.0	-20.4
35.0	-16.9
45.0	-11.8
60.0	1.1
80.0	30.2
90.0	45.0
100.0	54.5

NACA 1-85-100;
Lip radius, 0.084 cm;
Contraction ratio, 1.201;
Diffuser area ratio, 1.373

x/X	y/Y
0	0
.1	-10.9
.2	-16.3
.3	-19.2
.5	-23.2
.6	-27.5
1.1	-34.9
2.1	-44.8
3.0	-49.1
4.1	-50.9
13.9	-48.6
25.0	-45.9
35.0	-41.1
45.0	-34.1
60.0	-16.6
80.0	22.5
90.0	42.1
100.0	54.5

NACA 1-89-100;
Lip radius, 0.061 cm;
Contraction ratio, 1.006;
Diffuser area ratio, 1.052

x/X	y/Y
0	0
.1	-2.5
12.5	1.4
25.0	5.6
35.0	7.0
45.0	9.1
60.0	14.5
80.0	27.1
90.0	33.7
100.0	37.9

NACA 1-89-100;
Lip radius, 0.061 cm;
Contraction ratio, 1.195;
Diffuser area ratio, 1.250

x/X	y/Y
0	0
.1	-15.2
.2	-22.6
.3	-26.7
.5	-32.8
.6	-38.3
1.1	-48.6
2.1	-62.4
3.0	-68.3
4.1	-71.0
13.9	-67.9
25.0	-64.3
35.0	-59.5
45.0	-52.5
60.0	-35.0
80.0	-4.8
90.0	24.9
100.0	37.9

TABLE III.- PRESSURE ORIFICE LOCATIONS ON INLET

[Ordinates in percent]

(a) External surface

NACA 1-85-100;
NACA 1-89-100;
Contraction ratio, ≈1.0

Orifice locations for –		
x/X	ϕ, deg	
	0	180
0	X	X
.31	X	
.62	X	X
1.25	X	X
1.88	X	X
2.5	X	X
3.12	X	X
3.75	X	X
4.38	X	X
5	X	X
7.5	X	X
10	X	X
12.5	X	
15	X	X
17.5	X	
20	X	X
30	X	X
40	X	X
50	X	X
60	X	X
70	X	X
80	X	X
90	X	X

NACA 1-85-100;
Contraction ratios, 1.046,
1.093, and 1.201;
NACA 1-89-100;
Contraction ratio, 1.195

Orifice locations for –		
x/X	ϕ, deg	
	0	180
0	X	X
.31	X	
.62	X	X
1.25	X	X
1.88	X	X
2.5	X	X
3.12	X	X
3.75	X	X
4.38	X	
5	X	X
7.5	X	X
10	X	X
12.5	X	
15	X	X
17.5	X	
20	X	X
30	X	X
40	X	X
50	X	X
60	X	X
70	X	X
80	X	X
90	X	X

(b) Internal surface

NACA 1-85-100;
NACA 1-89-100;
Contraction ratio, ≈1.0

Orifice locations for –		
x/X	ϕ, deg	
	0	180
0.62	X	X
1.25	X	X
1.88	X	X
3.12	X	X
3.75	X	X

NACA 1-85-100;
Contraction ratios, 1.046,
1.093, and 1.201;
NACA 1-89-100;
Contraction ratio, 1.195

Orifice locations for –		
x/X	ϕ, deg	
	0	180
0.17	X	X
.33	X	X
.56	X	X
1.11	X	
2.22	X	
4.06	X	

TABLE IV.- PRESSURE ORIFICE LOCATIONS

ON AFTERBODY

[Ordinates in percent]

x/X
122.2
138.9
166.7
183.3
200.0
216.7
238.9
255.6
266.7
272.2
277.8
283.3

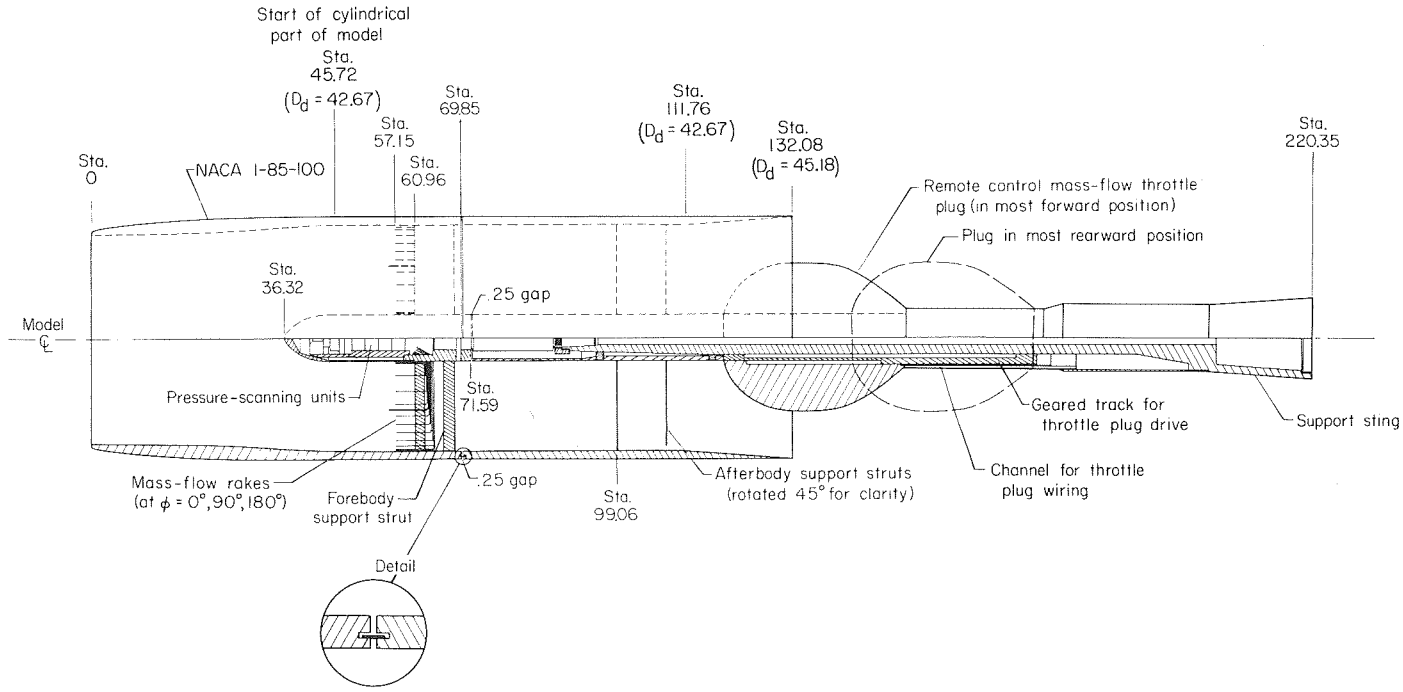

Figure 1.- Simplified cross-sectional sketch of complete model with NACA 1-85-100 inlet. All dimensions are in centimeters unless otherwise noted.

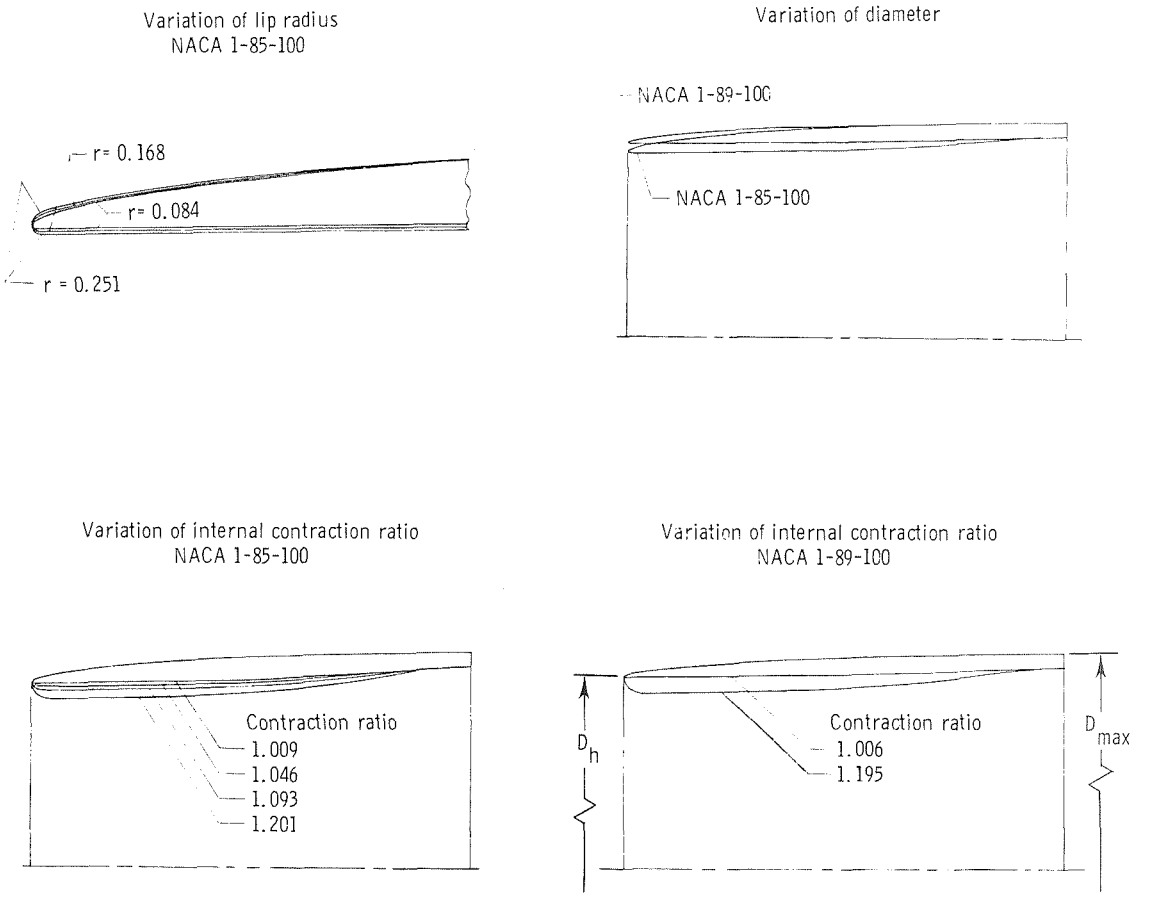

Inlet designation	Lip radius, cm	Internal contraction ratio, A_h/A_{min}	A_h/A_{max}
NACA 1-85-100	0.084	1.009	0.7286
	.168	1.017	
	.251	1.026	
	.084	1.046	
		1.093	
		1.201	
NACA 1-89-100	0.061	1.006	0.7968
		1.195	

Figure 2.- Sketch showing variations in inlet geometry included in investigation.

Pressure probe radial location, R/R_w
0.2131
.2268
.3305
.4720
.5851
.6373 *
.6893
.7622
.8373
.9058
.9549
.9808
.9952
* Static pressure probe

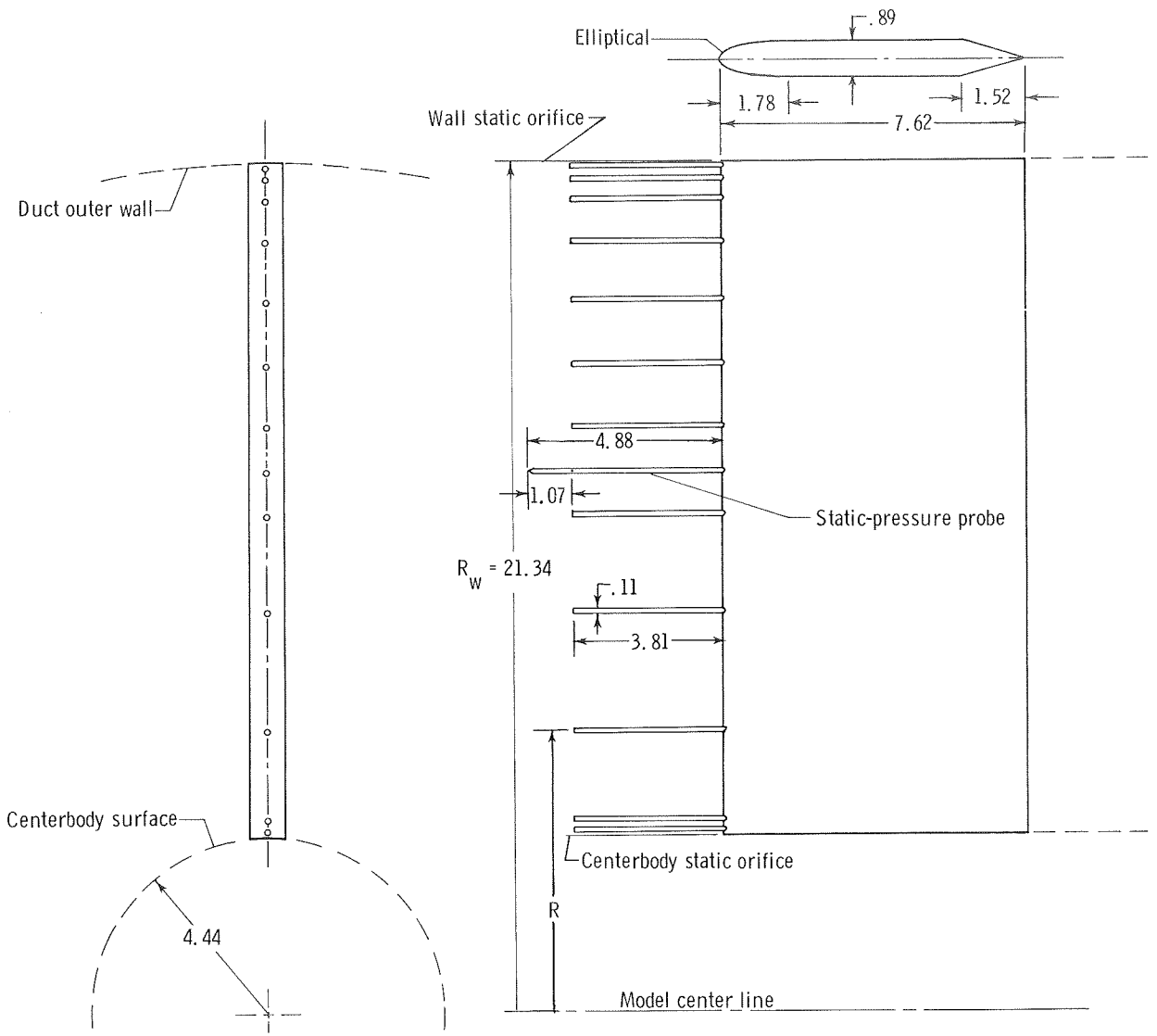

Figure 3.- Pressure instrumentation (on struts at $\phi = 0^o$, 90^o, and 180^o) used to obtain data for mass-flow computations. All dimensions are in centimeters unless otherwise noted.

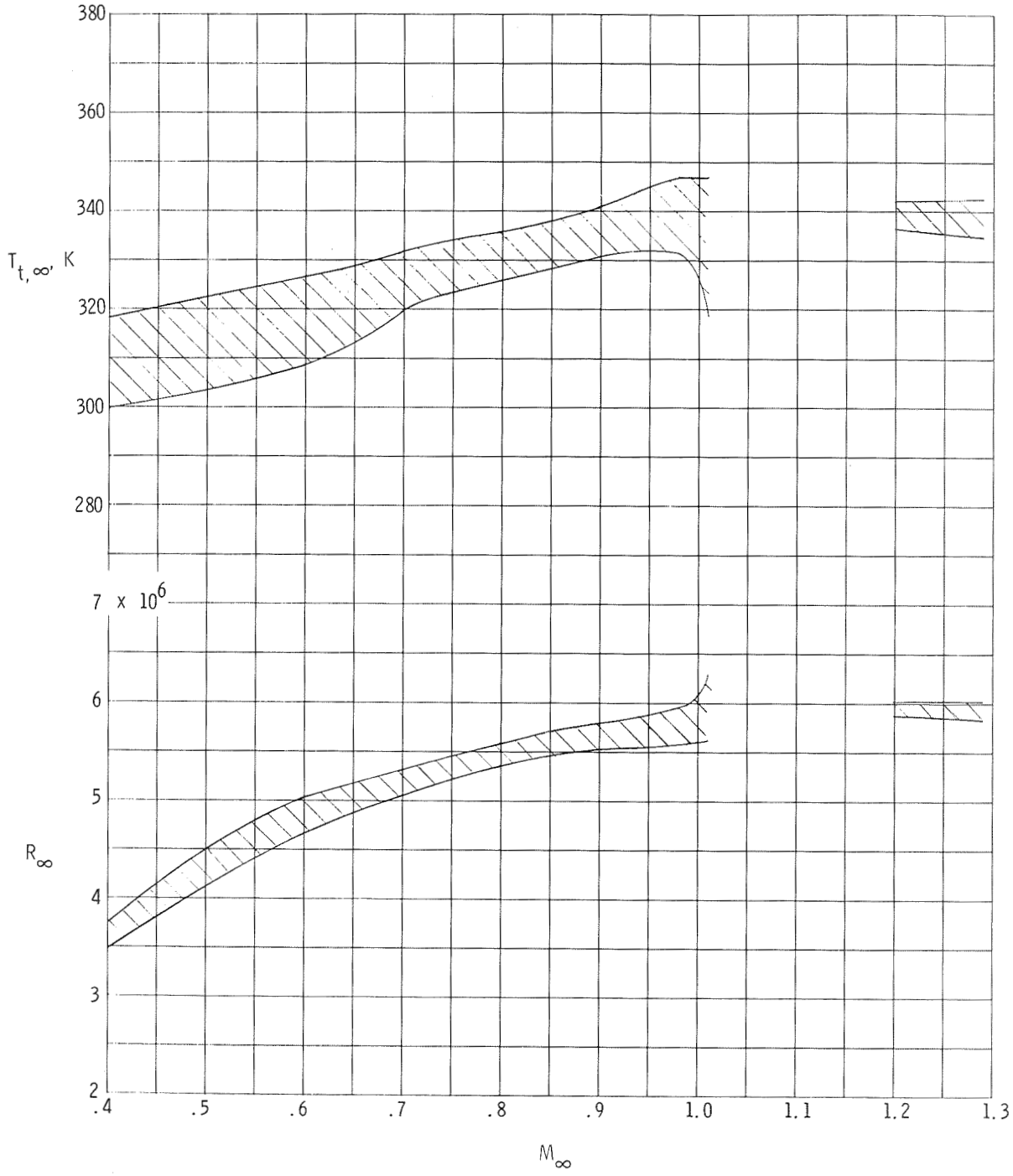

Figure 4.- Variation of Reynolds number (based on maximum model diameter) and free-stream stagnation temperature with free-stream Mach number.

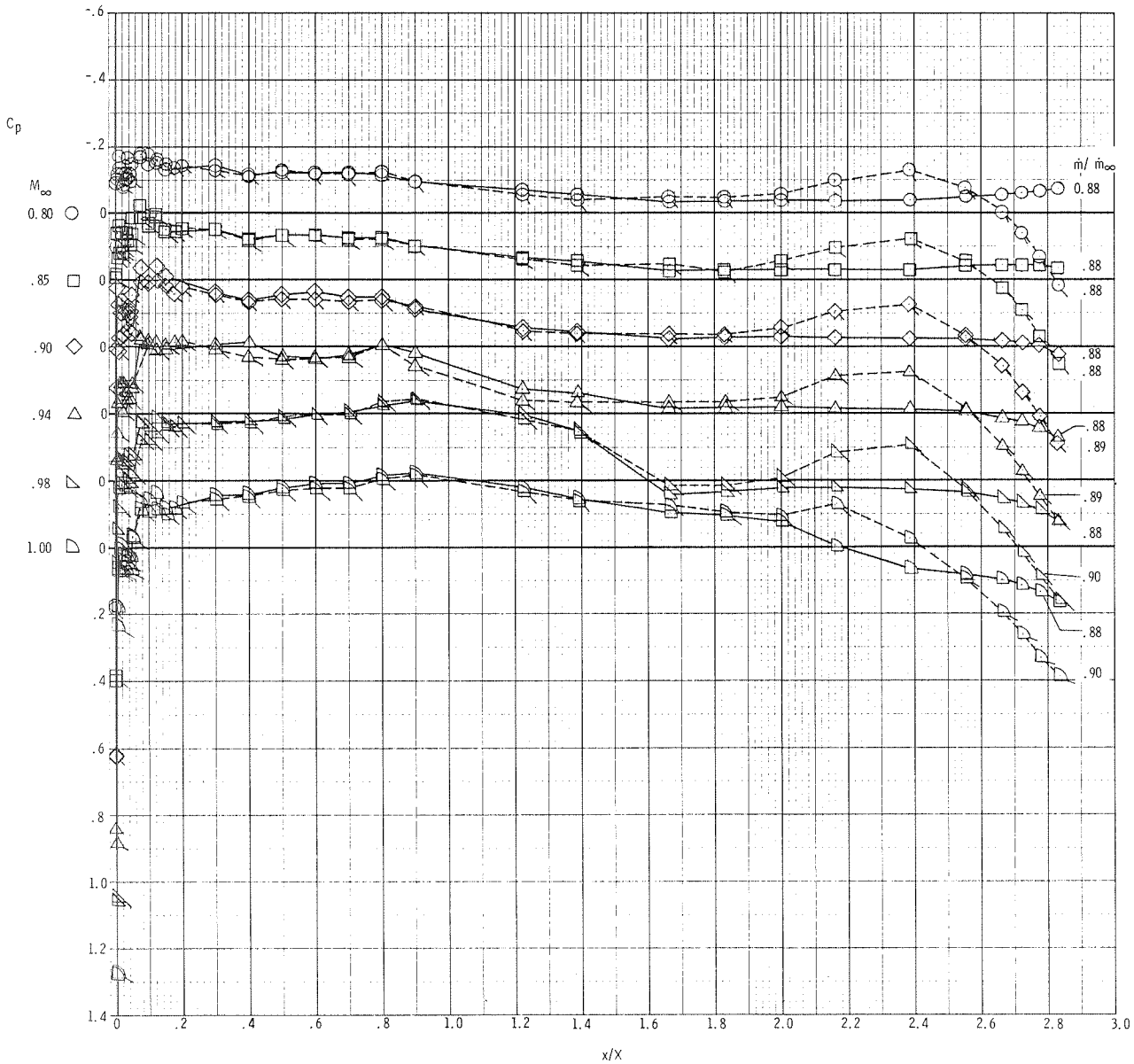

Figure 5.- Comparison of pressure-coefficient distributions along upper surface of present model (cylindrical afterbody) with those of reference 19 (boattailed afterbody) with NACA 1-85-100 (lip radius 0.084 cm, contraction ratio 1.009) inlet. Dashed line and flagged symbols indicate boattailed afterbody.

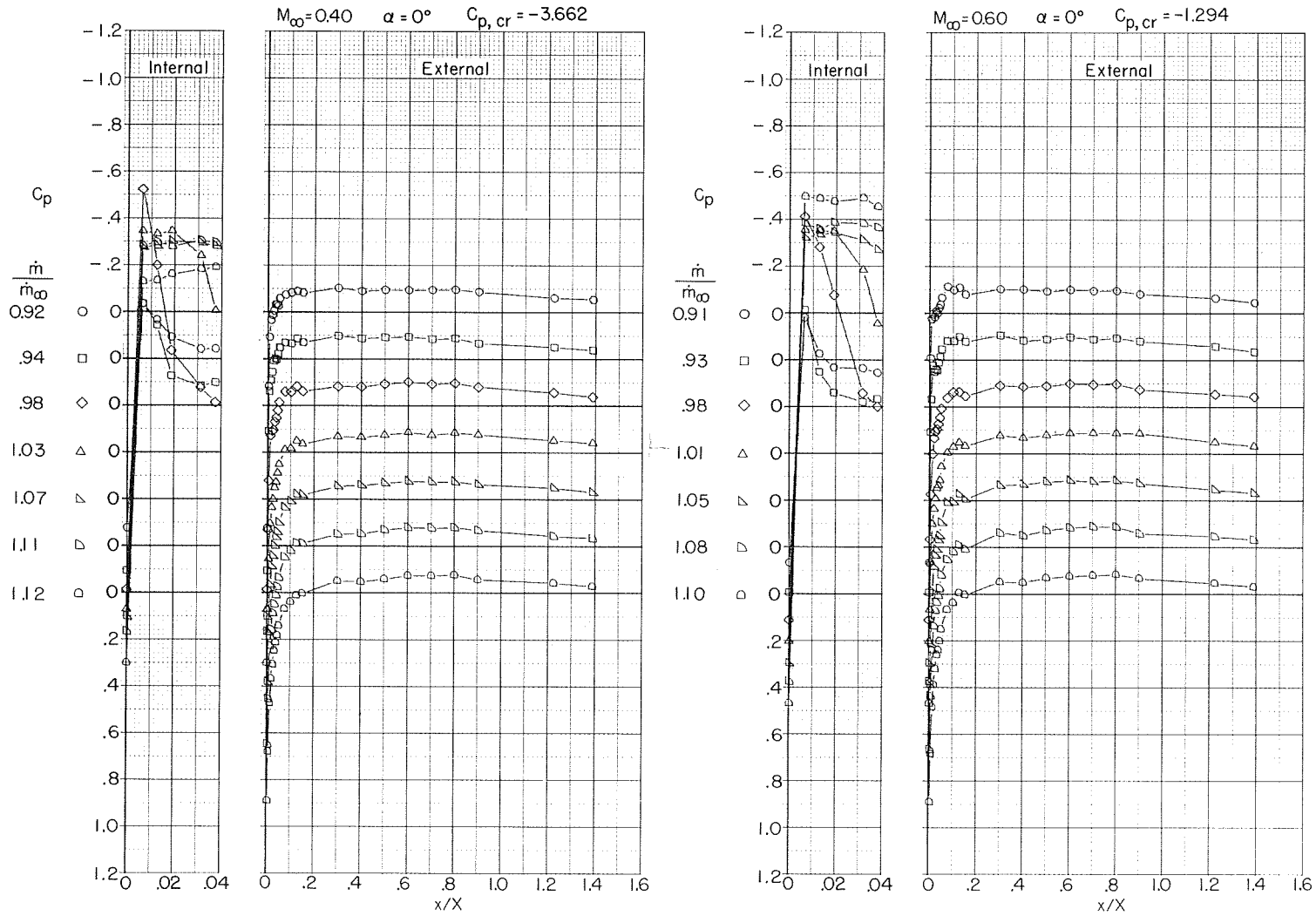

(a) M_∞ = 0.40 and 0.60.

Figure 6.- Variation with length of local pressure coefficient of NACA 1-85-100 inlet (lip radius 0.084 cm, contraction ratio 1.009).

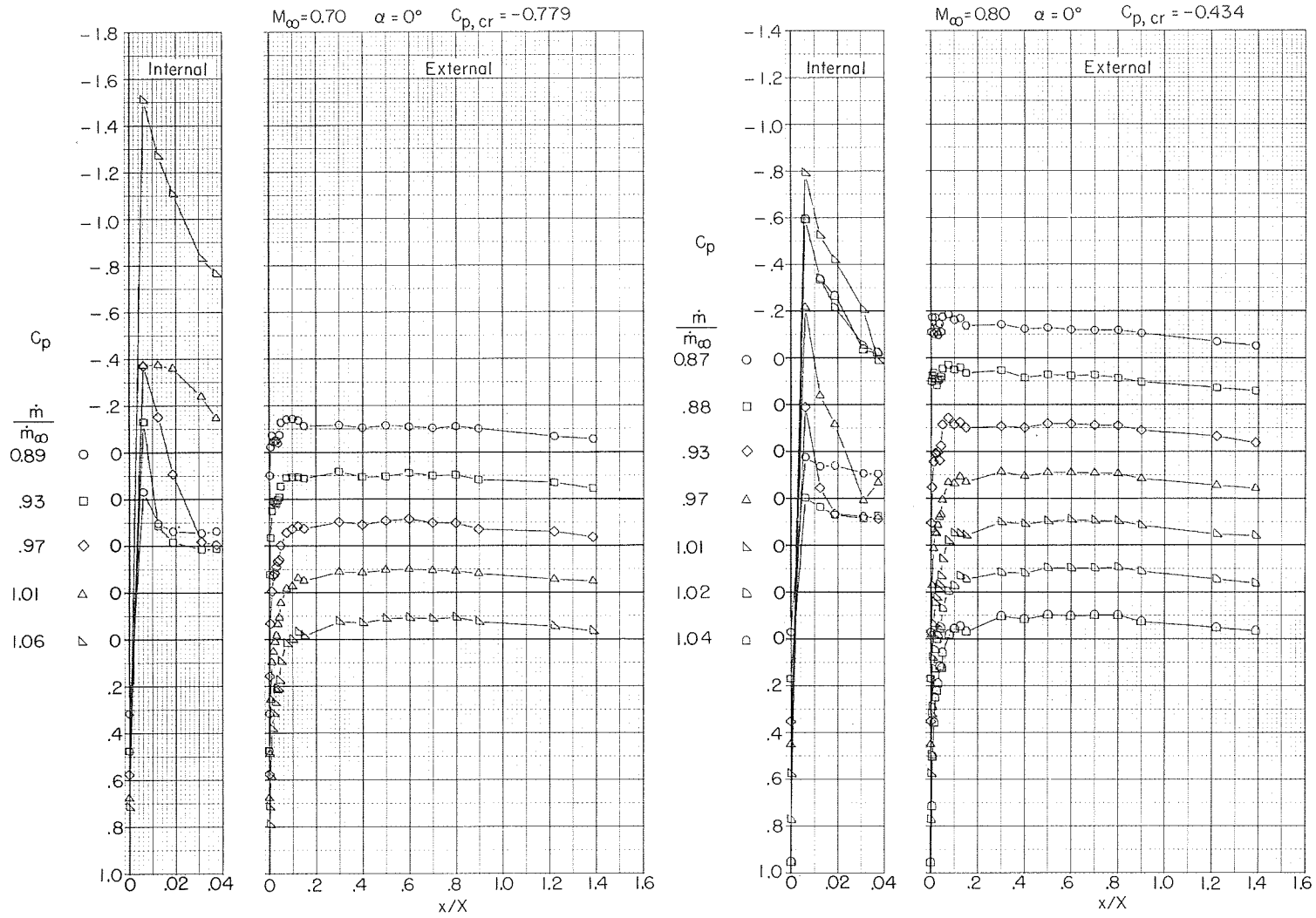

(b) M_∞ = 0.70 and 0.80.

Figure 6.- Continued.

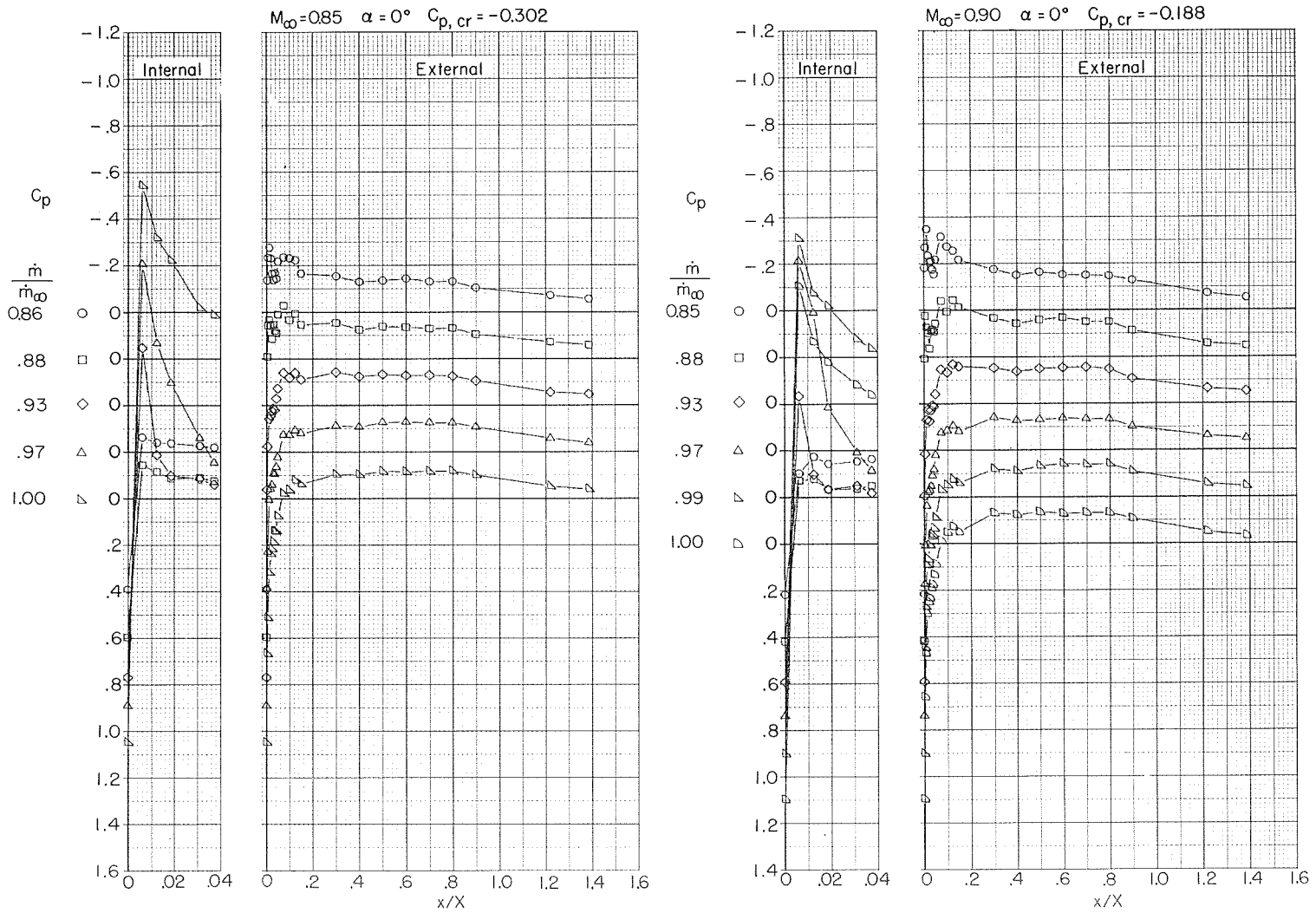

(c) M_∞ = 0.85 and 0.90.

Figure 6.- Continued.

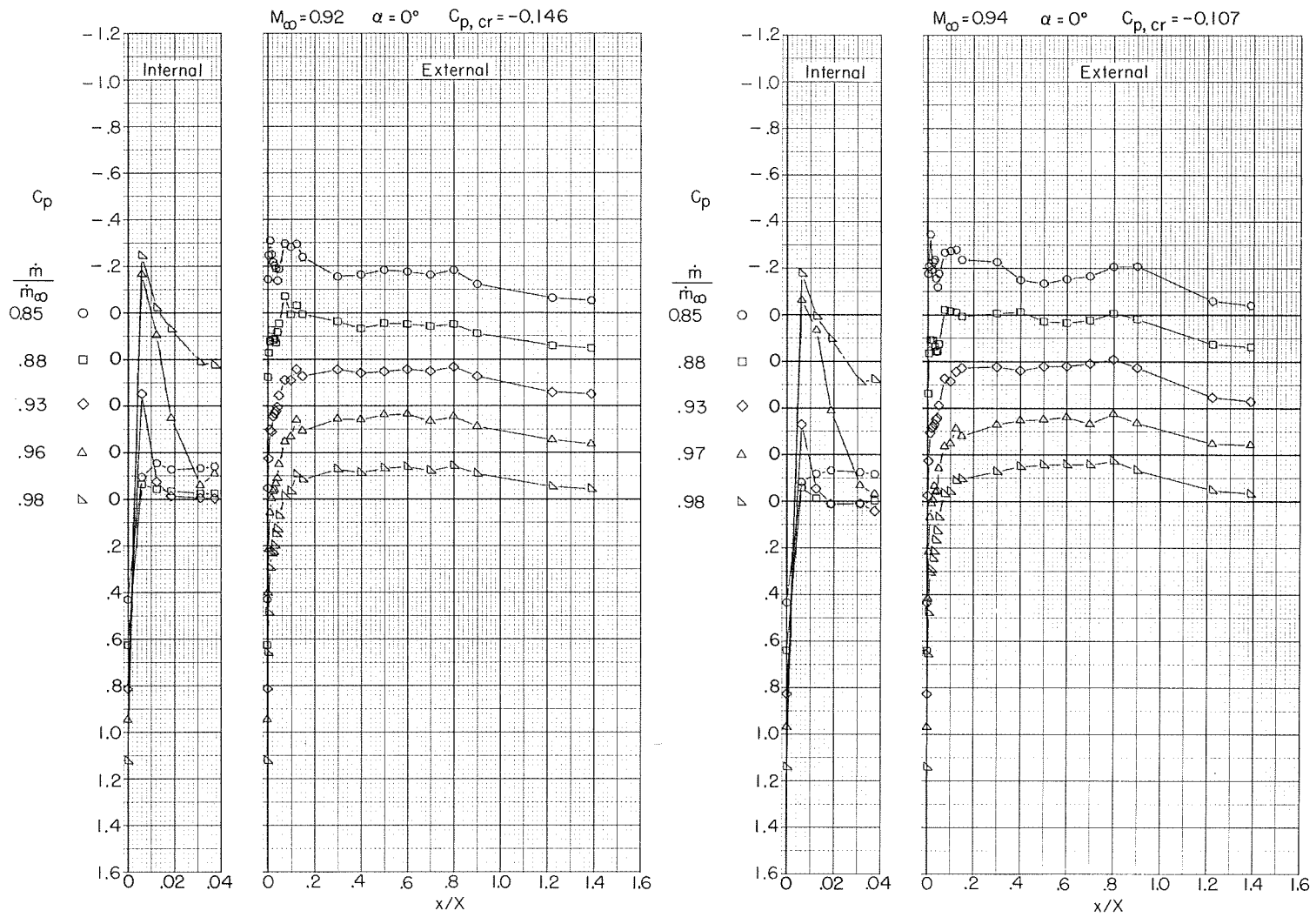

(d) M_∞ = 0.92 and 0.94.

Figure 6.- Continued.

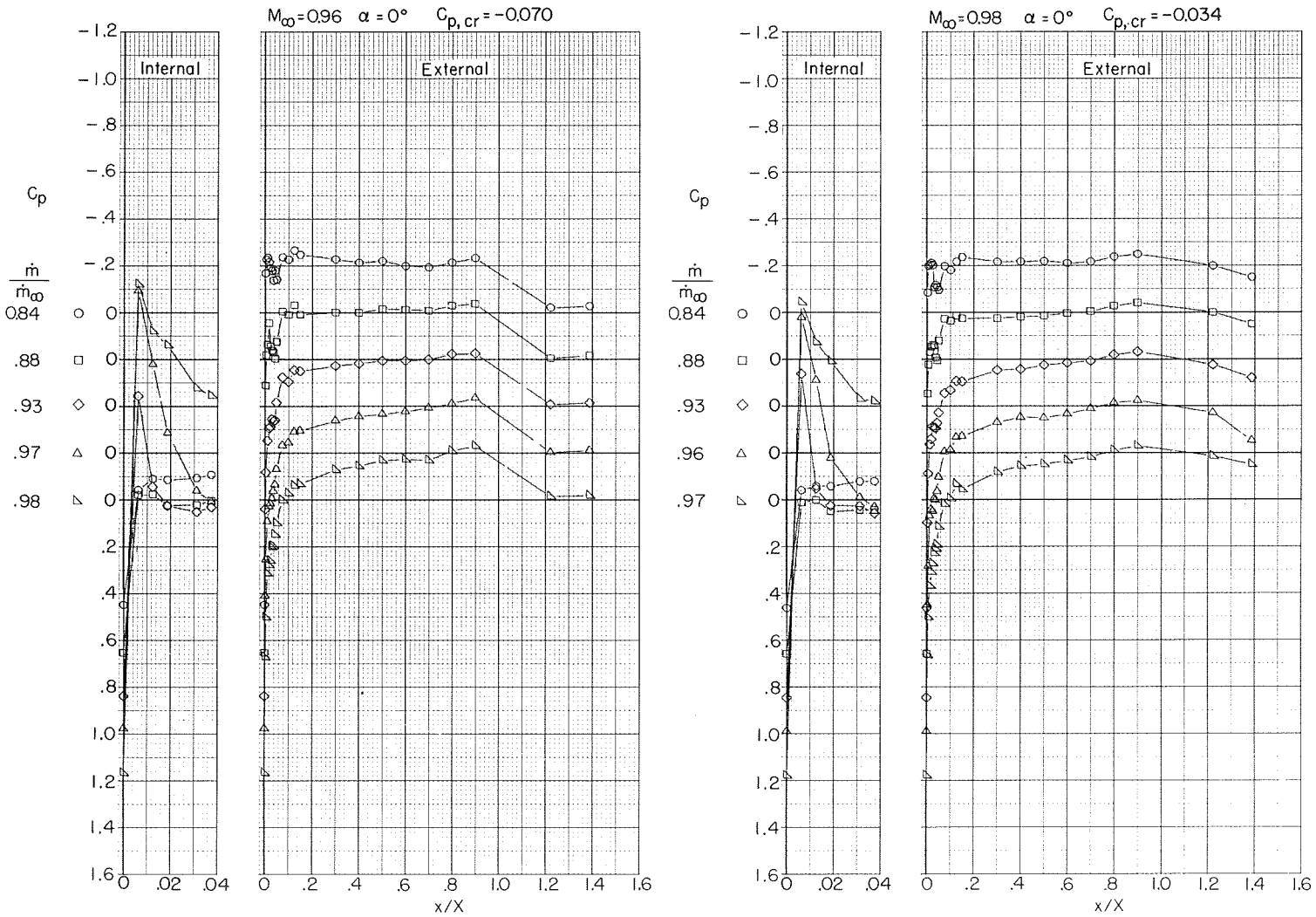

(e) M_∞ = 0.96 and 0.98.

Figure 6.- Continued.

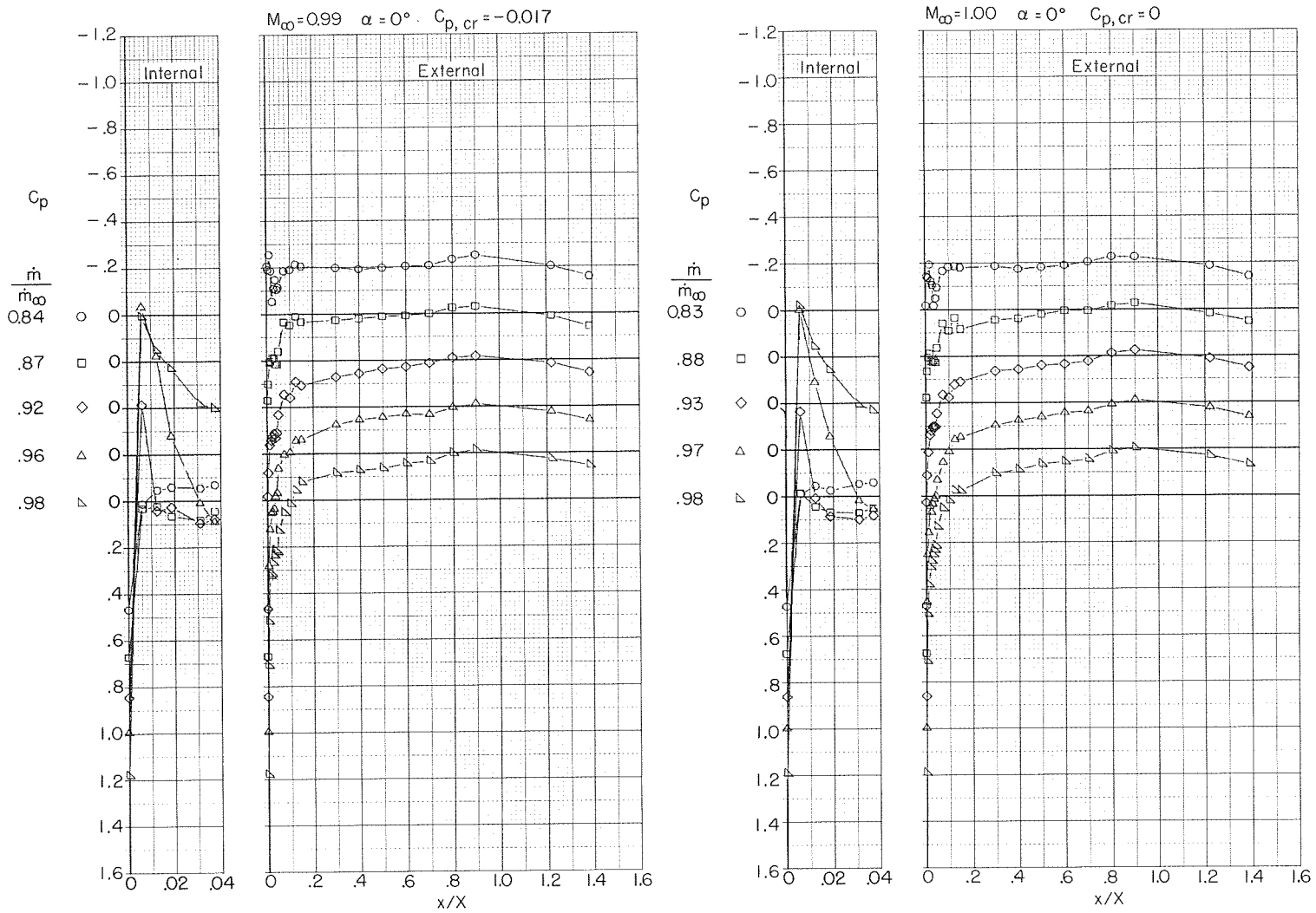

(f) M_∞ = 0.99 and 1.00.

Figure 6.- Continued.

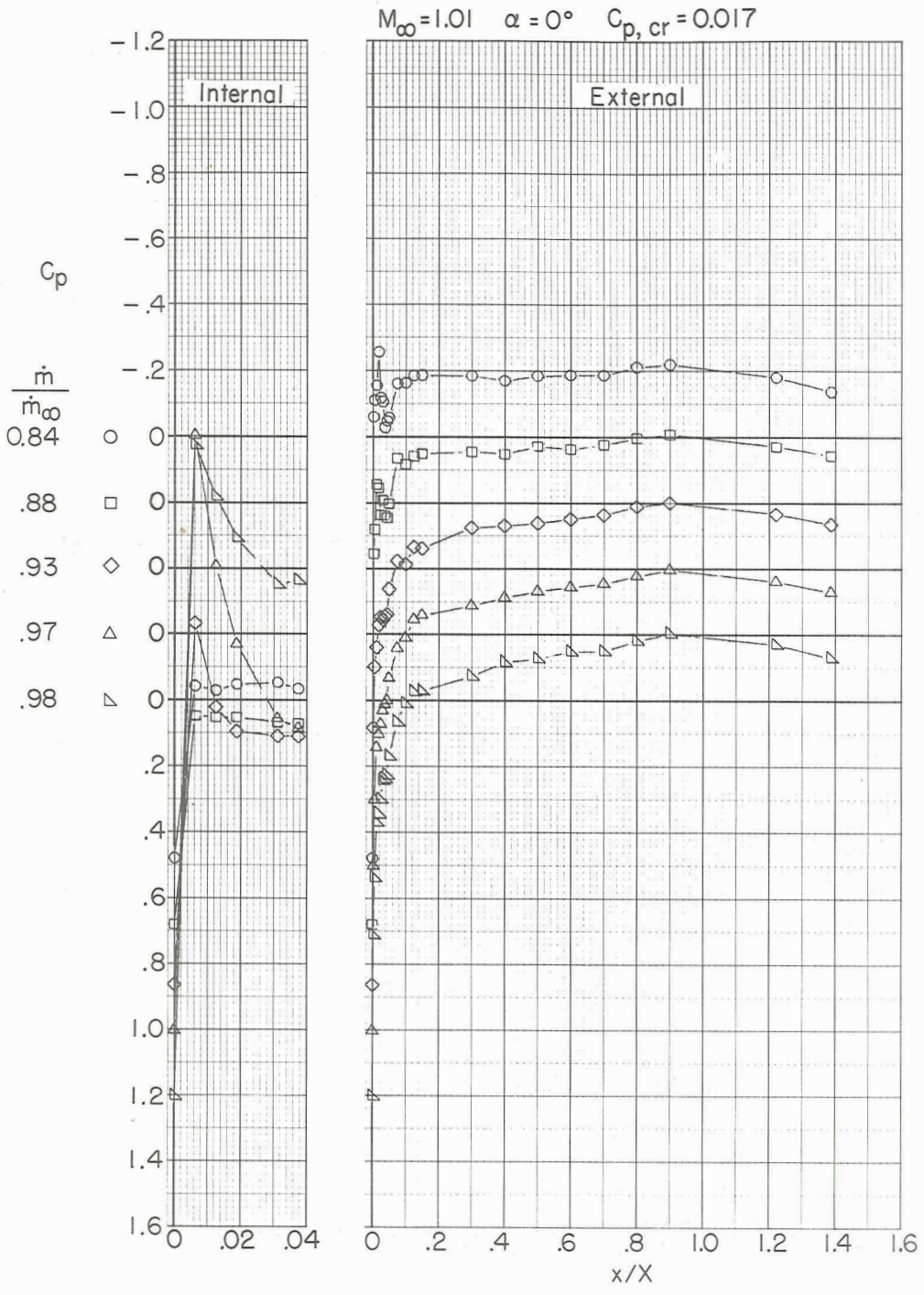

(g) $M_\infty = 1.01$.

Figure 6.- Concluded.

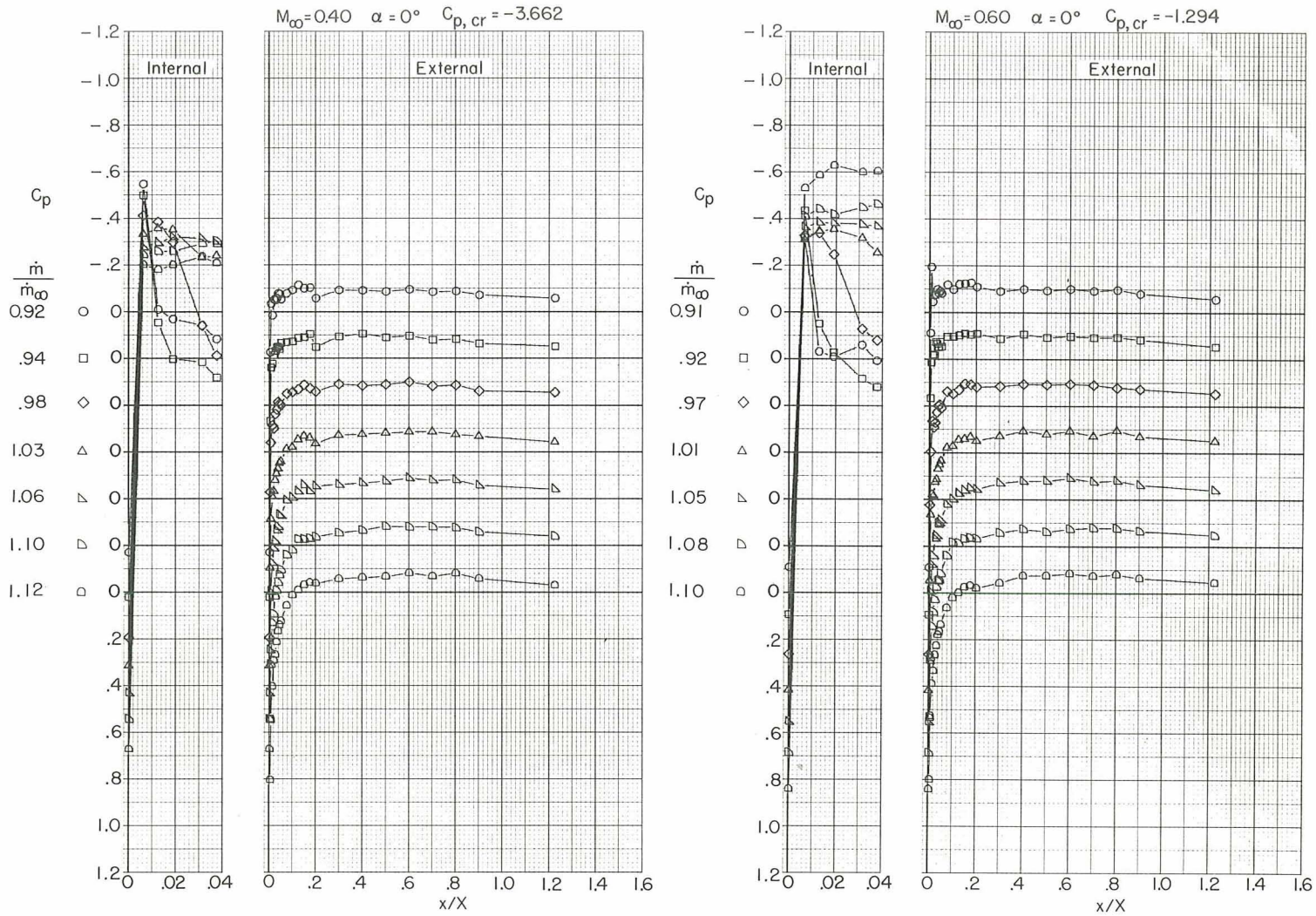

(a) M_∞ = 0.40 and 0.60.

Figure 7.- Variation with length of local pressure coefficient of NACA 1-85-100 inlet (lip radius 0.168 cm, contraction ratio 1.017).

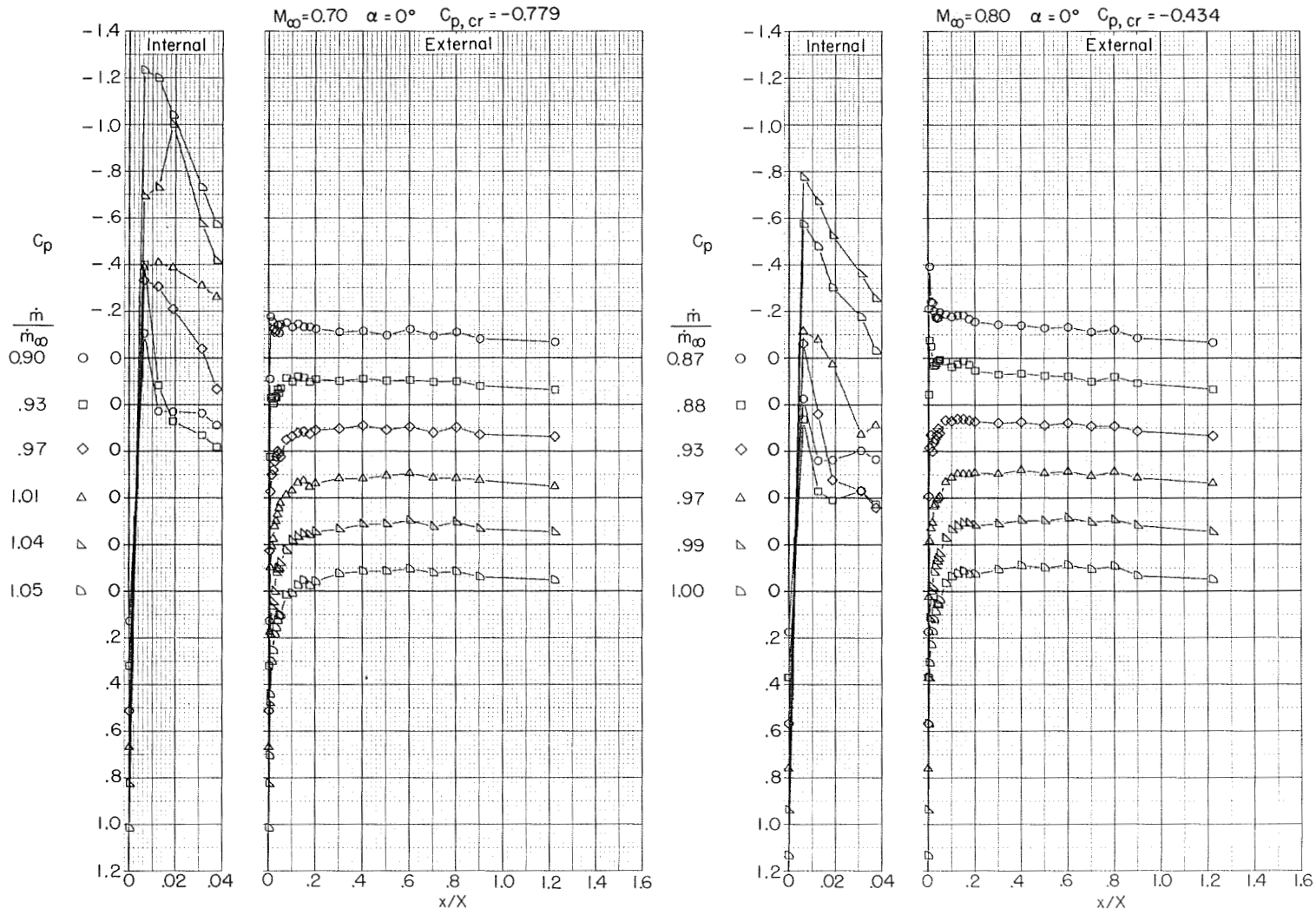

(b) M_∞ = 0.70 and 0.80.

Figure 7.- Continued.

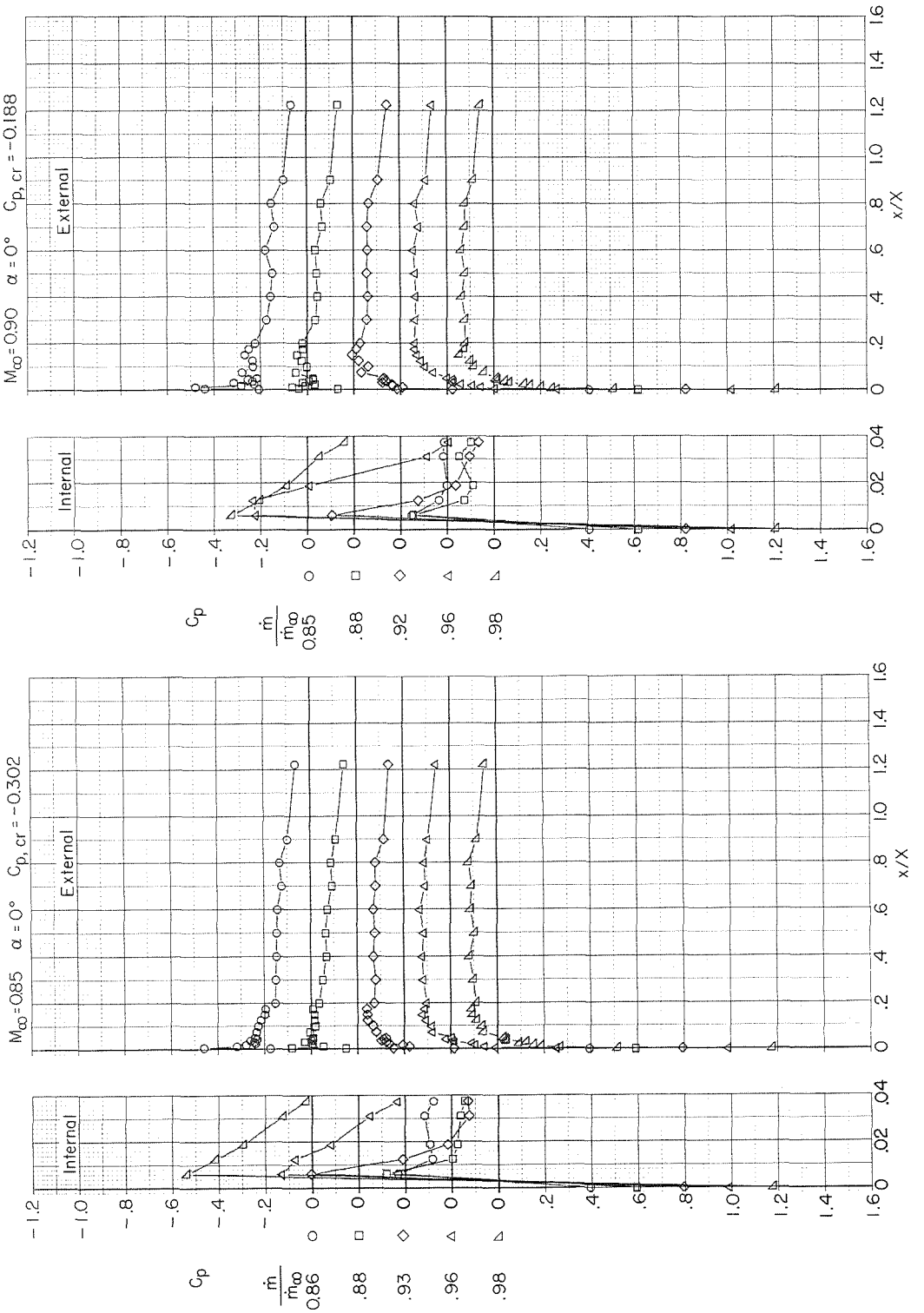

(c) M_∞ = 0.85 and 0.90.

Figure 7.- Continued.

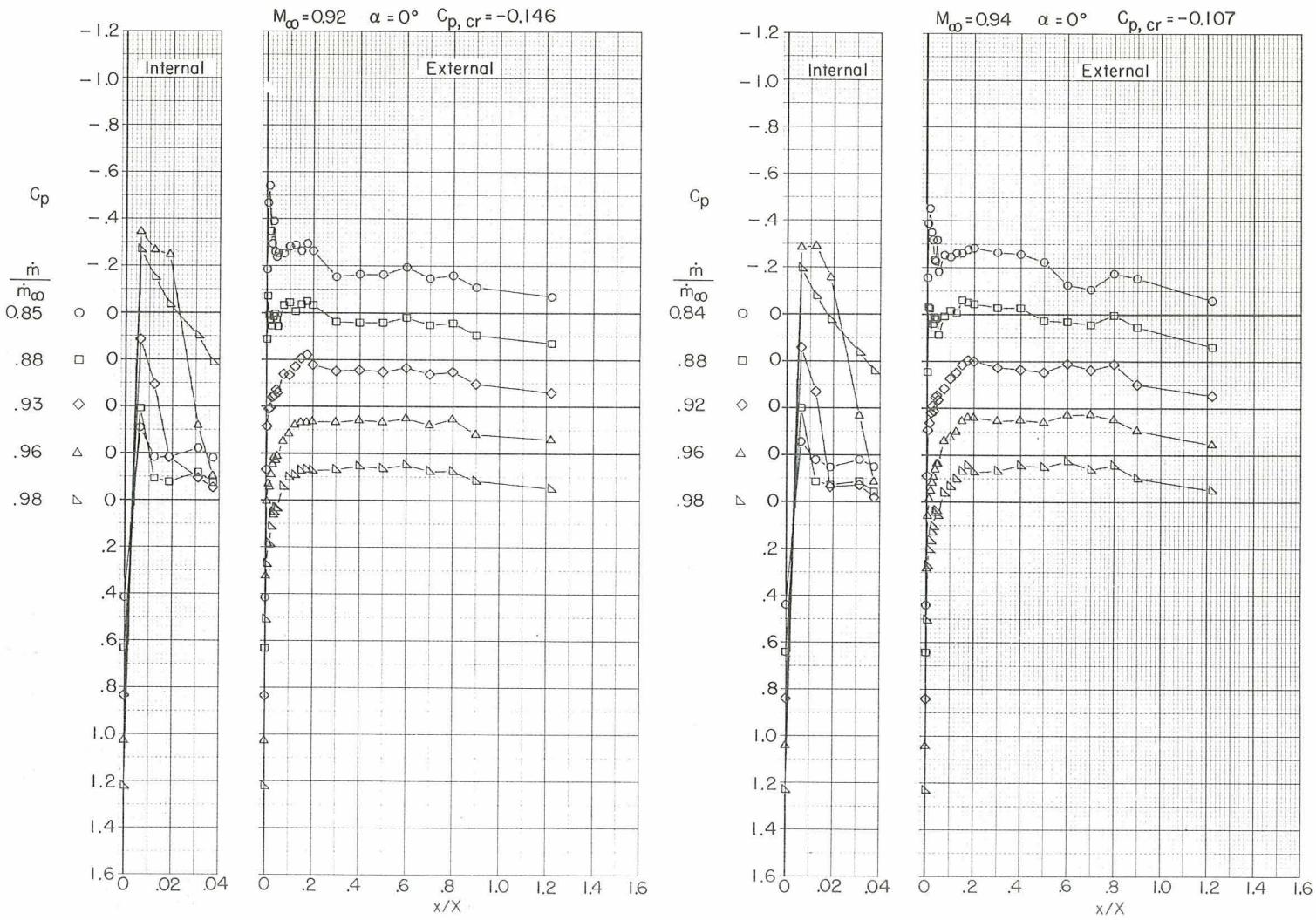

(d) M_∞ = 0.92 and 0.94.

Figure 7.- Continued.

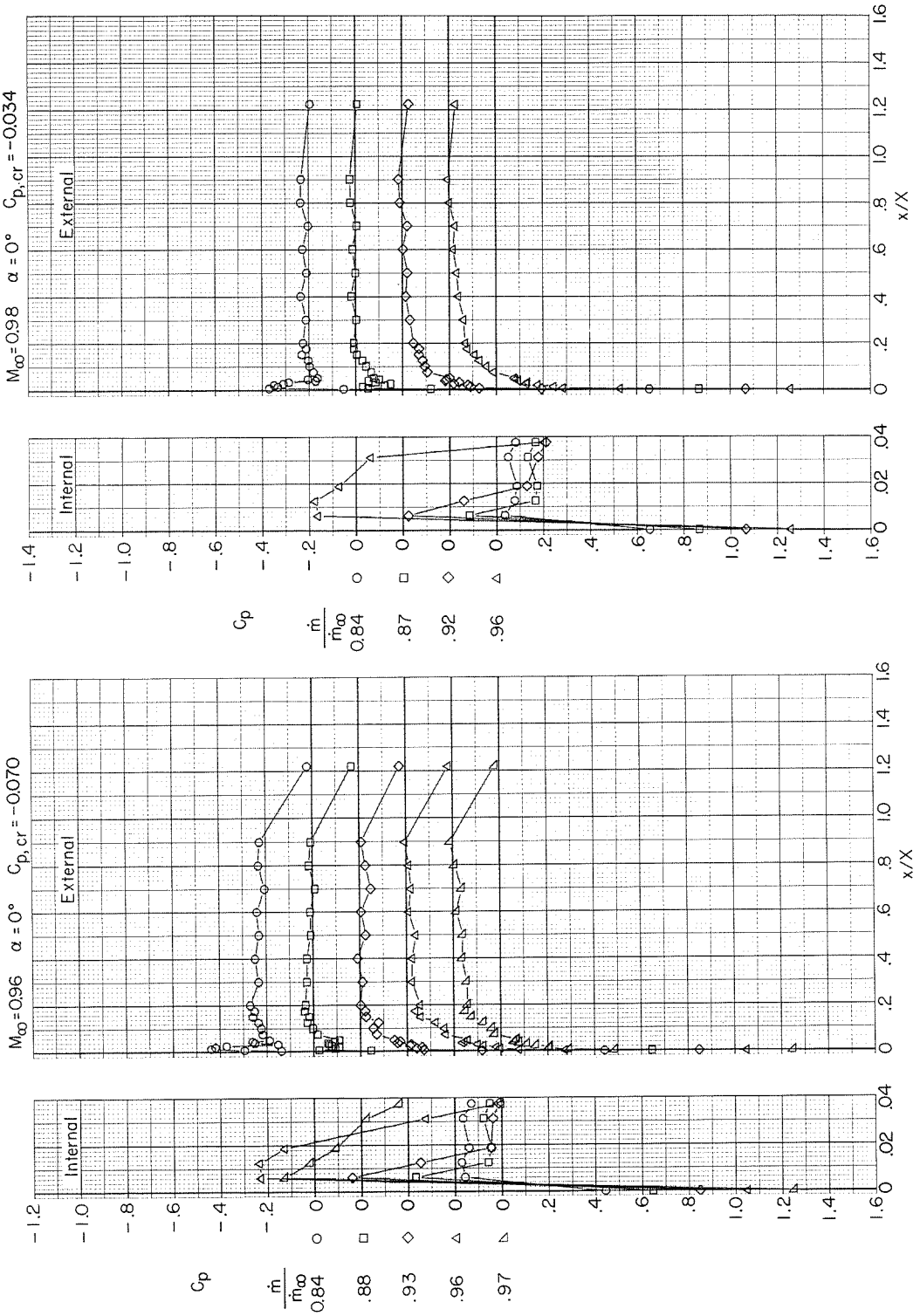

(e) M_∞ = 0.96 and 0.98.

Figure 7.- Continued.

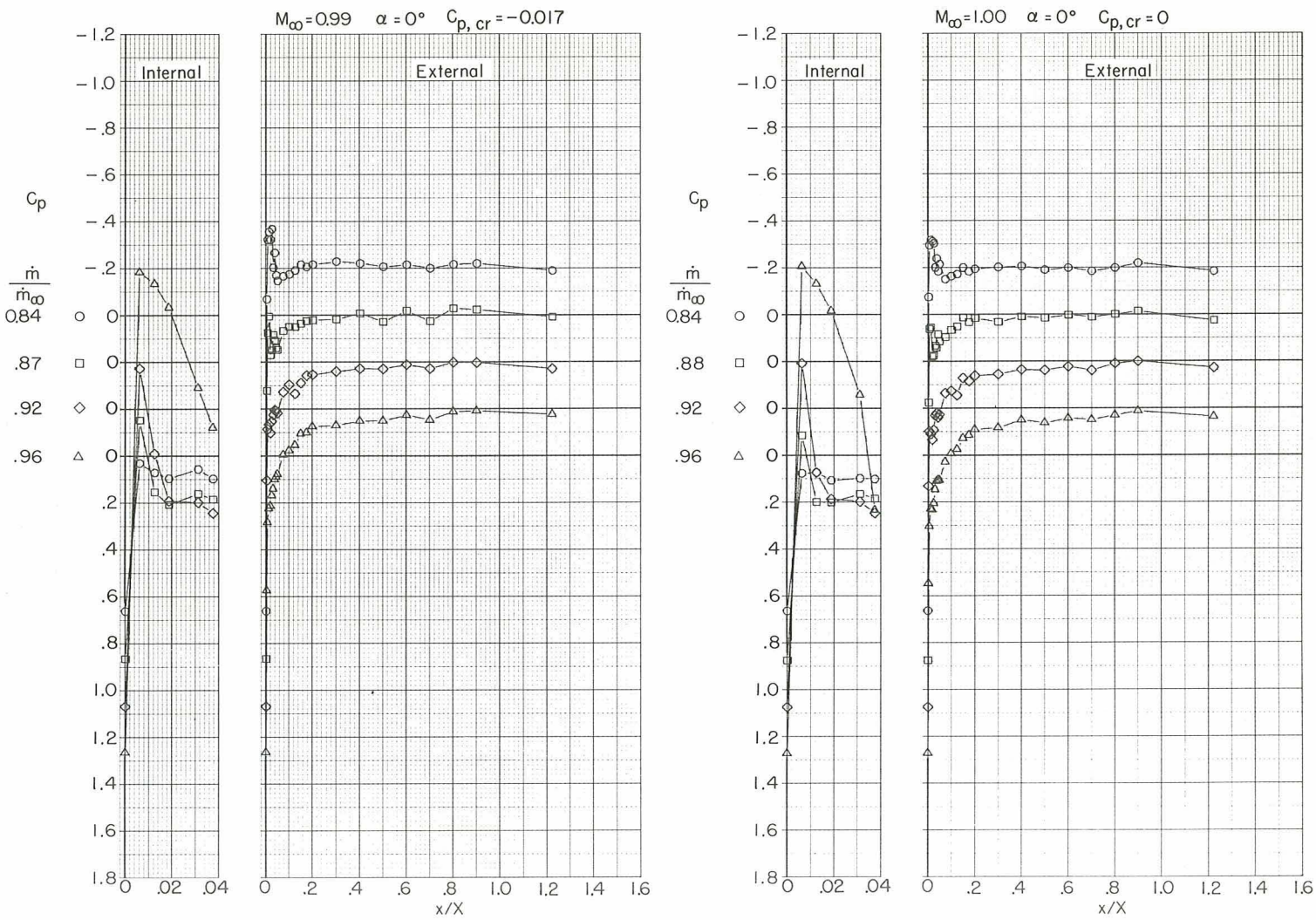

(f) M_∞ = 0.99 and 1.00.

Figure 7.- Continued.

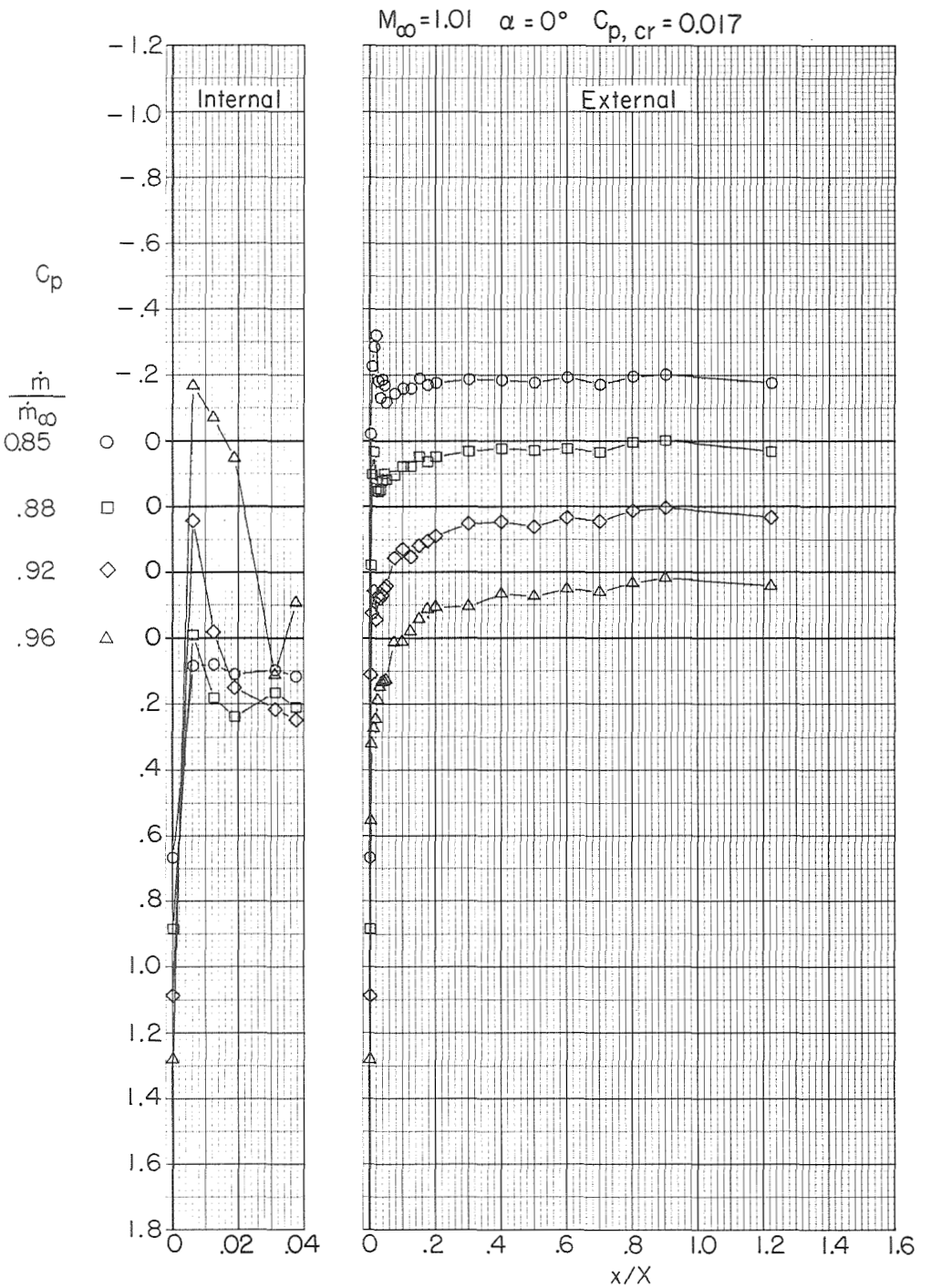

(g) $M_\infty = 1.01$.

Figure 7.- Concluded.

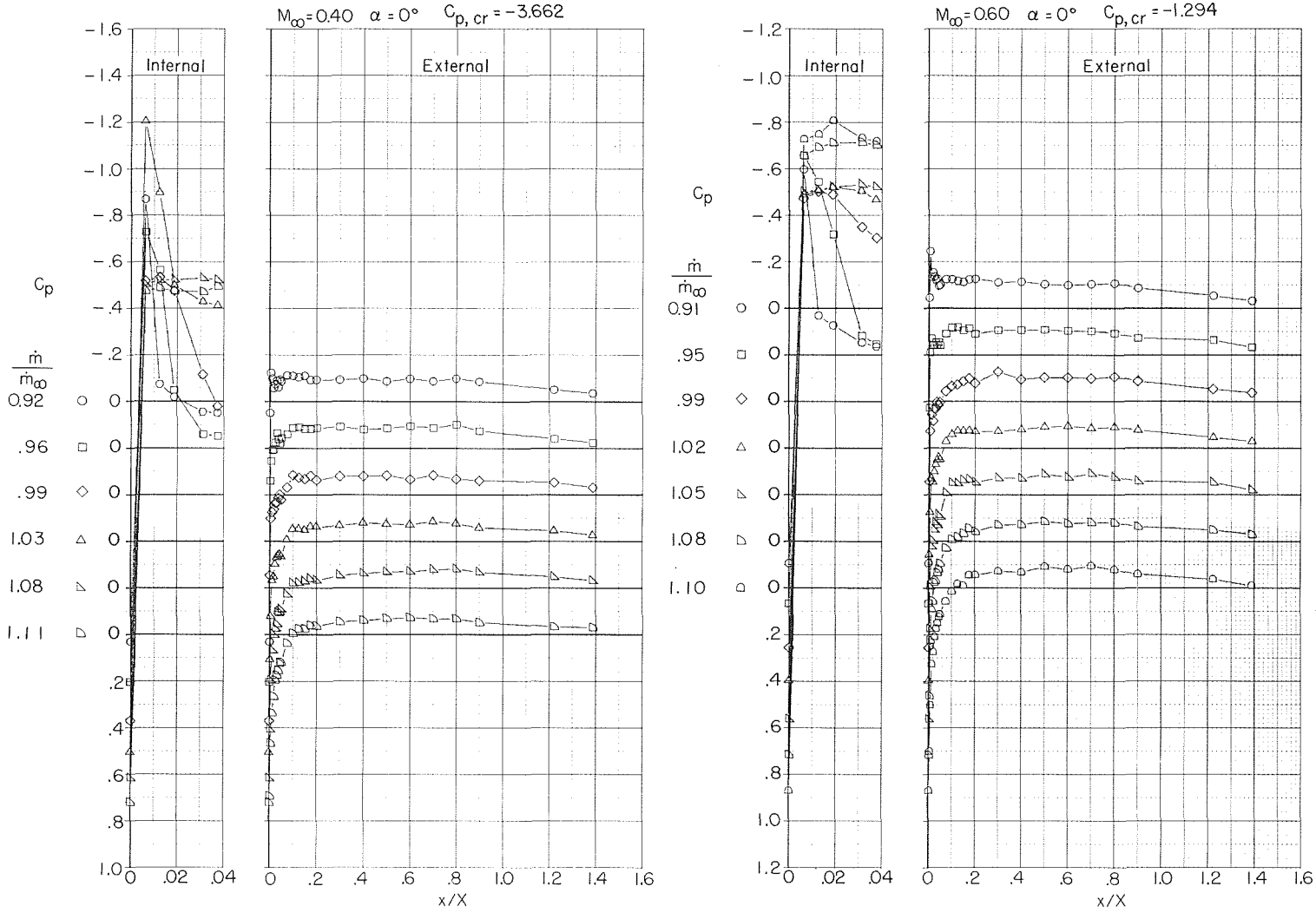

(a) M_∞ = 0.40 and 0.60.

Figure 8.- Variation with length of local pressure coefficient of NACA 1-85-100 inlet (lip radius 0.251 cm, contraction ratio 1.026).

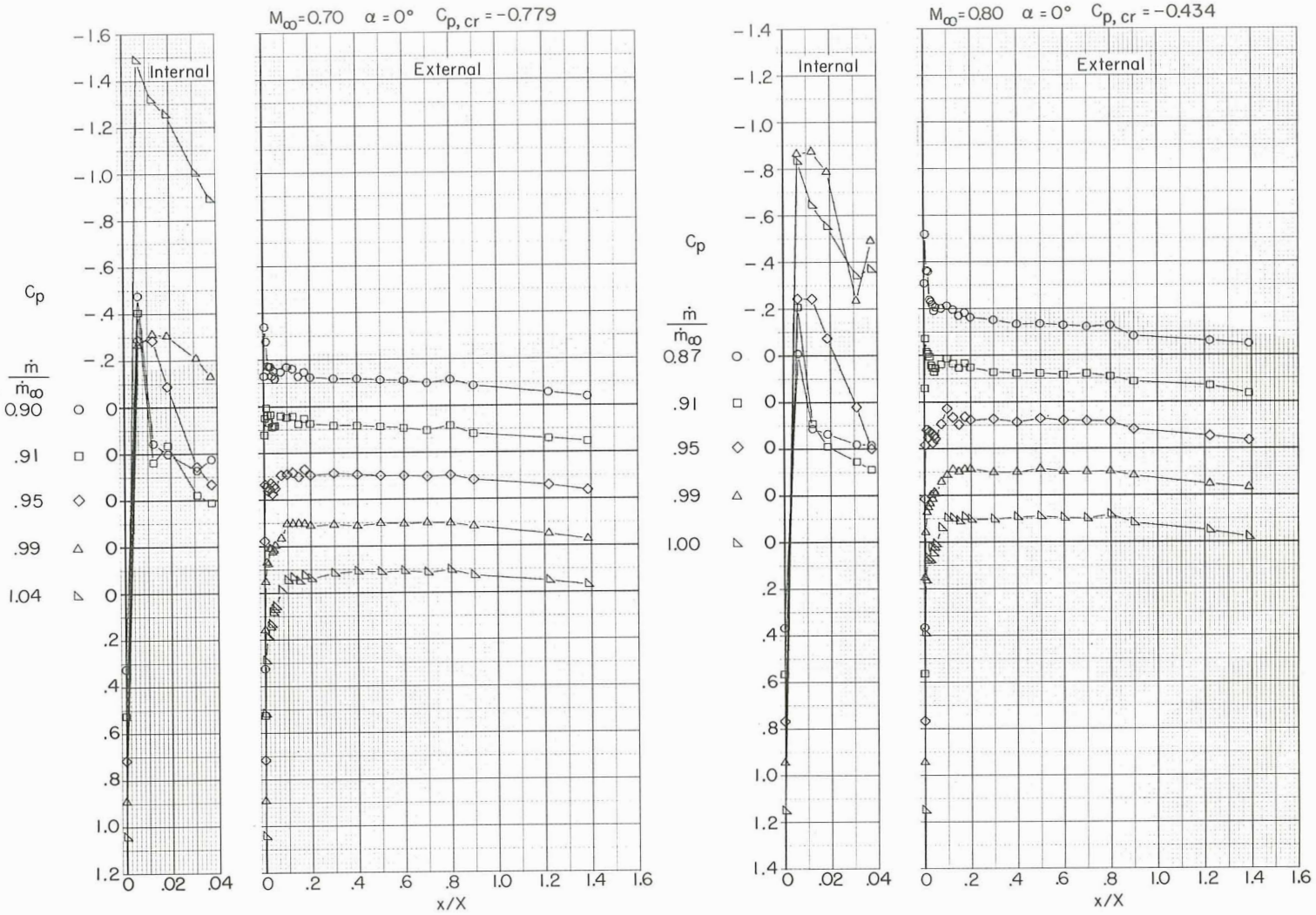

(b) M_∞ = 0.70 and 0.80.

Figure 8.- Continued.

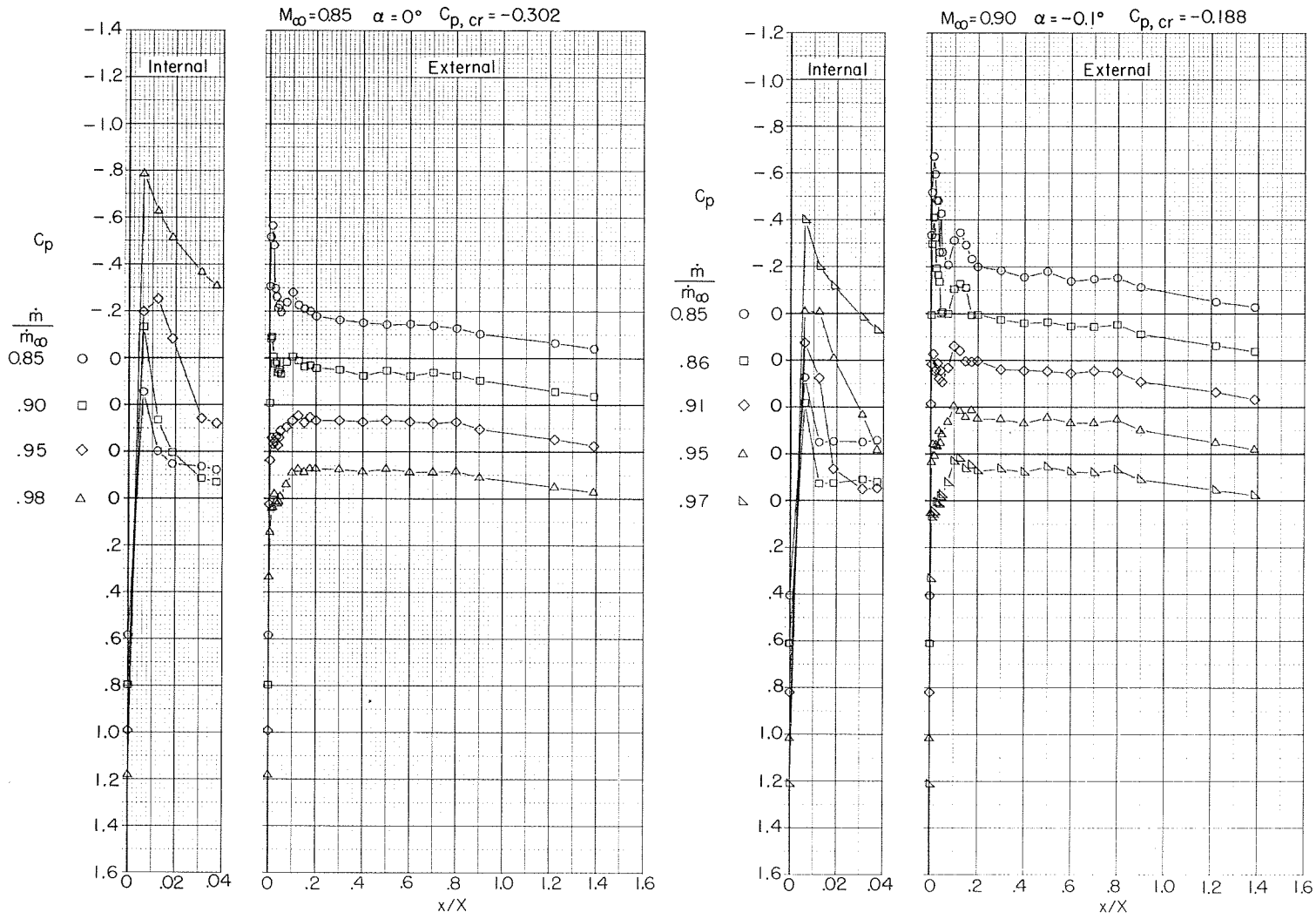

(c) M_∞ = 0.85 and 0.90.

Figure 8.- Continued.

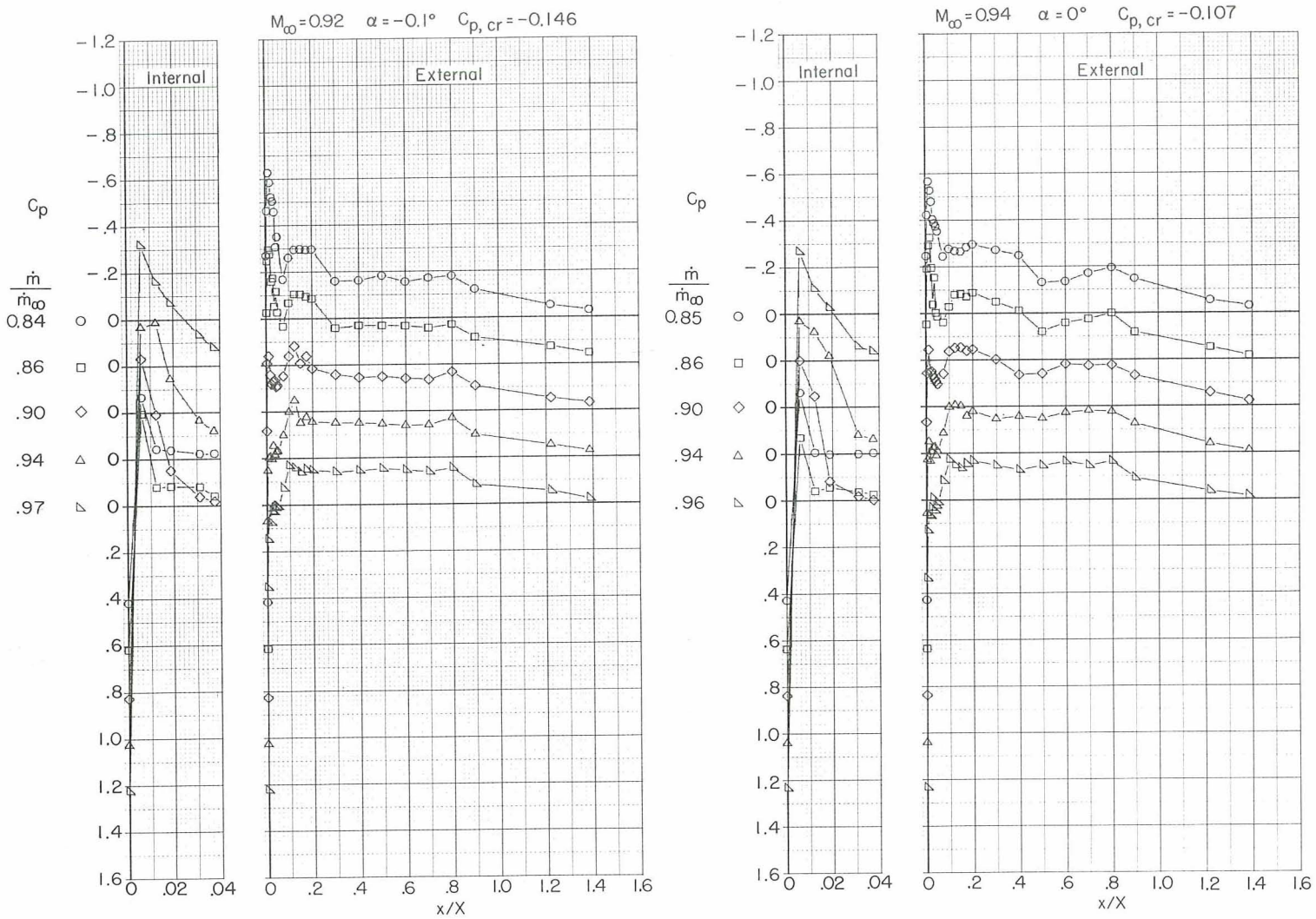

(d) $M_\infty = 0.92$ and 0.94.

Figure 8.- Continued.

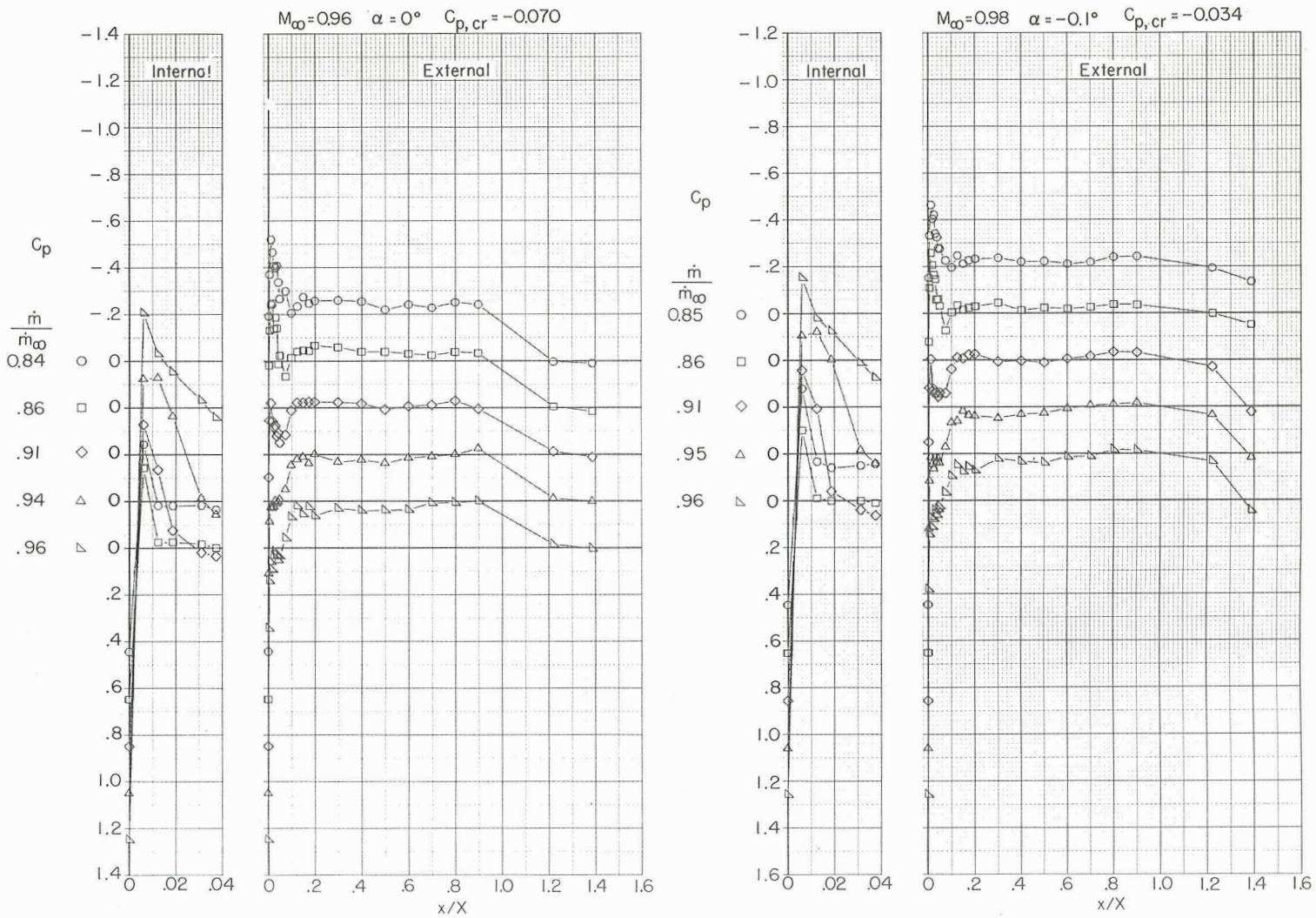

(e) M_∞ = 0.96 and 0.98.

Figure 8.- Continued.

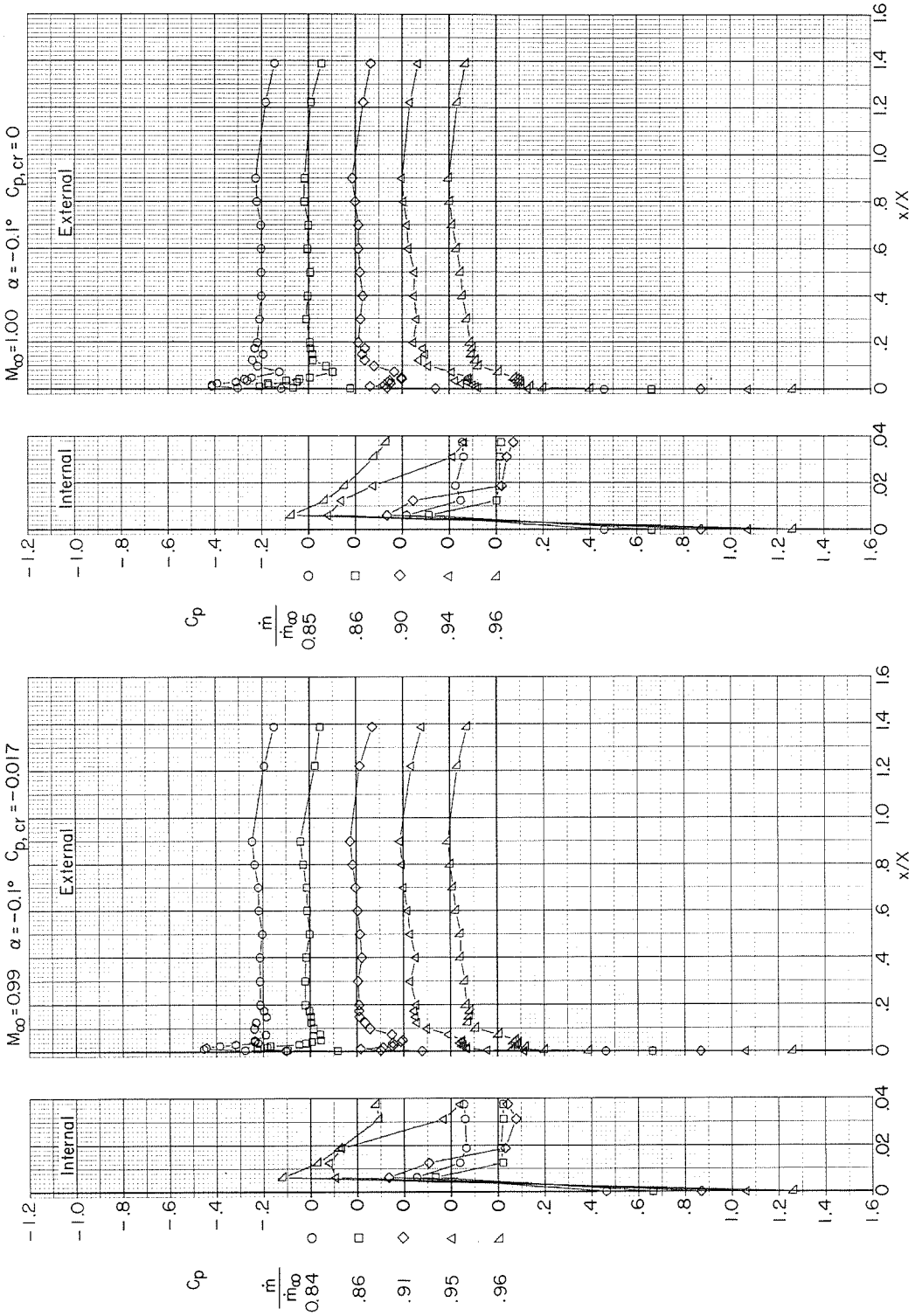

(f) M_∞ = 0.99 and 1.00.

Figure 8.- Continued.

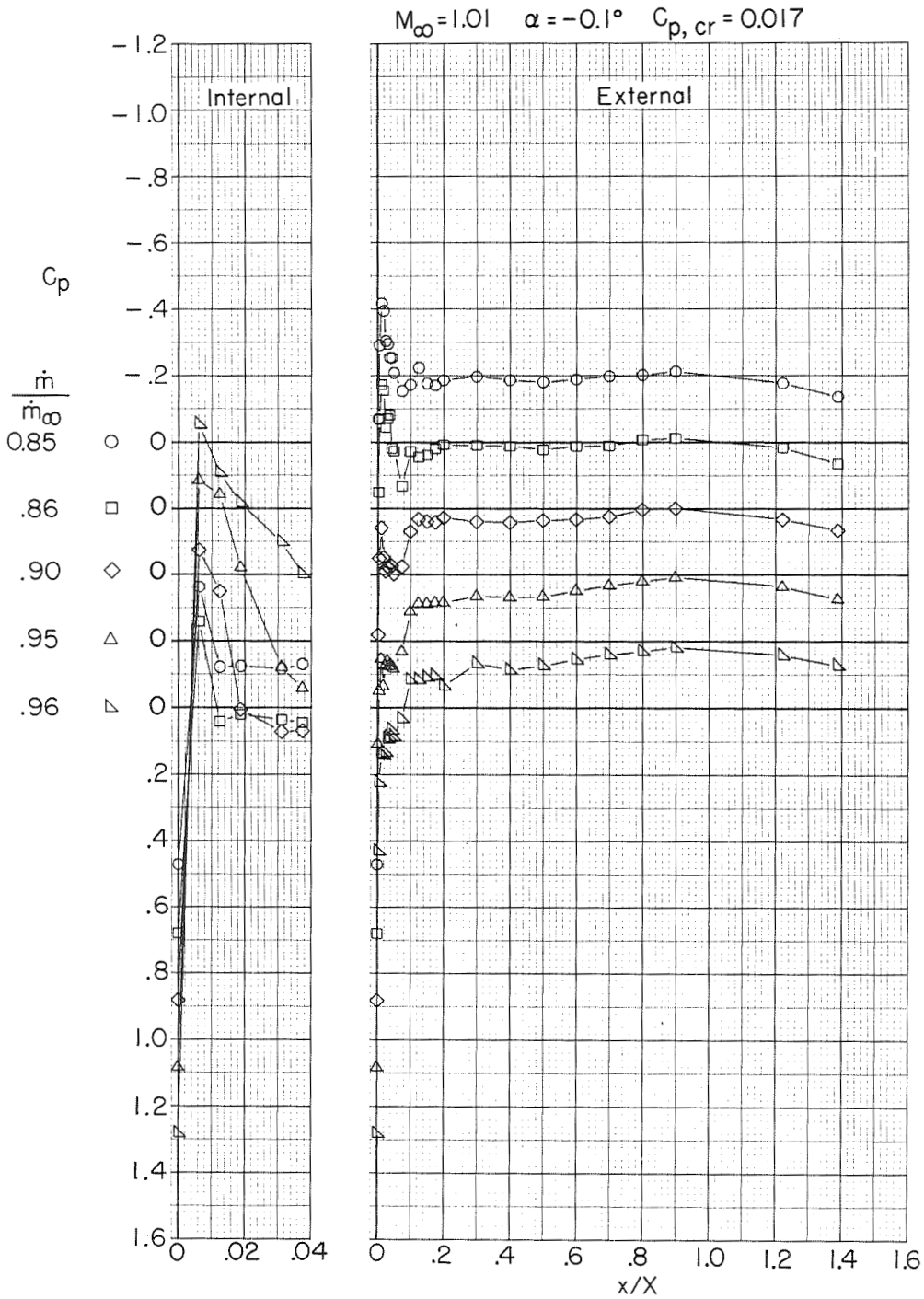

(g) $M_\infty = 1.01$.

Figure 8.- Concluded.

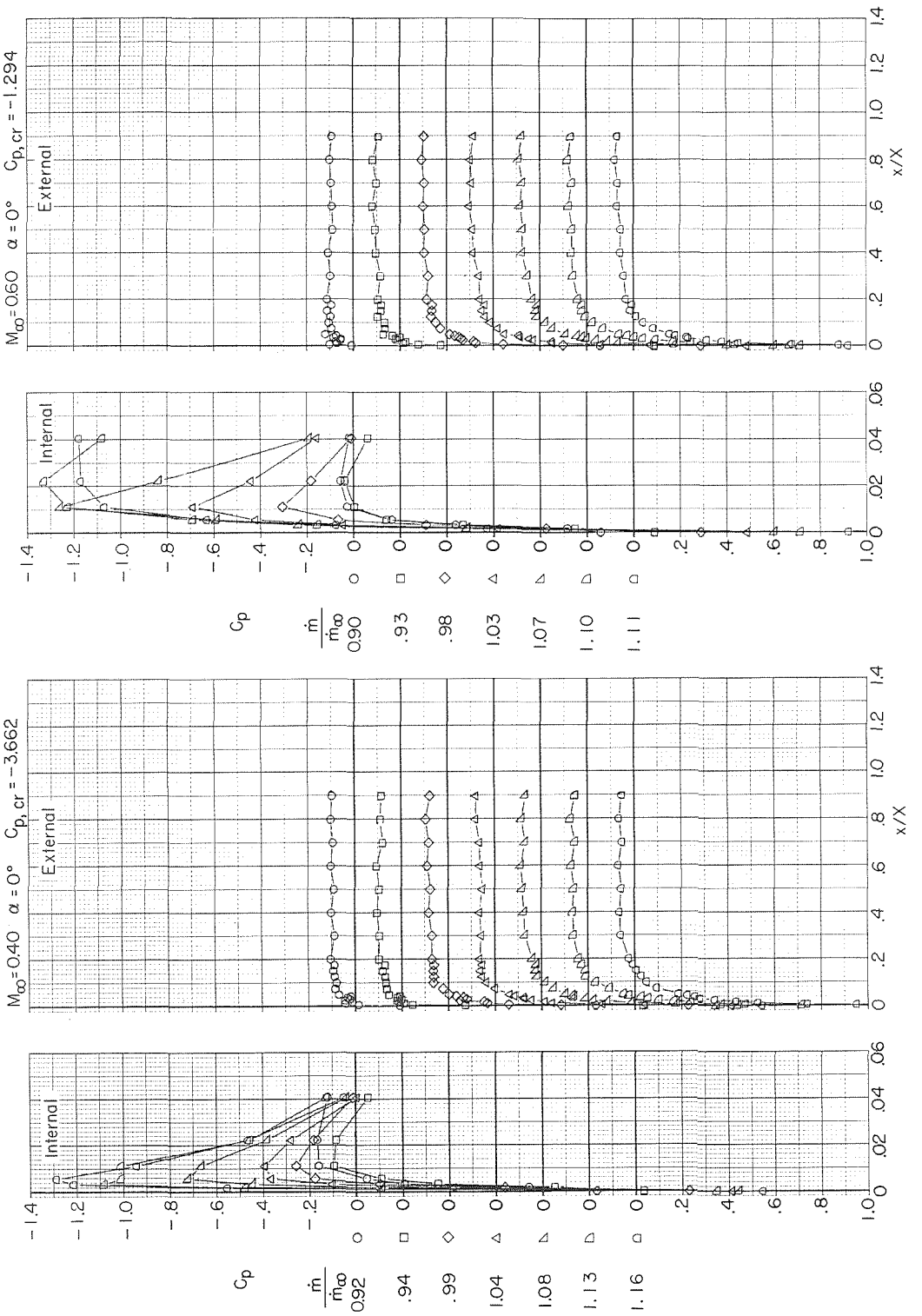

(a) M_∞ = 0.40 and 0.60.

Figure 9.- Variation with length of local pressure coefficient of NACA 1-85-100 inlet (lip radius 0.084 cm, contraction ratio 1.046).

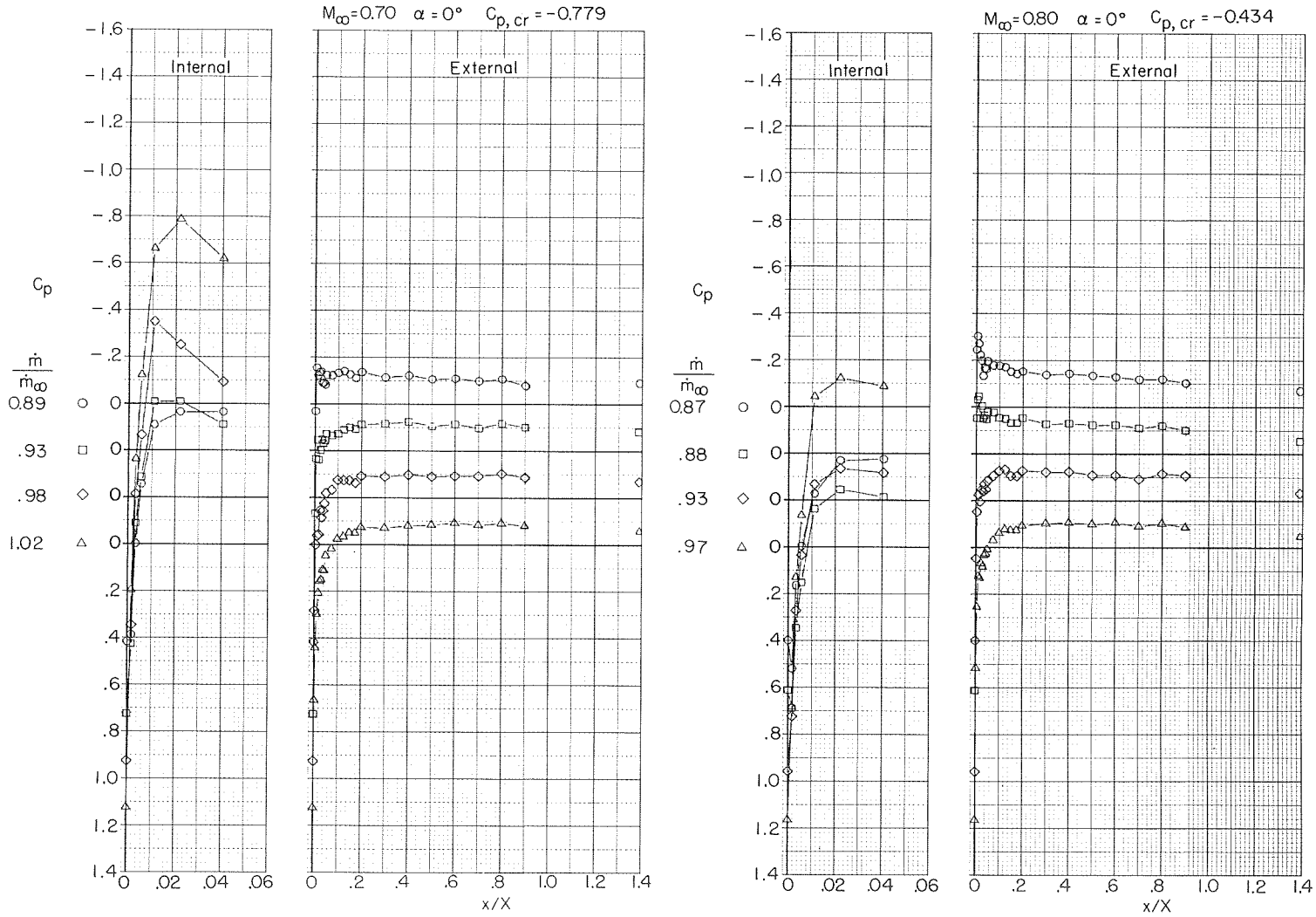

(b) M_∞ = 0.70 and 0.80.

Figure 9.- Continued.

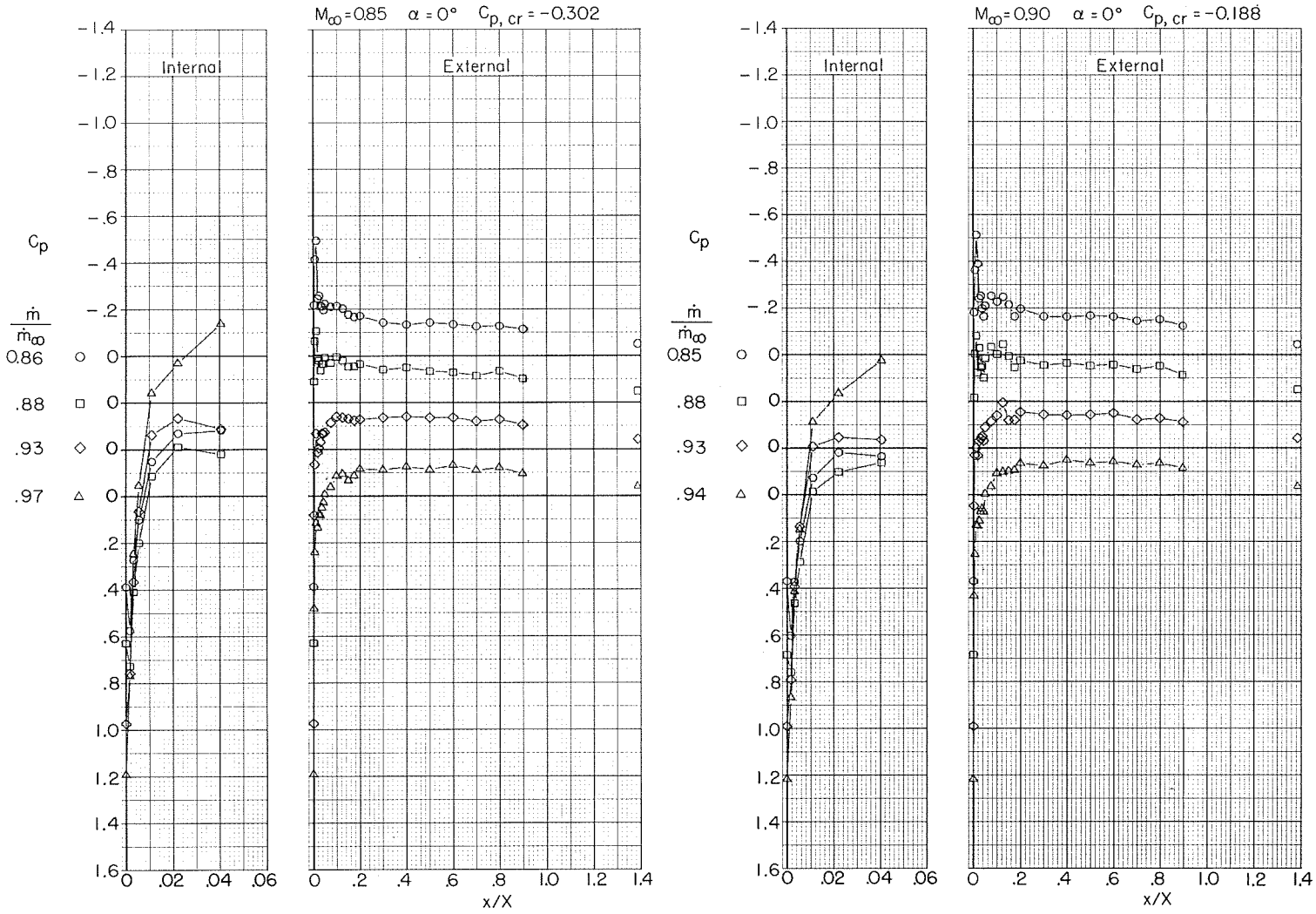

(c) M_∞ = 0.85 and 0.90.

Figure 9.- Continued.

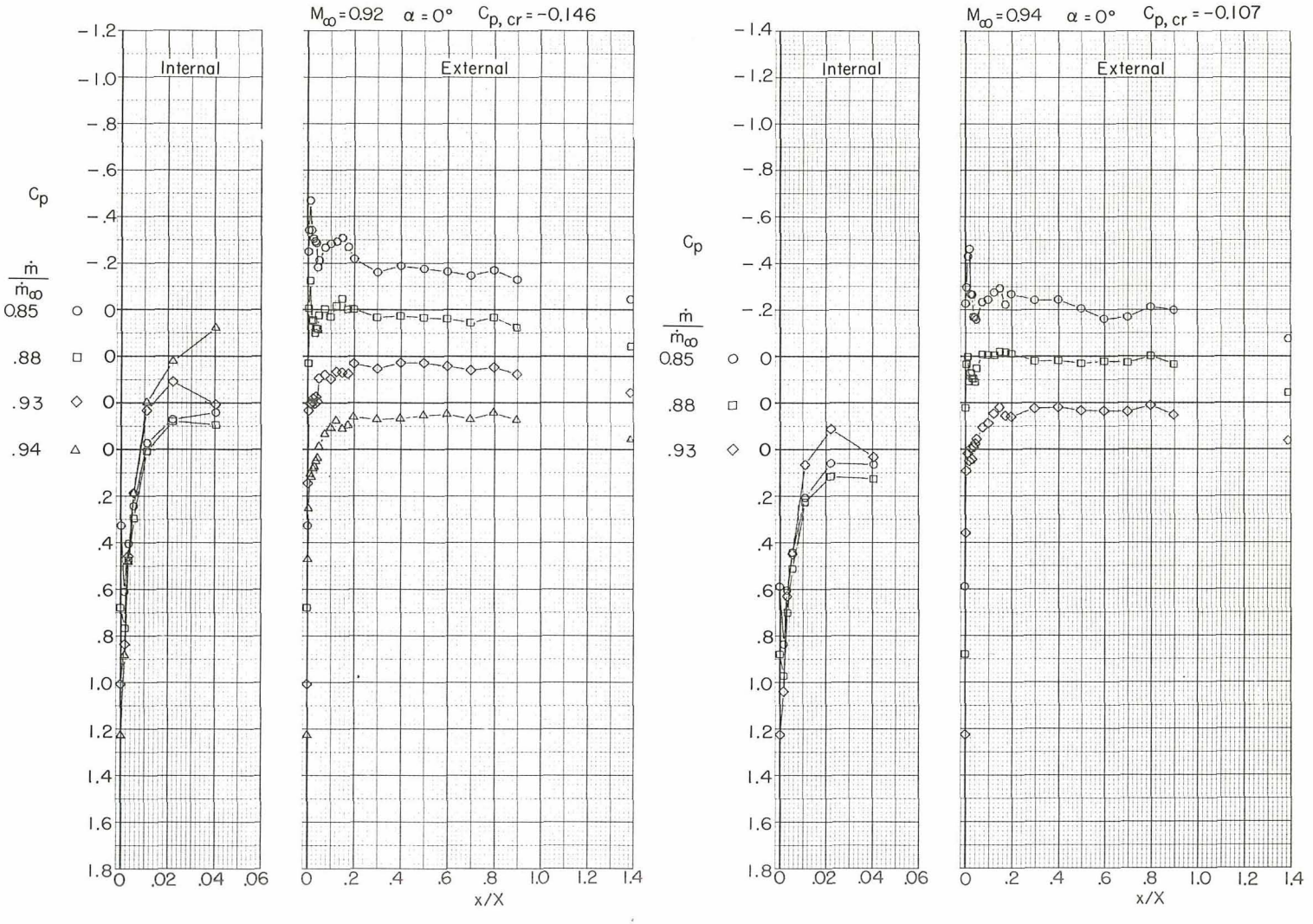

(d) $M_\infty = 0.92$ and 0.94.

Figure 9.- Continued.

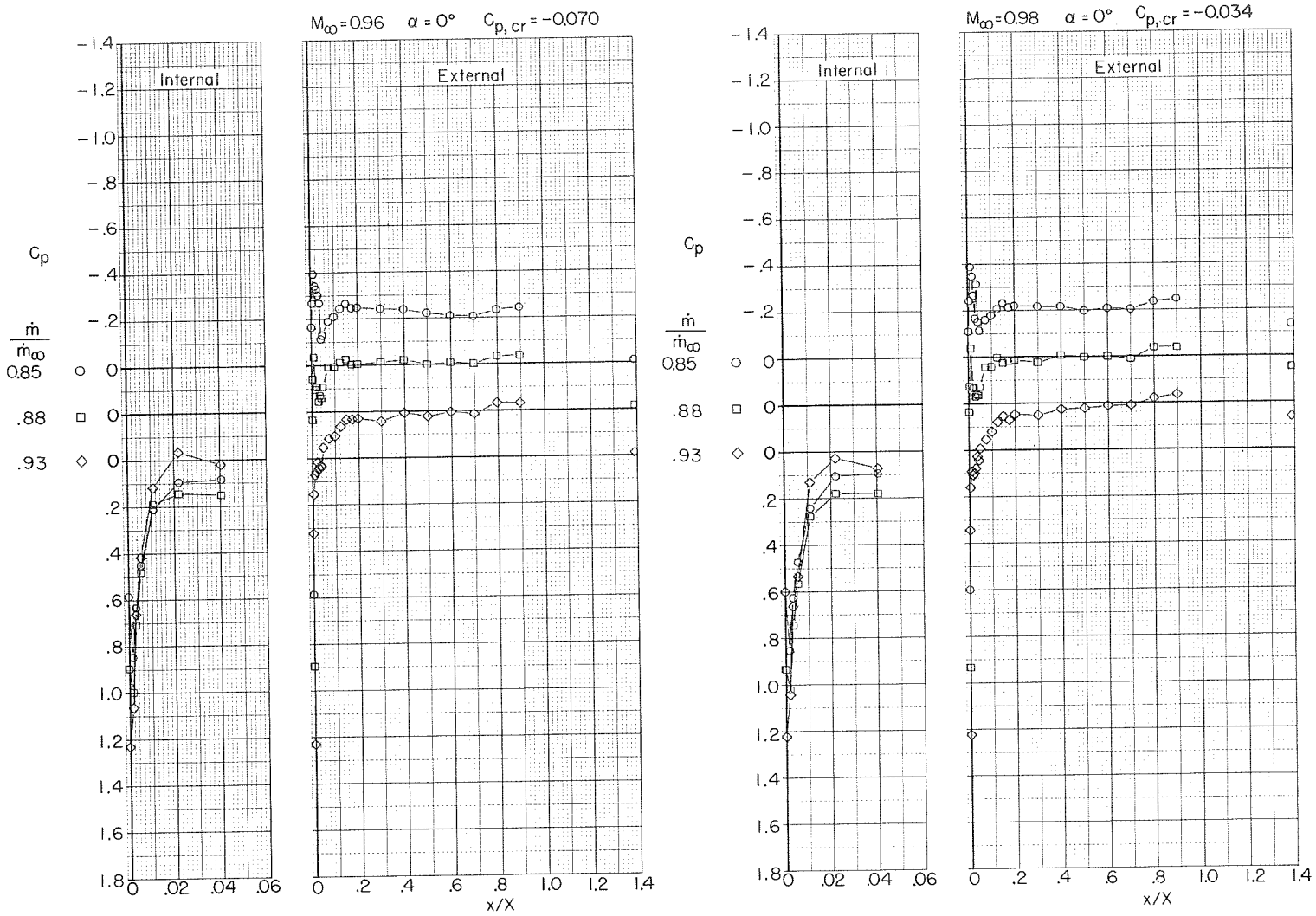

(e) M_∞ = 0.96 and 0.98.

Figure 9.- Continued.

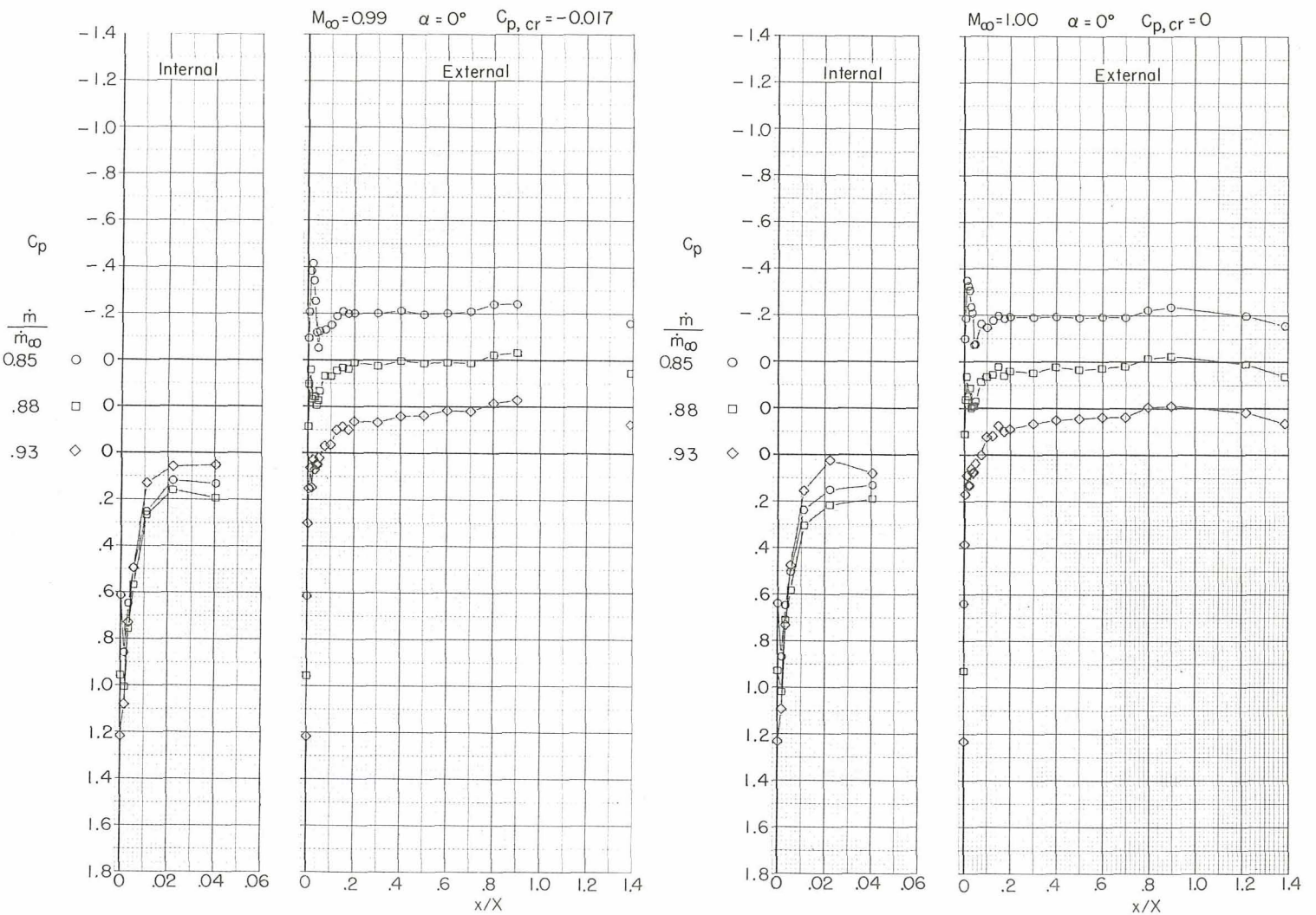

(f) M_∞ = 0.99 and 1.00.

Figure 9.- Continued.

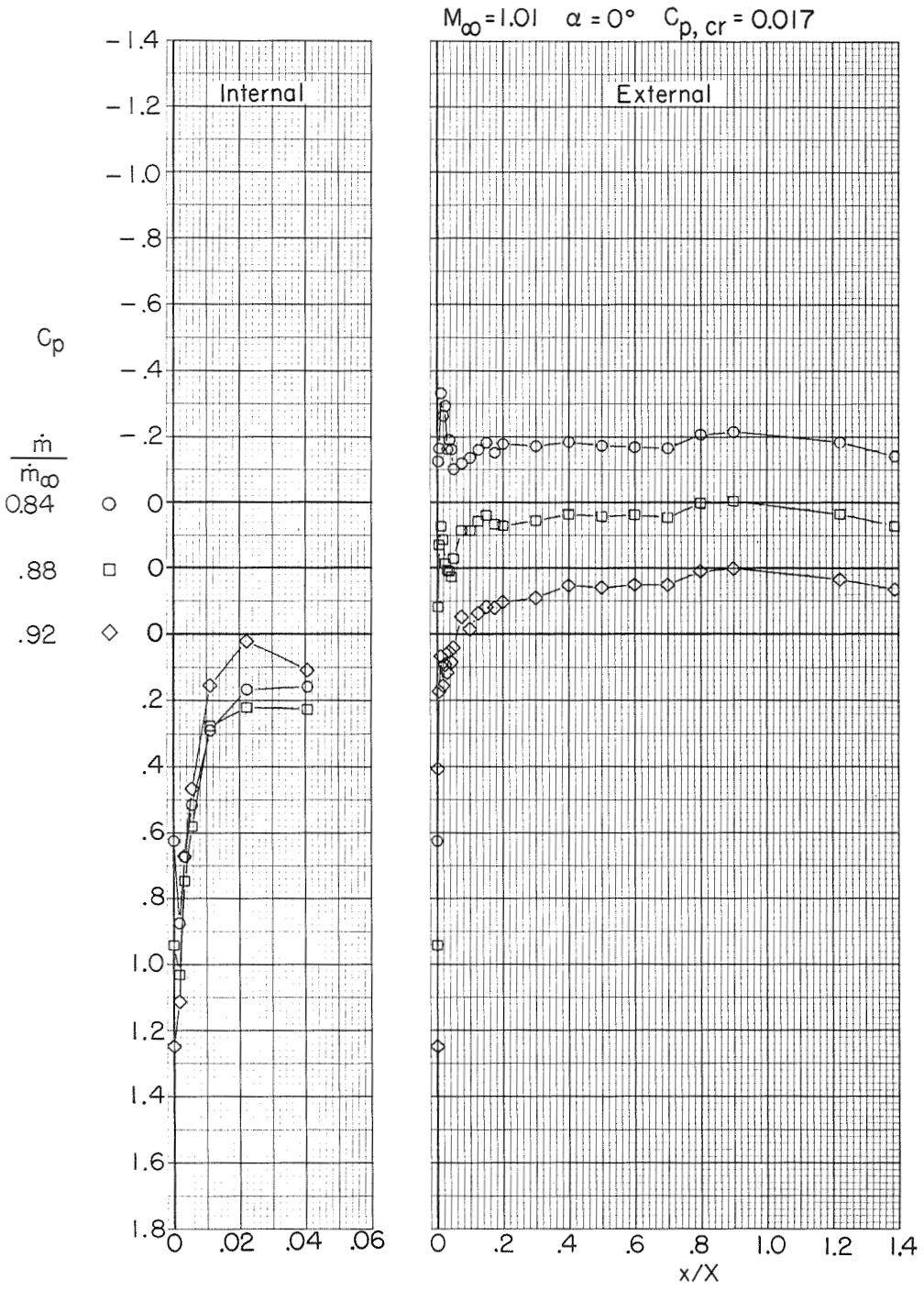

(g) $M_\infty = 1.01$.

Figure 9.- Concluded

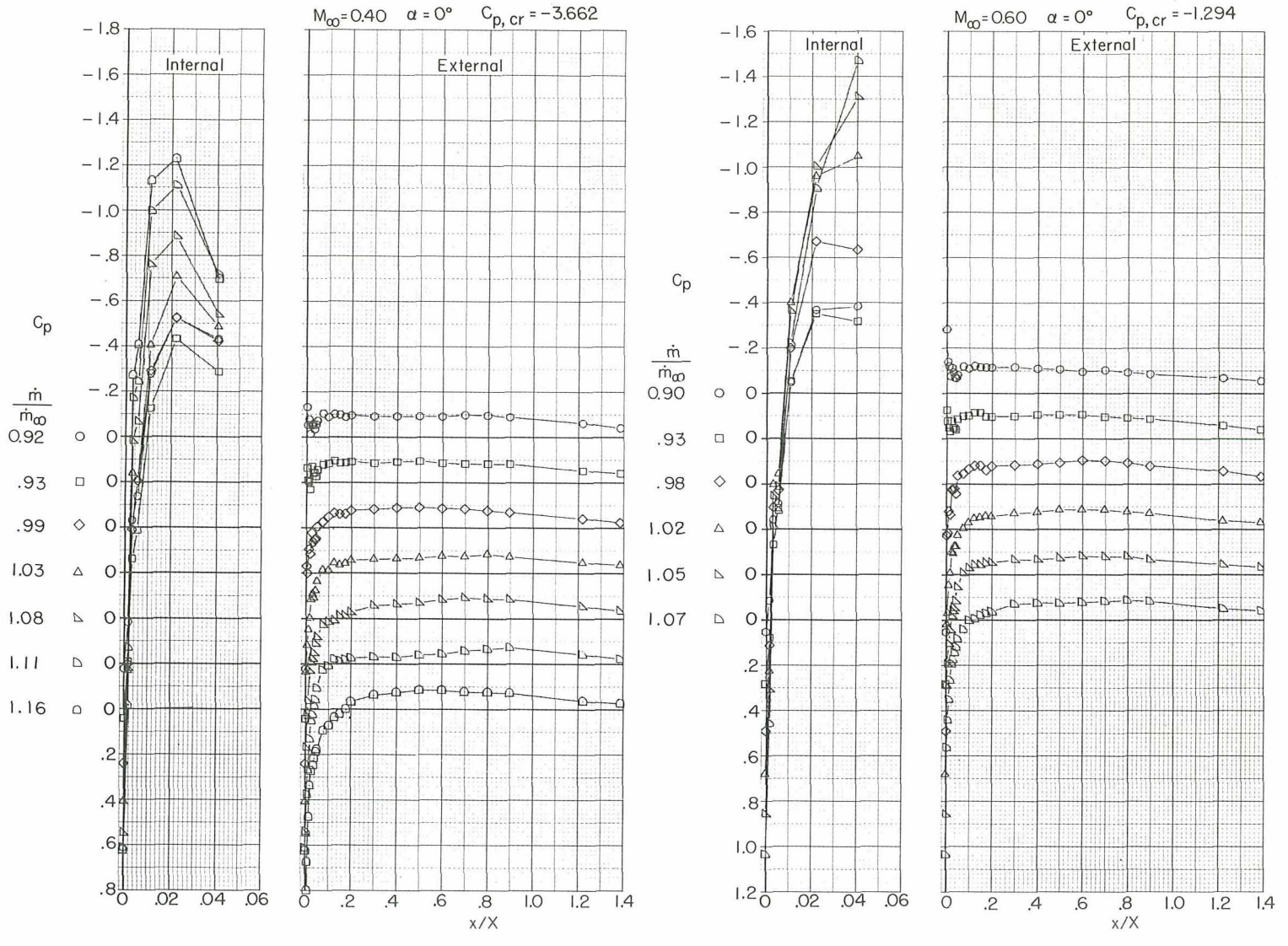

(a) M_∞ = 0.40 and 0.60.

Figure 10.- Variation with length of local pressure coefficient of NACA 1-85-100 inlet (lip radius 0.084 cm, contraction ratio 1.093).

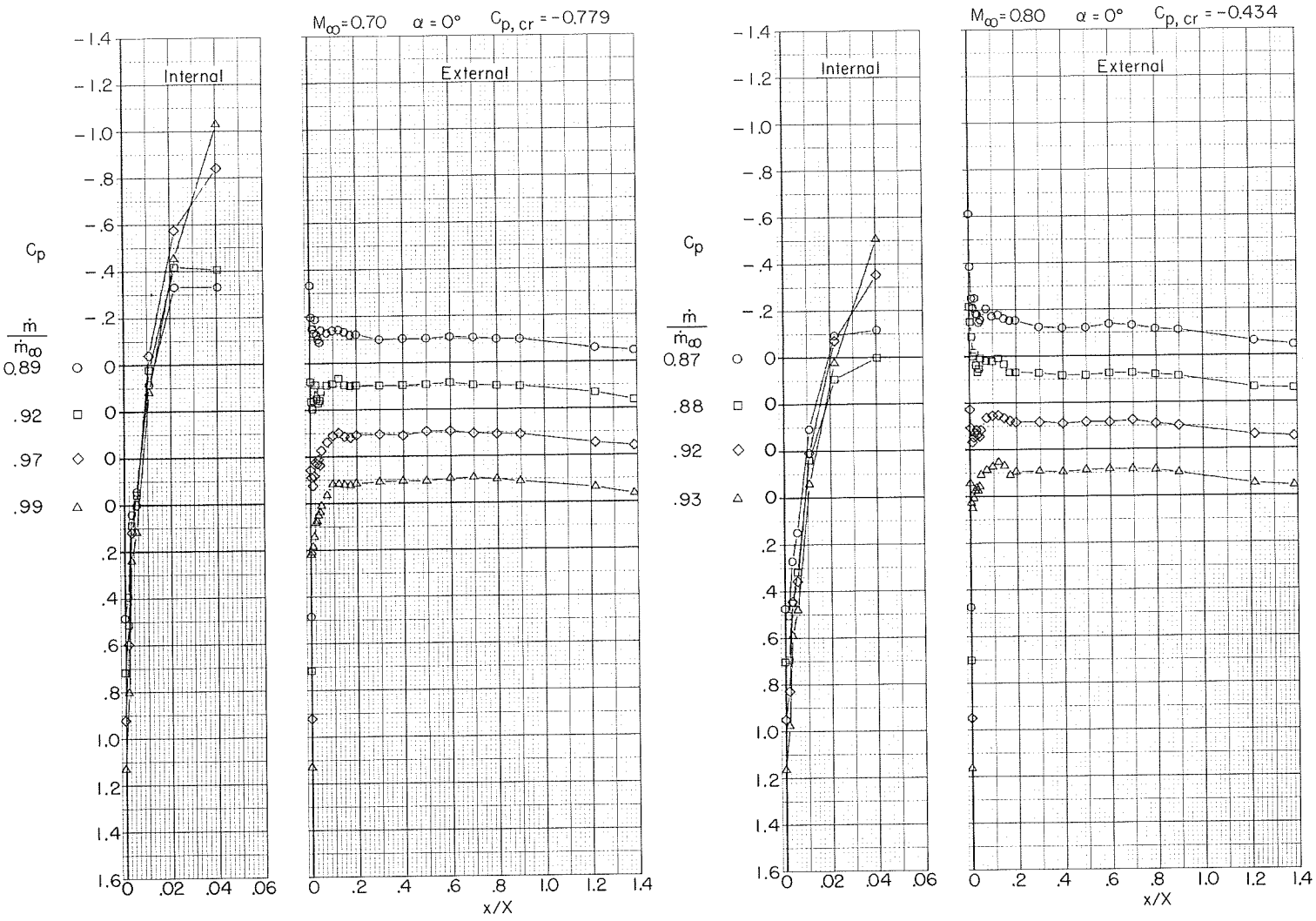

(b) M_∞ = 0.70 and 0.80.

Figure 10.- Continued.

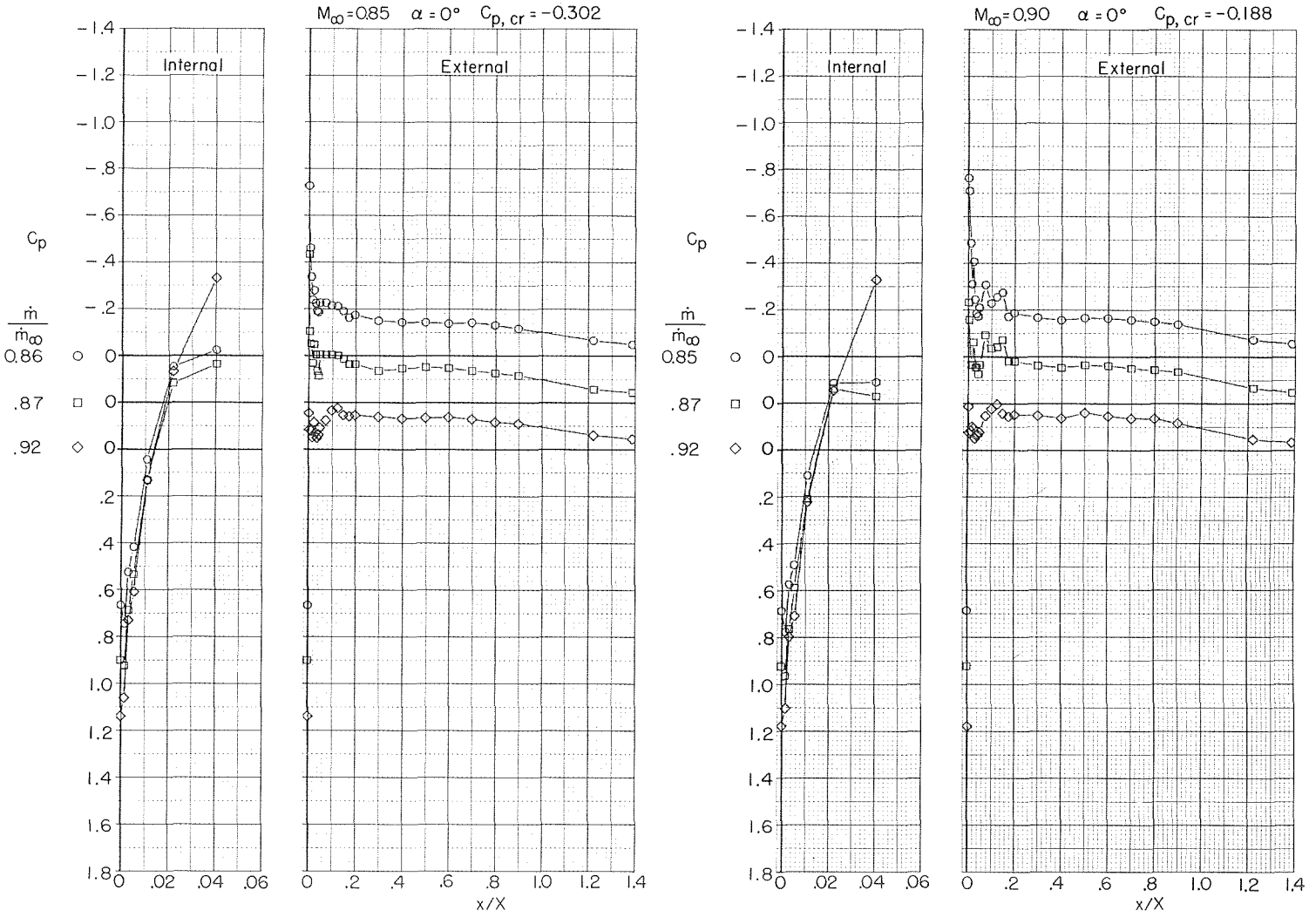

(c) M_∞ = 0.85 and 0.90.

Figure 10.- Continued.

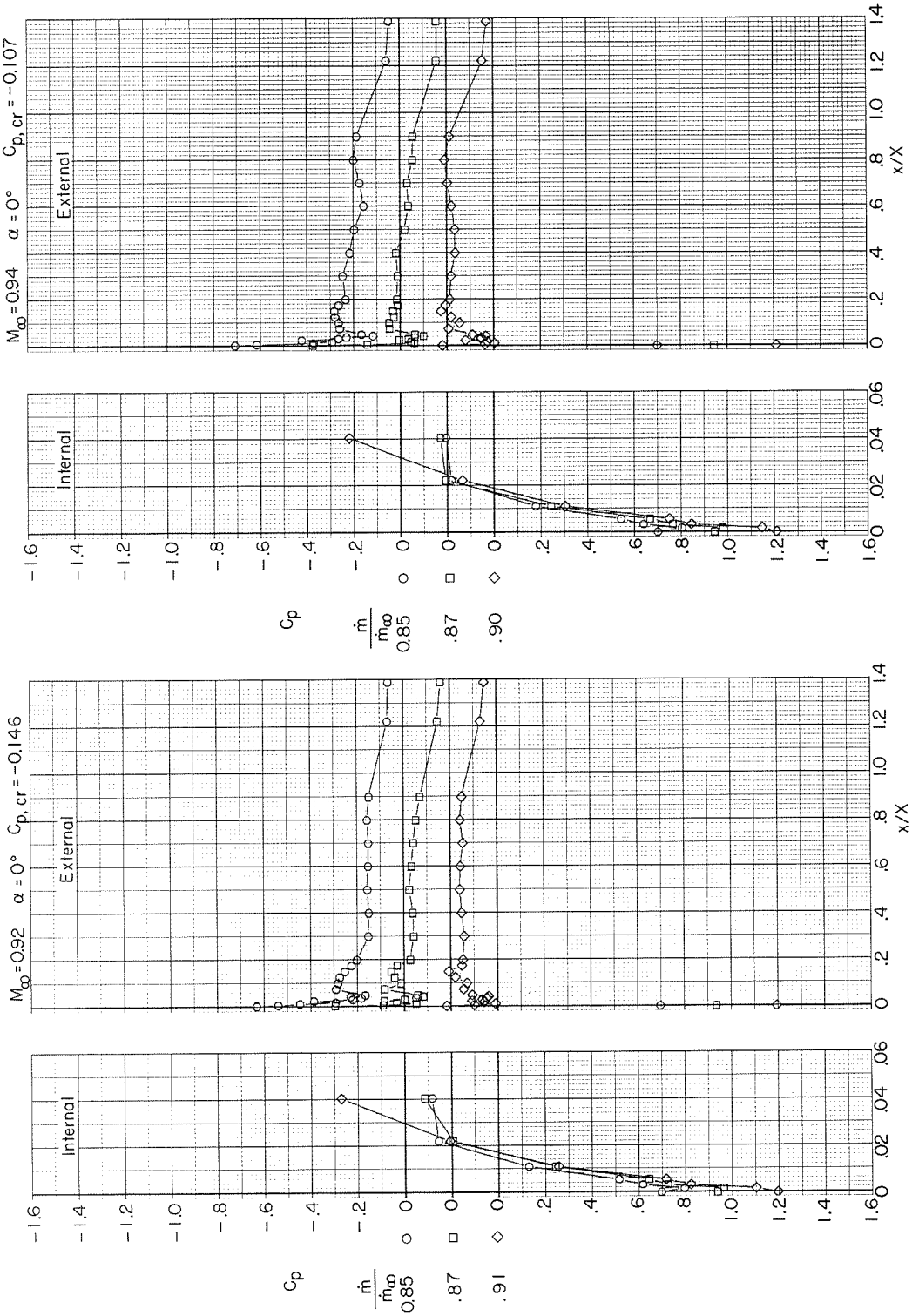

(d) M_∞ = 0.92 and 0.94.

Figure 10.- Continued.

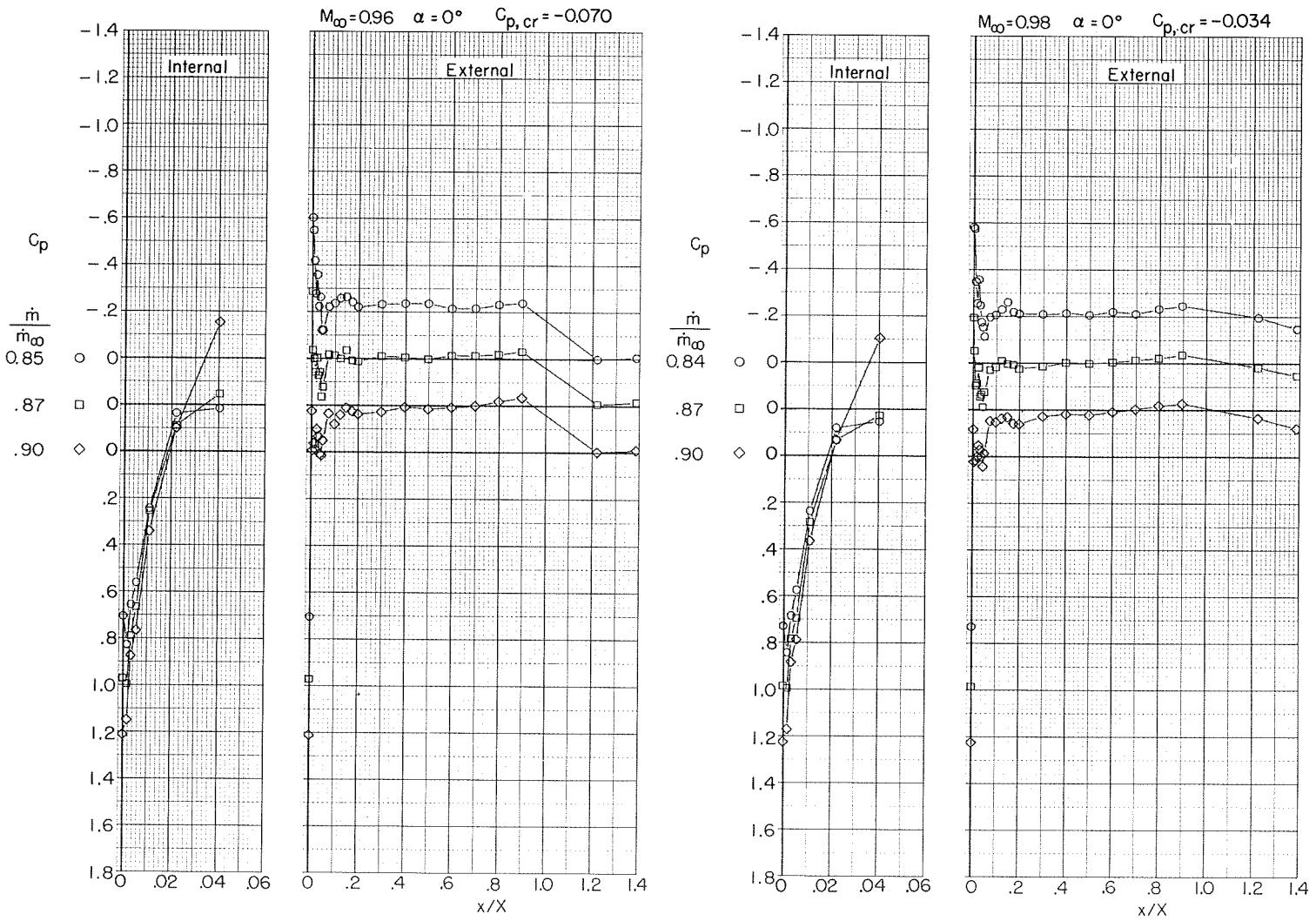

(e) M_∞ = 0.96 and 0.98.

Figure 10.- Continued.

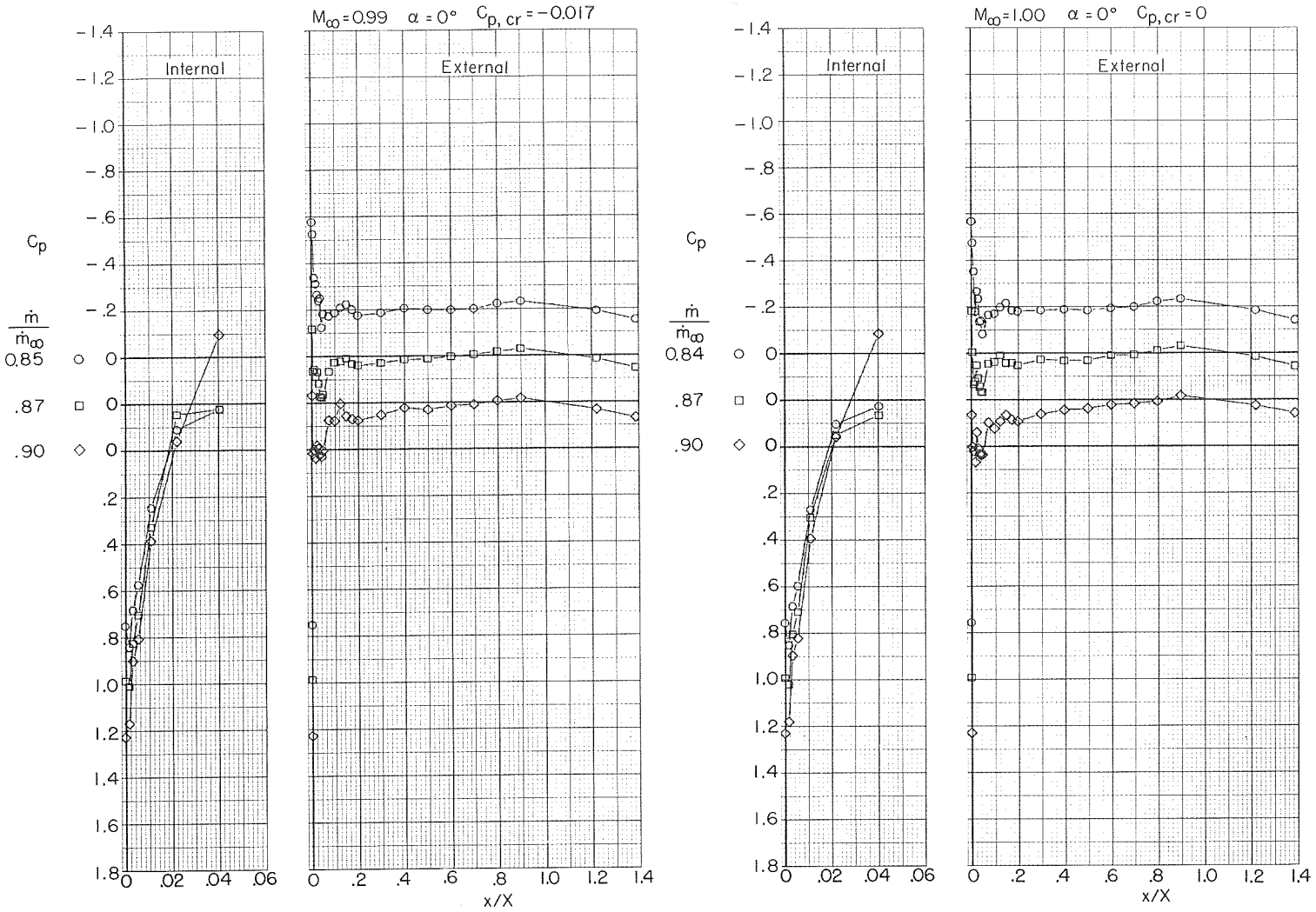

(f) M_∞ = 0.99 and 1.00.

Figure 10.- Continued.

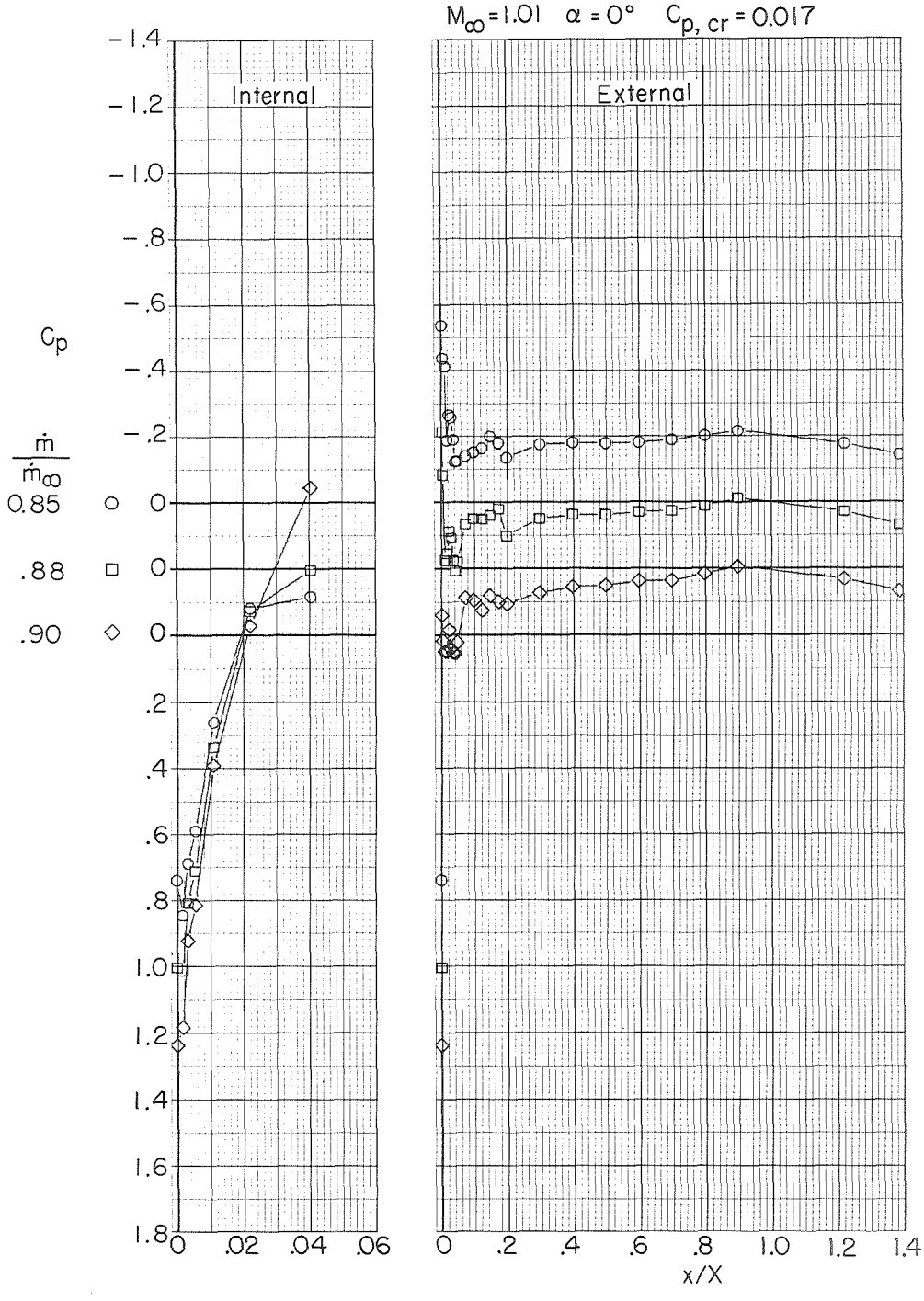

(g) $M_\infty = 1.01$.

Figure 10.- Concluded.

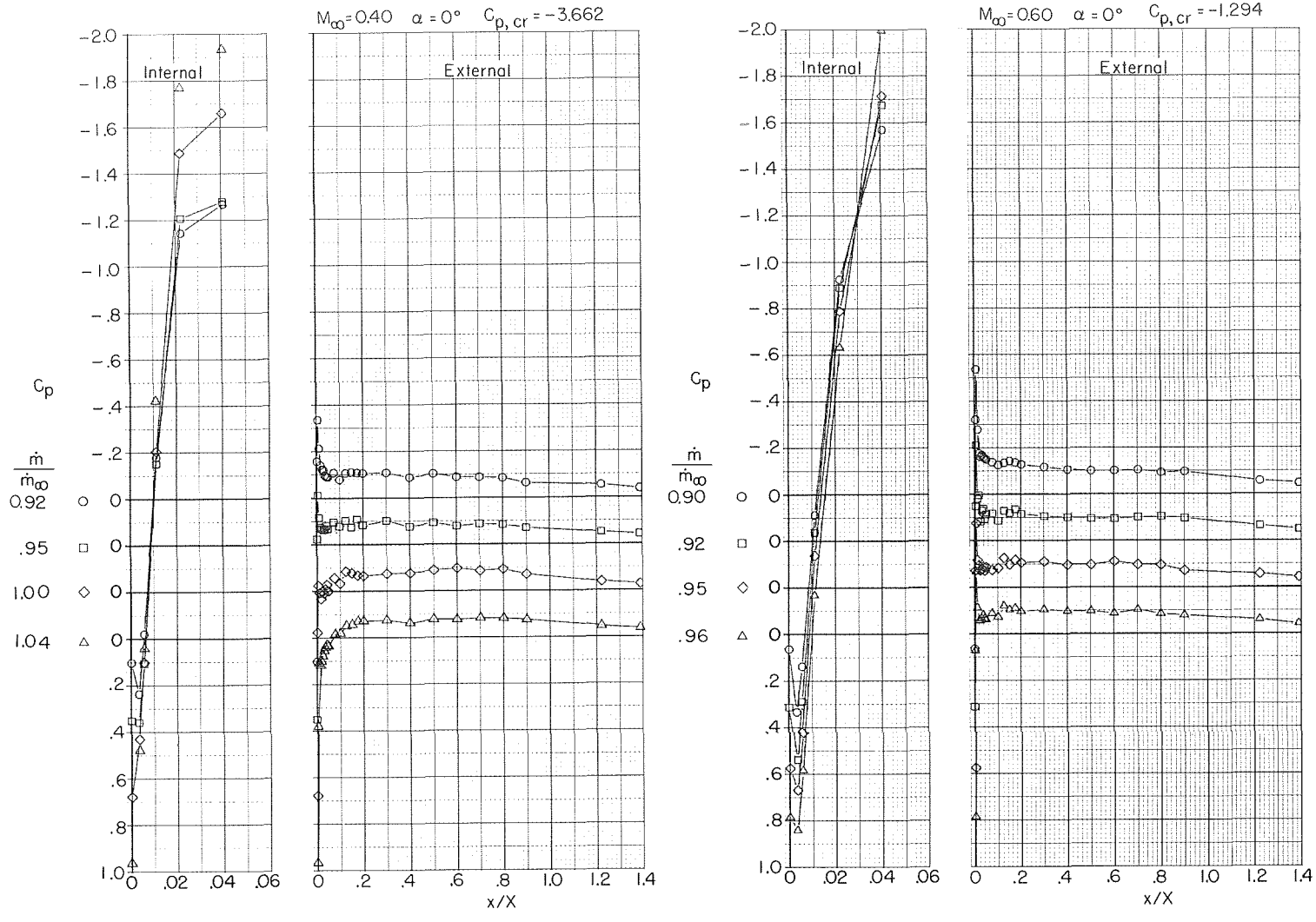

(a) M_∞ = 0.40 and 0.60.

Figure 11.- Variation with length of local pressure coefficient of NACA 1-85-100 inlet (lip radius 0.084 cm, contraction ratio 1.201).

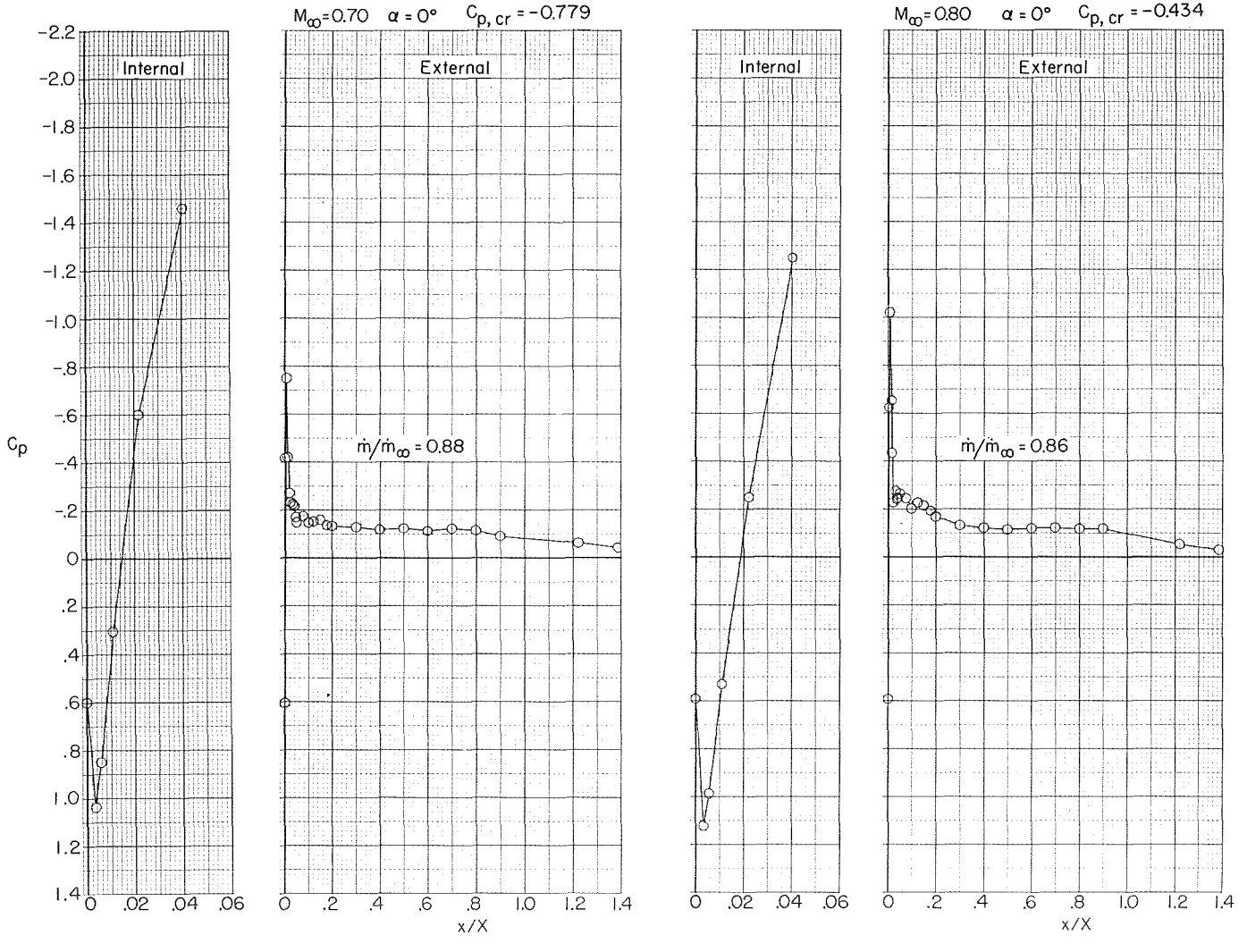

(b) M_∞ = 0.70 and 0.80.

Figure 11.- Continued.

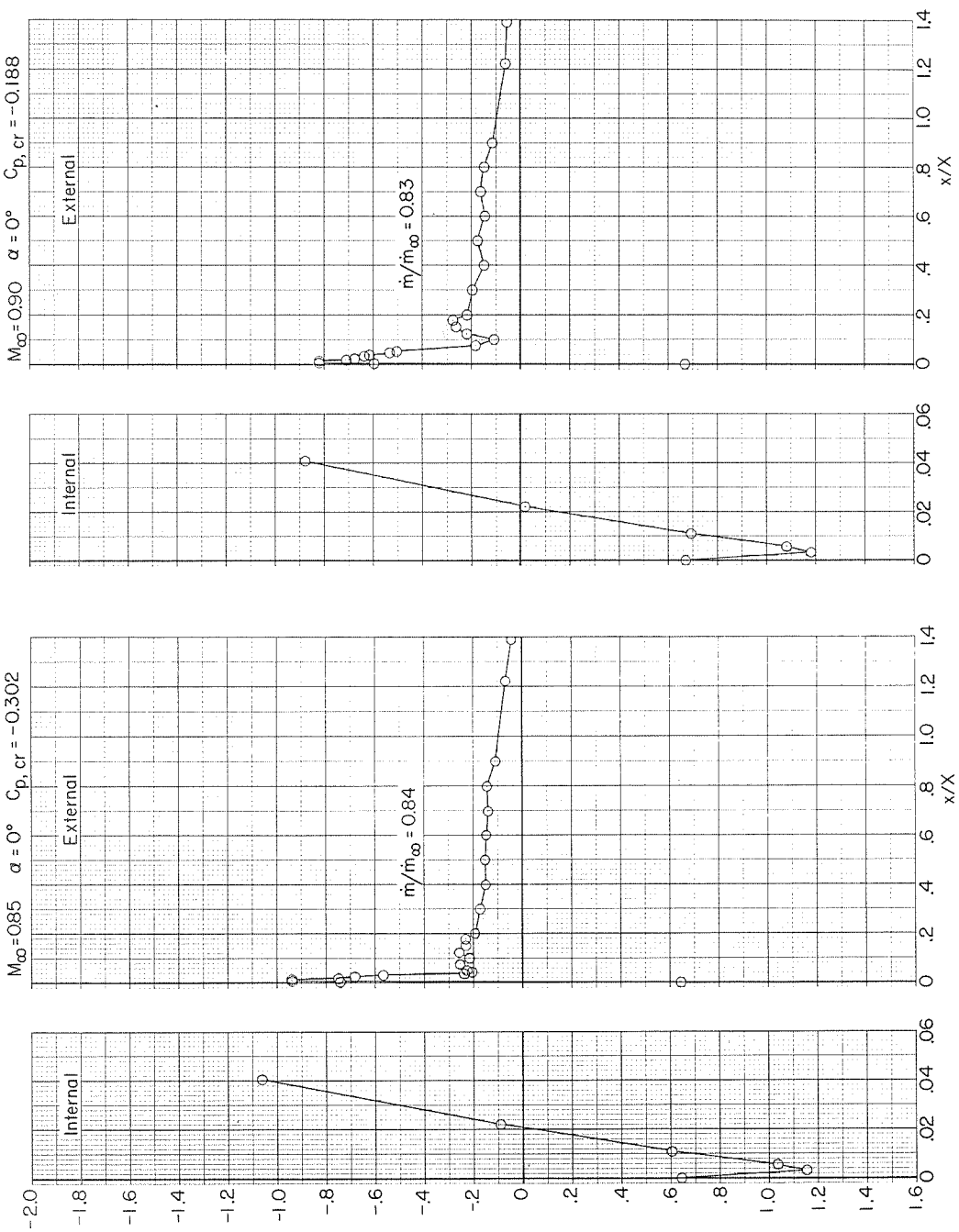

(c) M_∞ = 0.85 and 0.90.

Figure 11.- Continued.

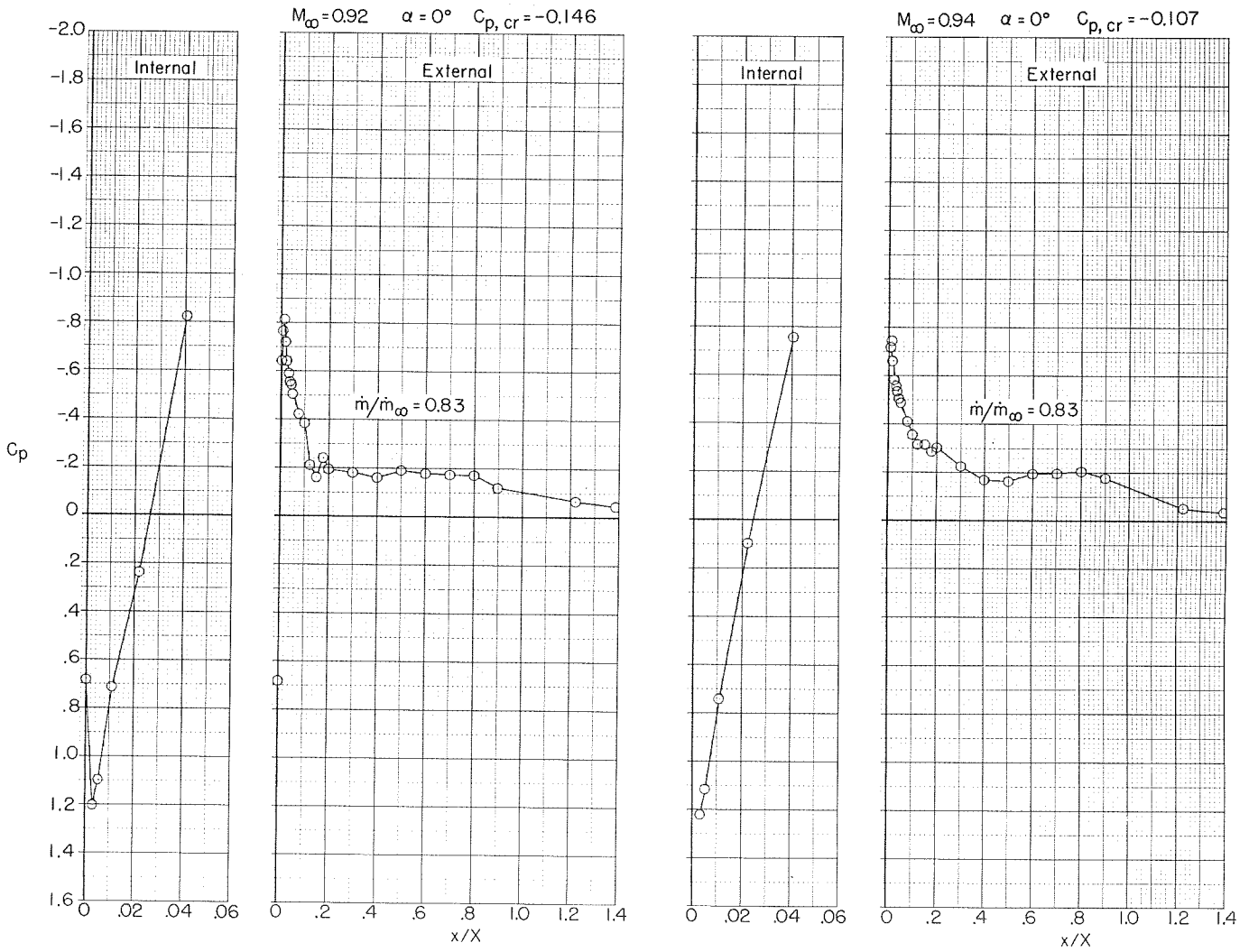

(d) $M_\infty = 0.92$ and 0.94.

Figure 11.- Continued.

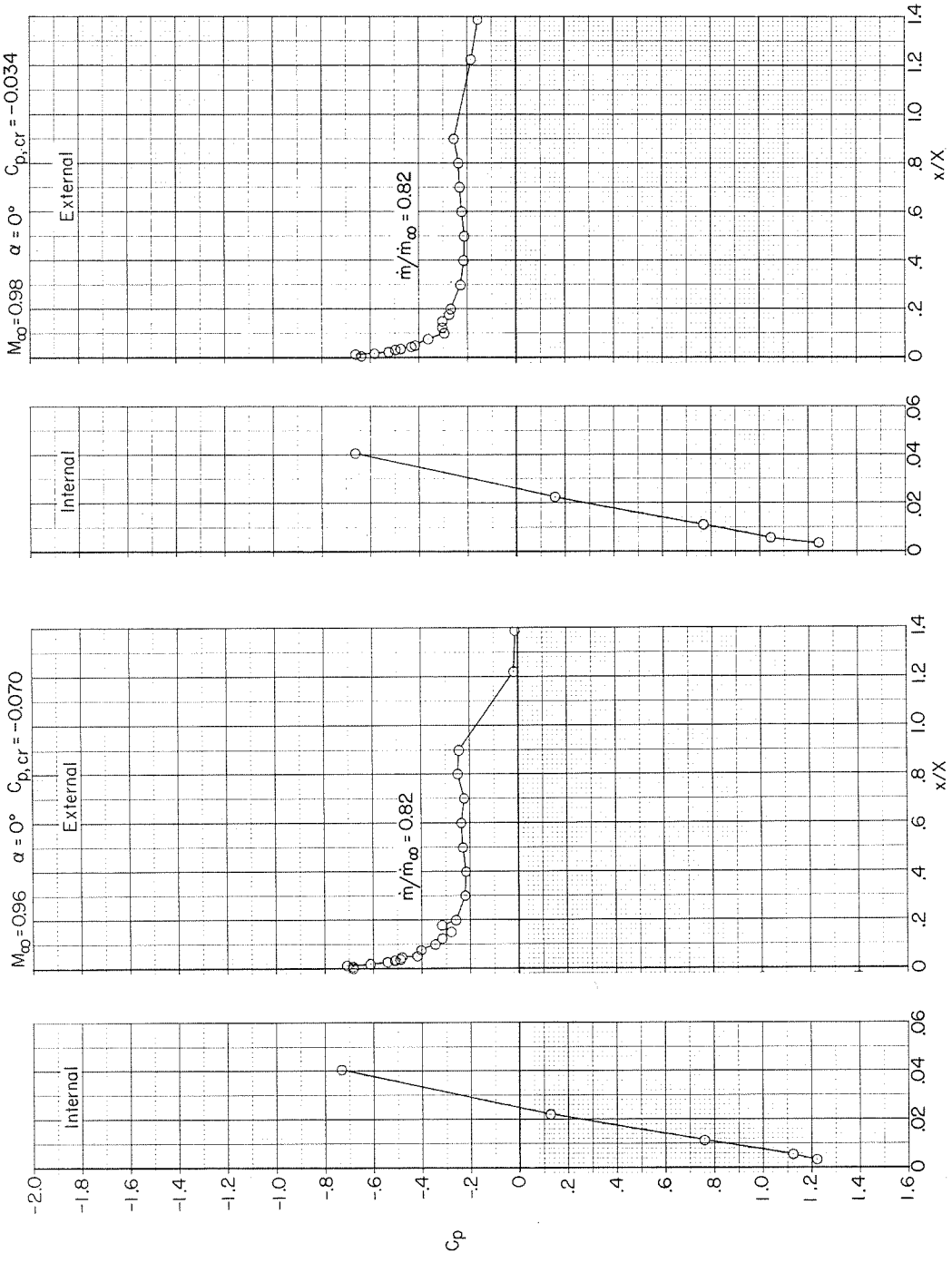

(e) M_∞ = 0.96 and 0.98.

Figure 11.- Continued.

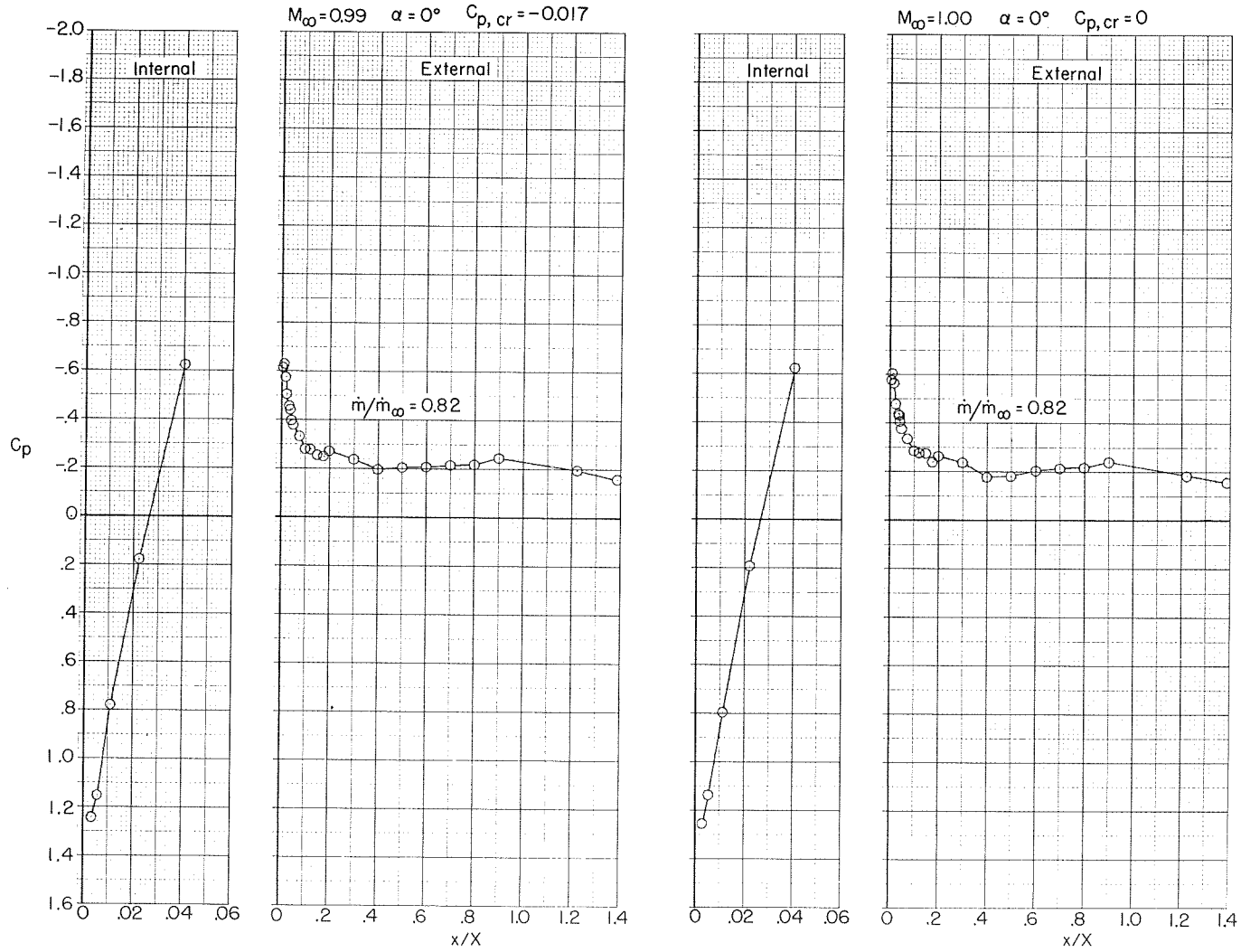

(f) M_∞ = 0.99 and 1.00.

Figure 11.- Continued.

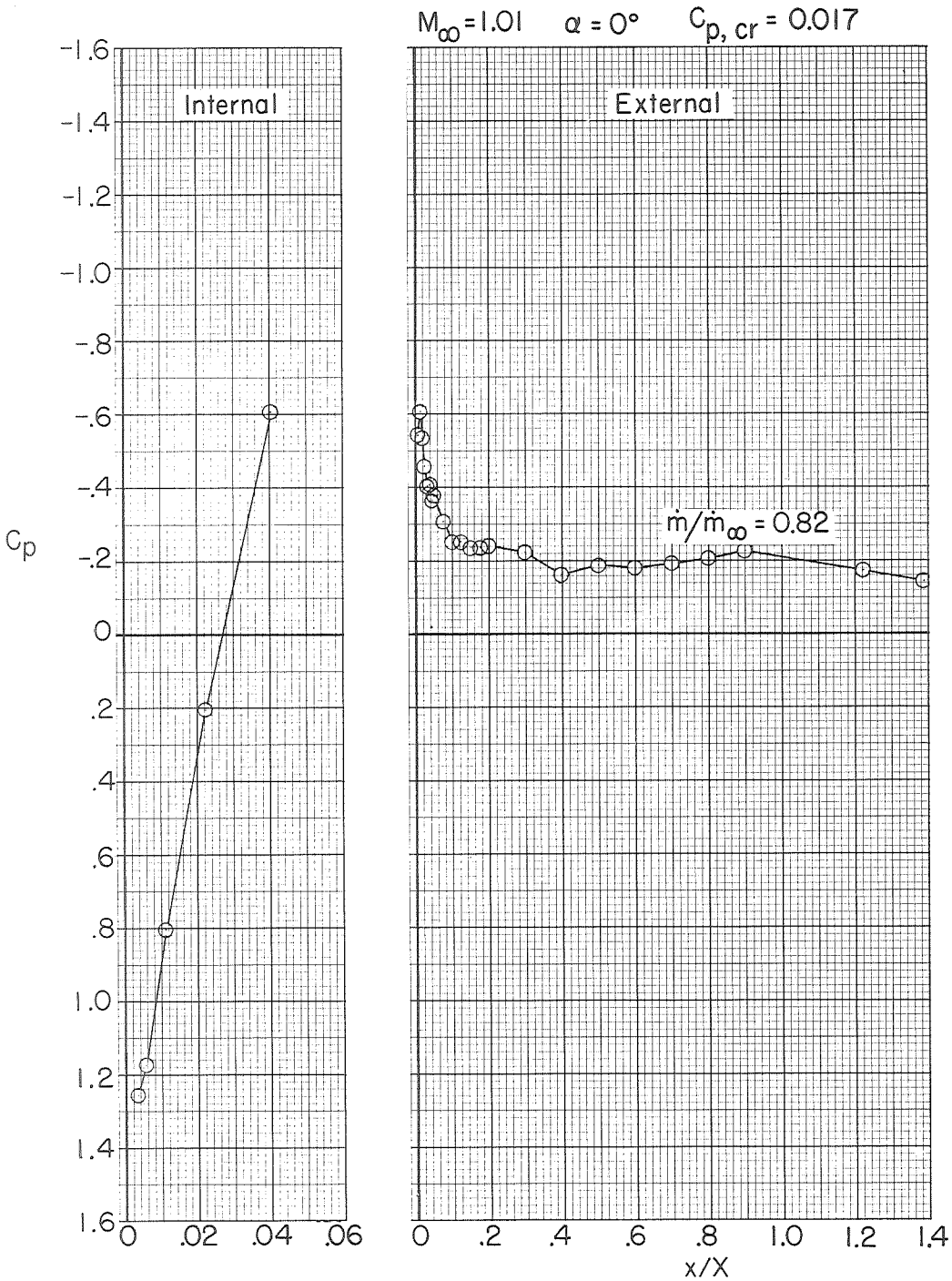

(g) $M_\infty = 1.01$.

Figure 11.- Concluded.

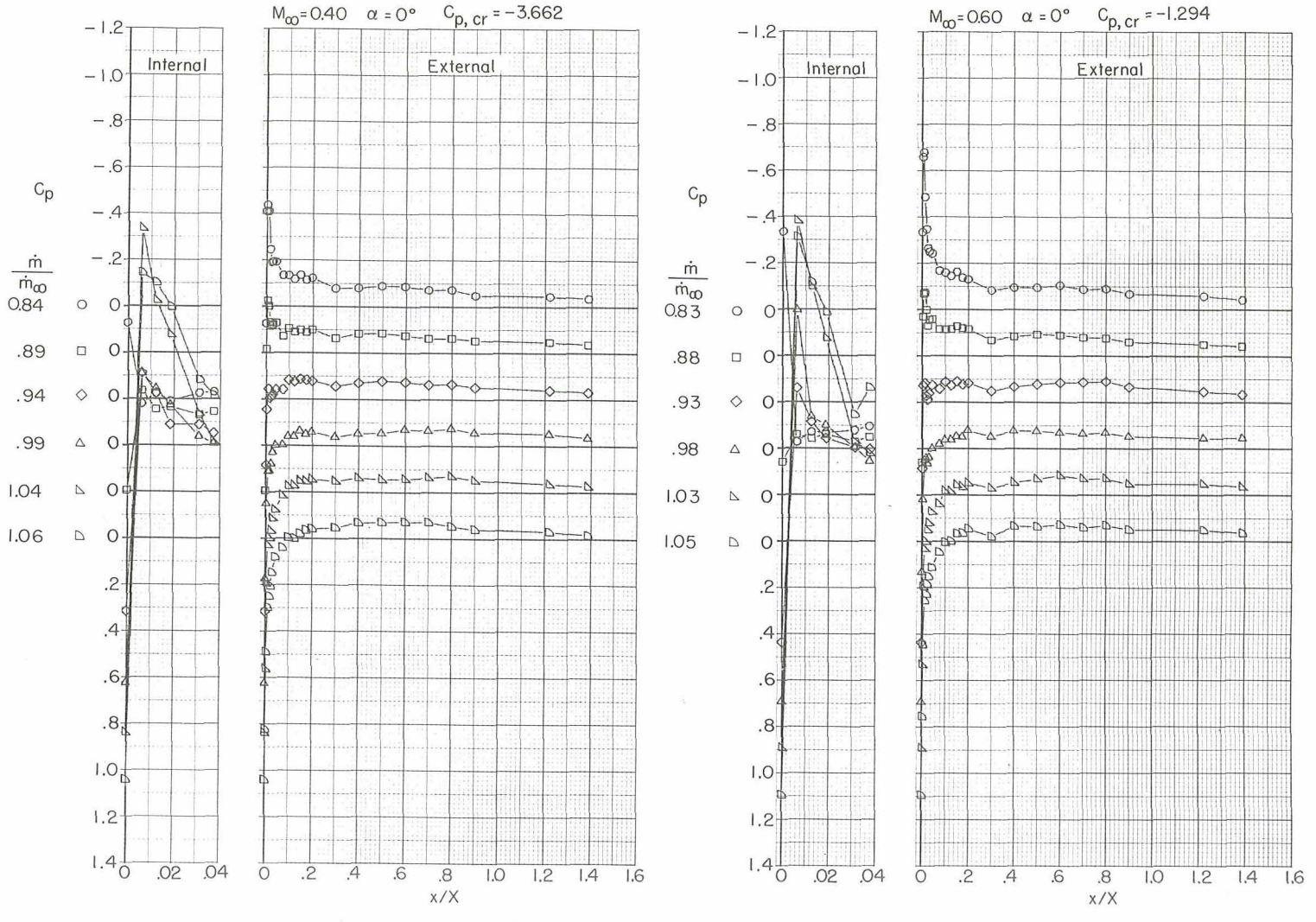

(a) M_∞ = 0.40 and 0.60.

Figure 12.- Variation with length of local pressure coefficient of NACA 1-89-100 inlet (lip radius 0.061 cm, contraction ratio 1.006).

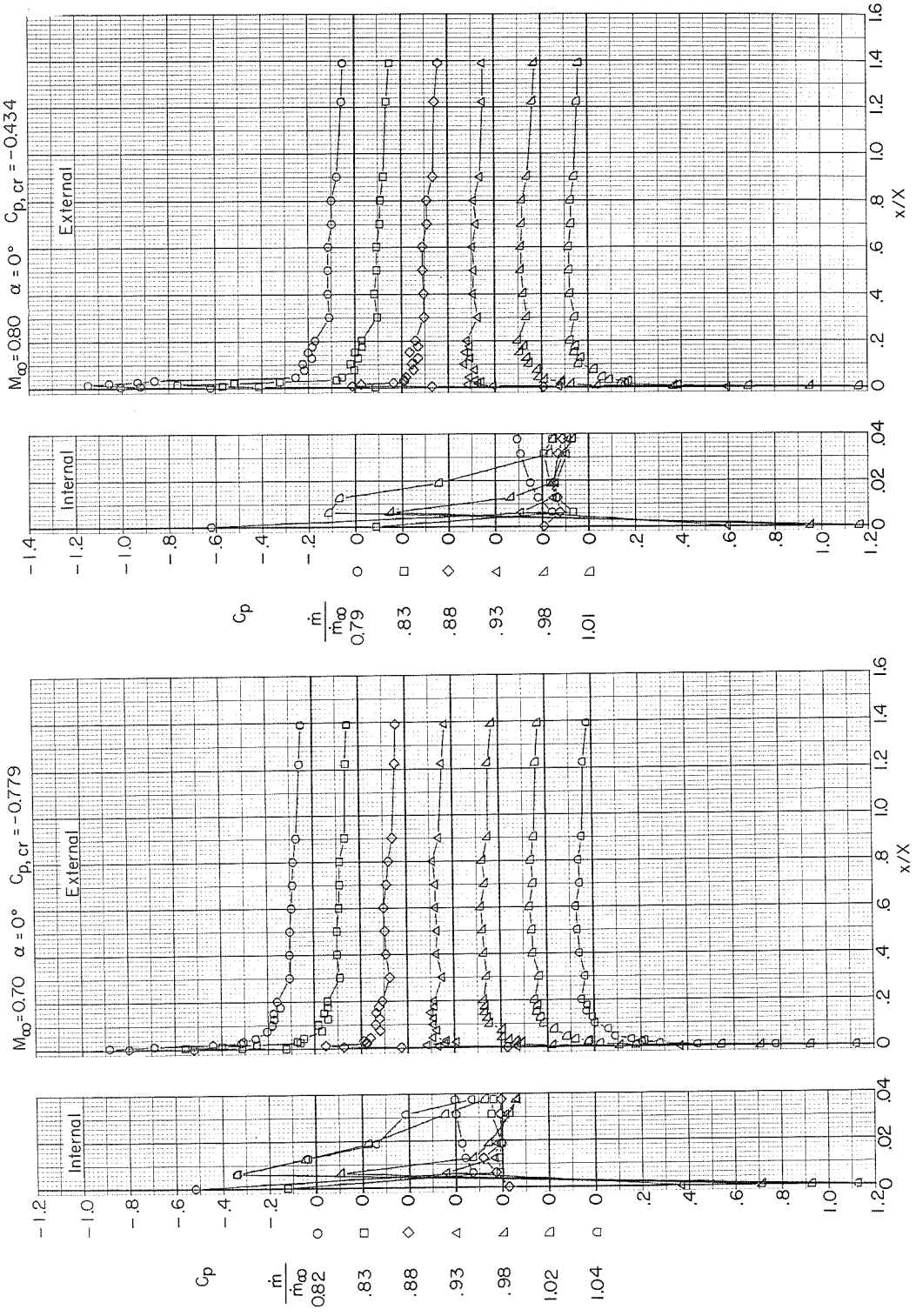

(b) M_∞ = 0.70 and 0.80.

Figure 12.- Continued.

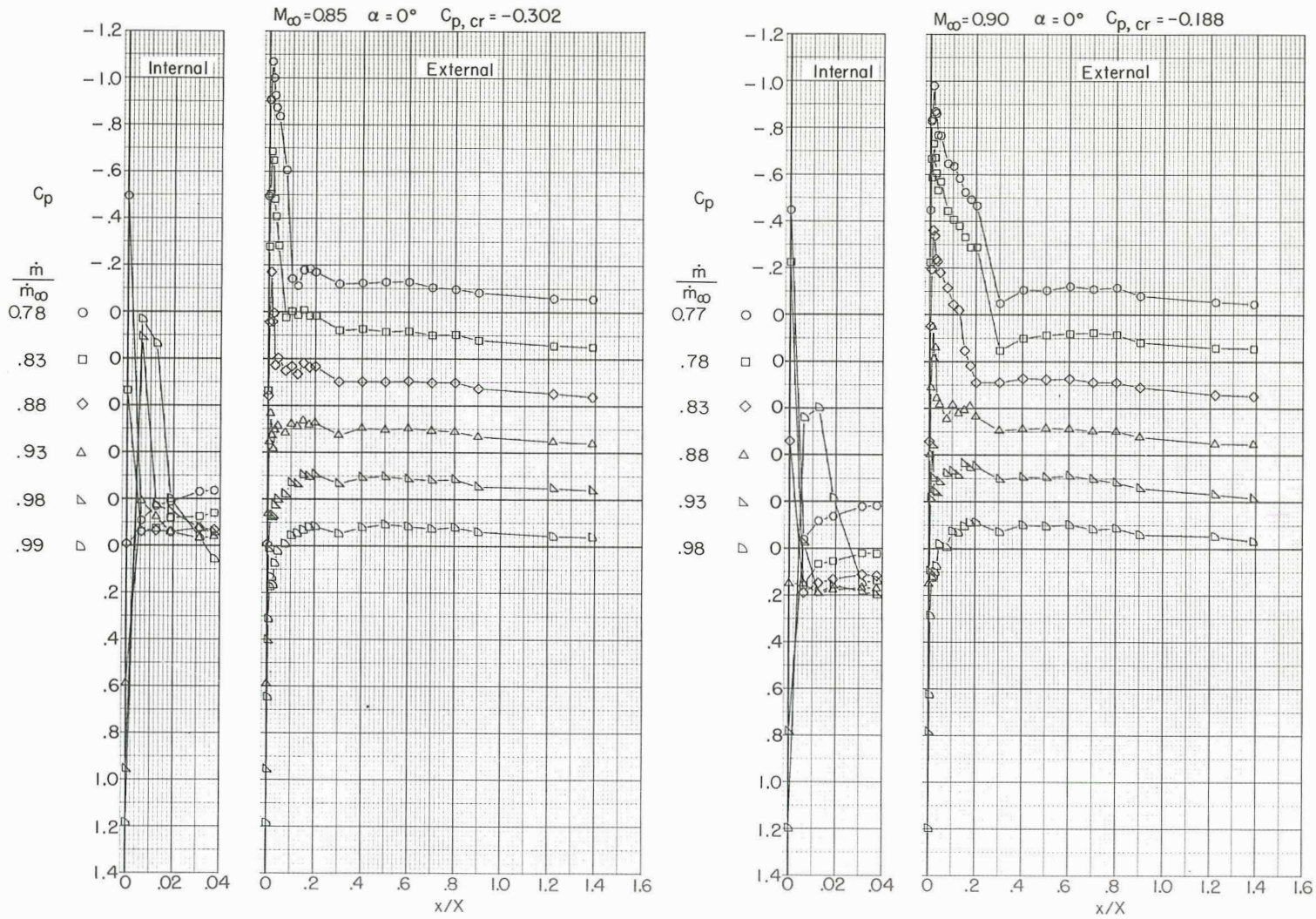

(c) M_∞ = .0.85 and 0.90.

Figure 12.- Continued.

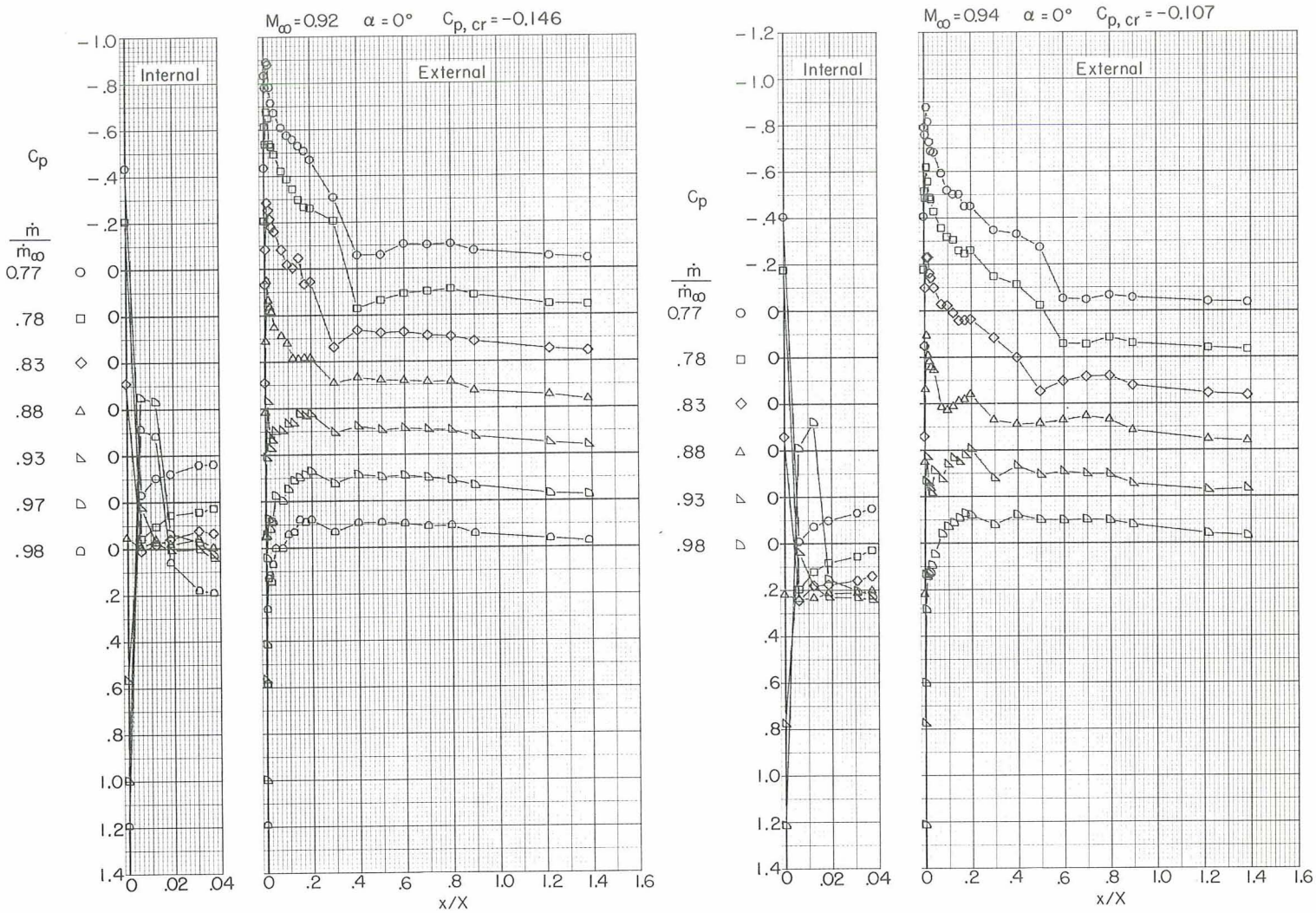

(d) M_∞ = 0.92 and 0.94.

Figure 12.- Continued.

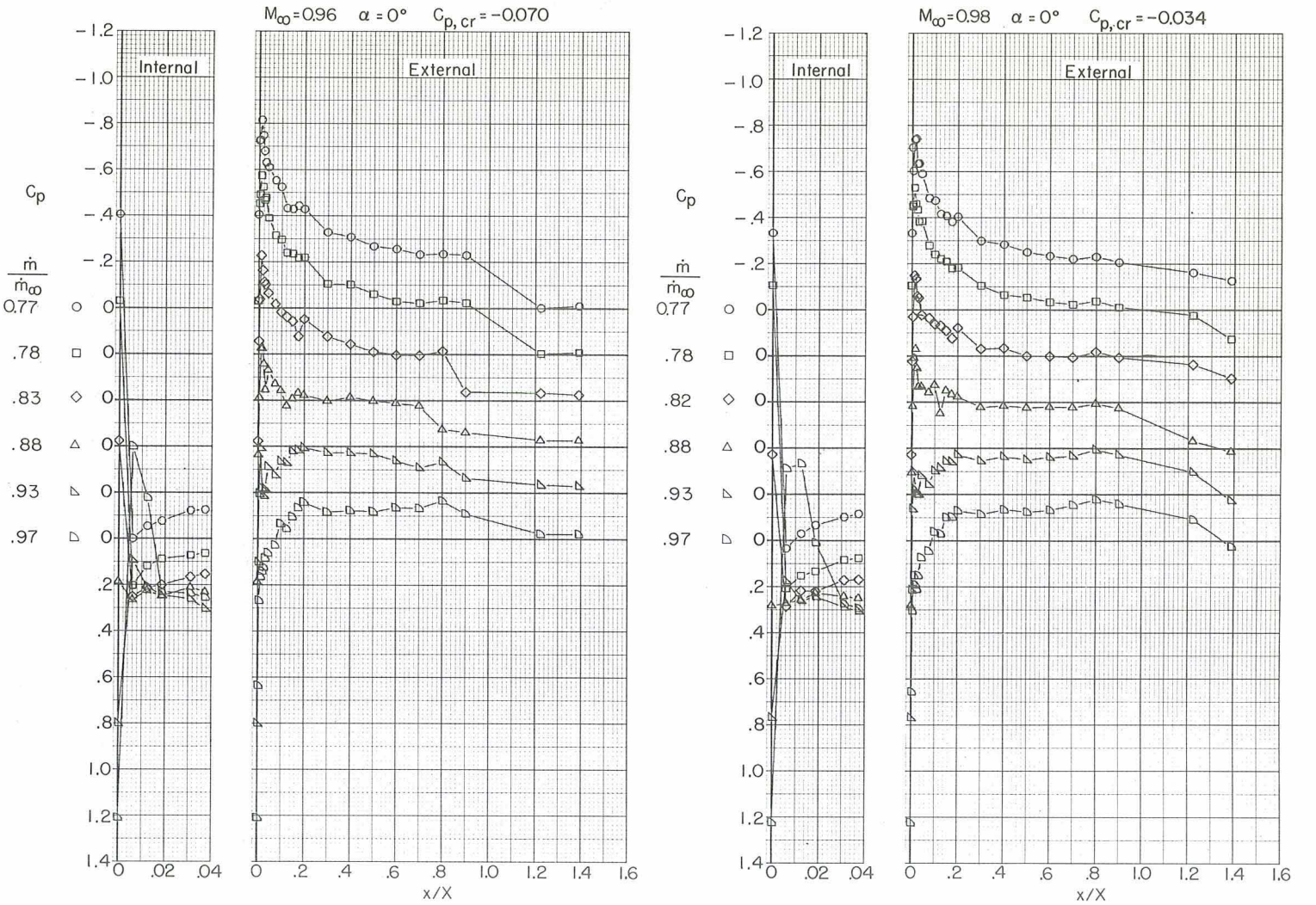

(e) M_∞ = 0.96 and 0.98.

Figure 12.- Continued.

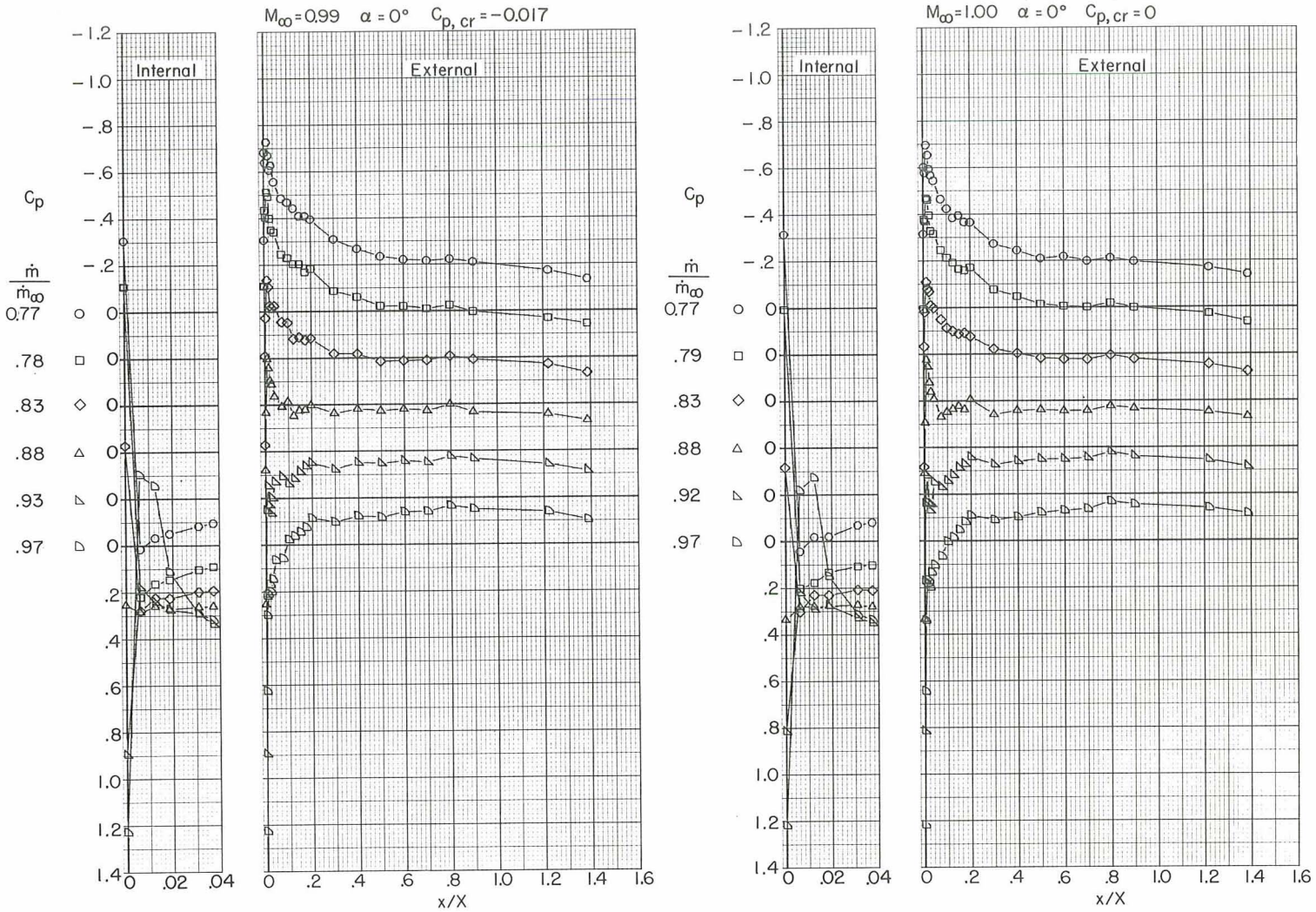

(f) M_∞ = 0.99 and 1.00.

Figure 12.- Continued.

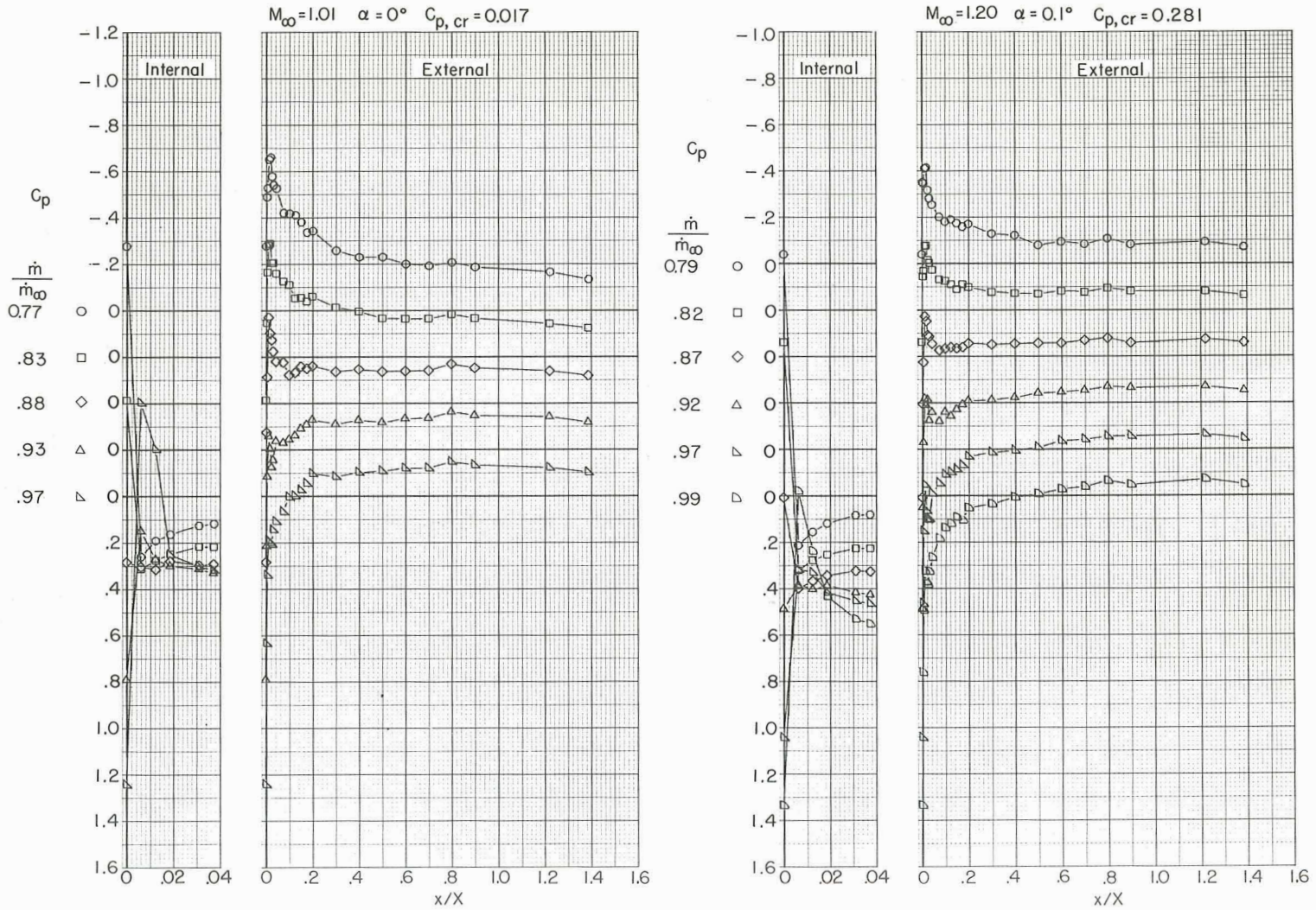

(g) M_∞ = 1.01 and 1.20.

Figure 12.- Continued.

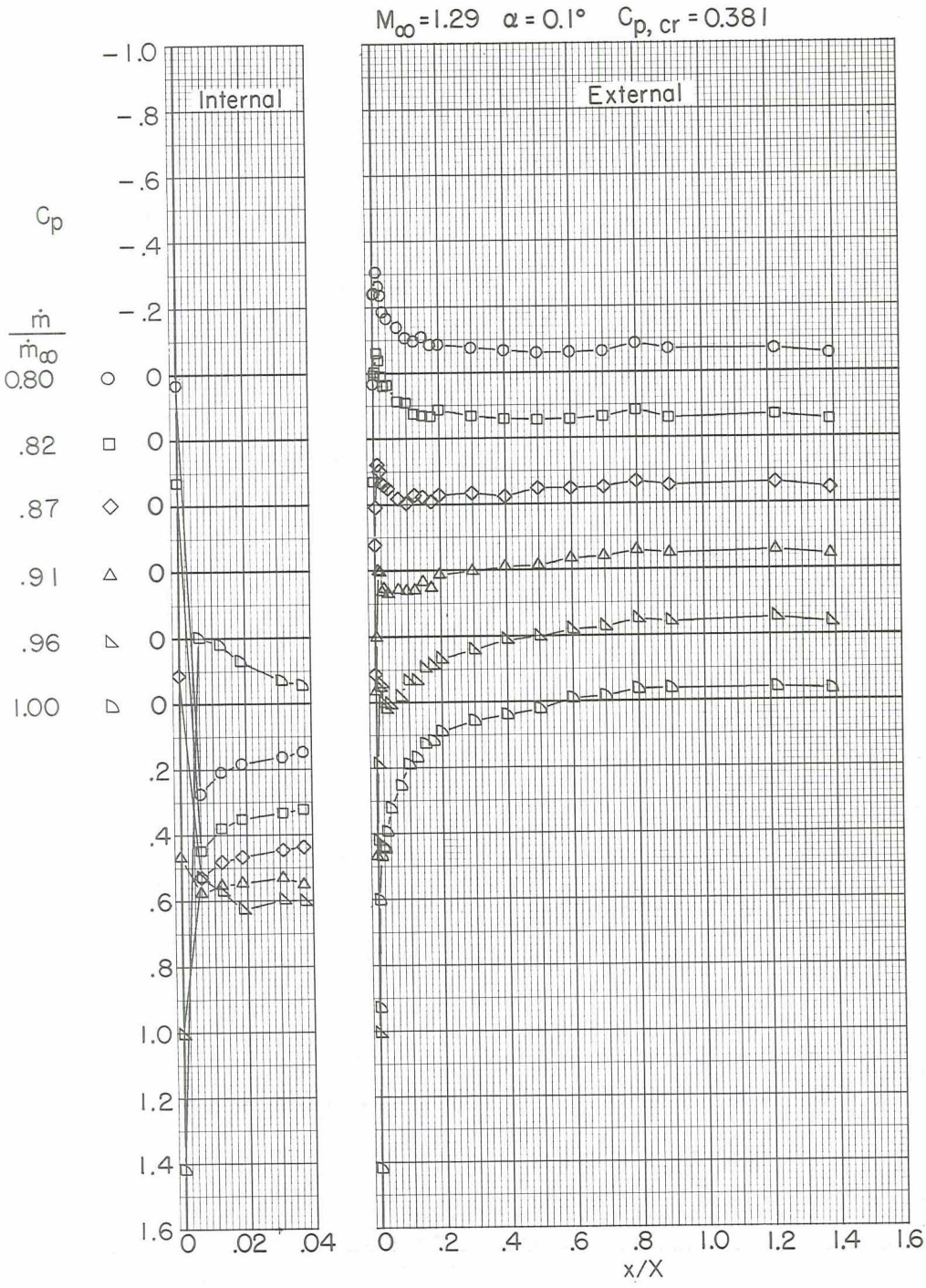

(h) $M_\infty = 1.29$.

Figure 12.- Concluded.

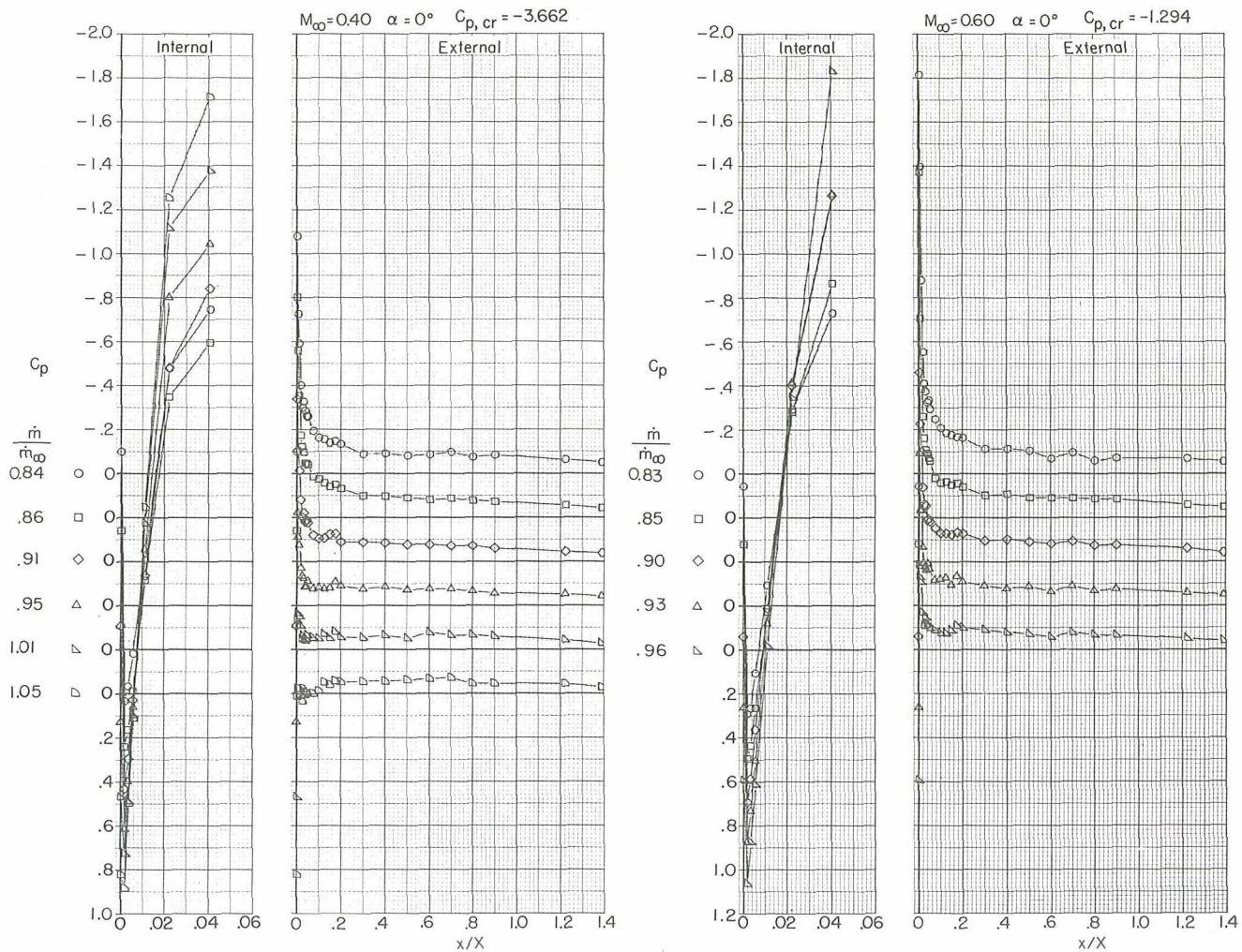

(a) M_∞ = 0.40 and 0.60.

Figure 13.- Variation with length of local pressure coefficient of NACA 1-89-100 inlet (lip radius 0.061 cm, contraction ratio 1.195).

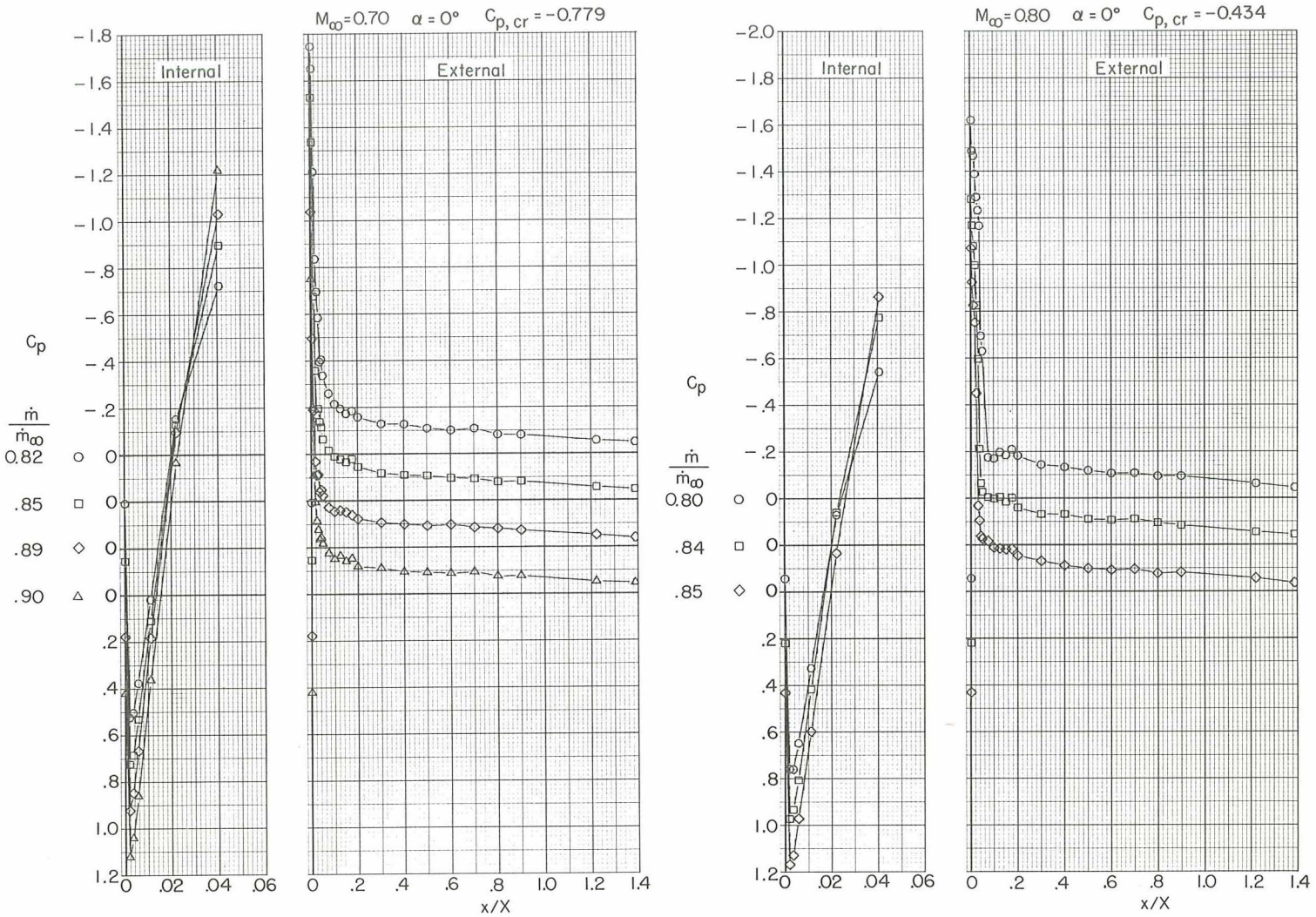

(b) M_∞ = 0.70 and 0.80.

Figure 13.- Continued.

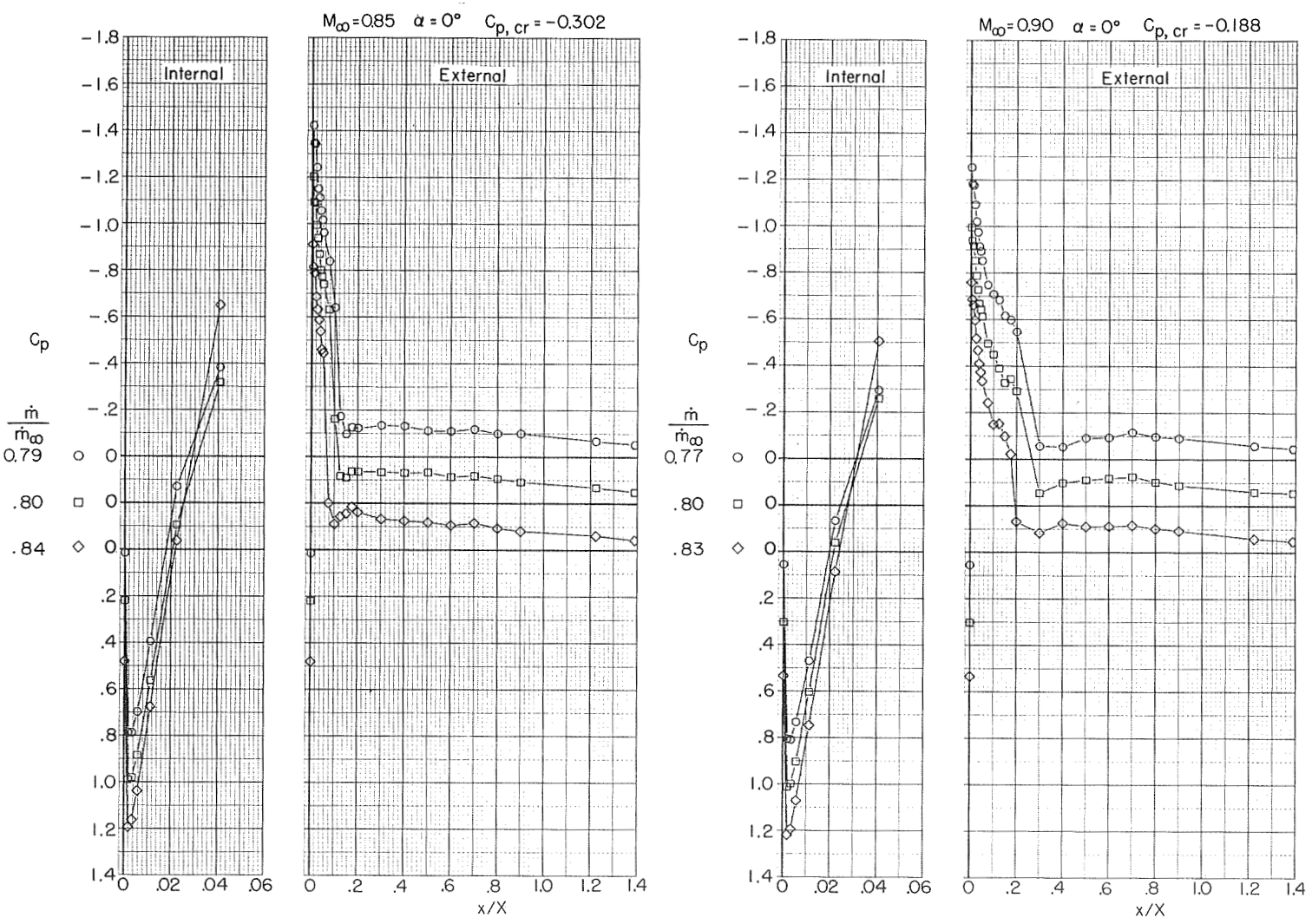

(c) M_∞ = 0.85 and 0.90.

Figure 13.- Continued.

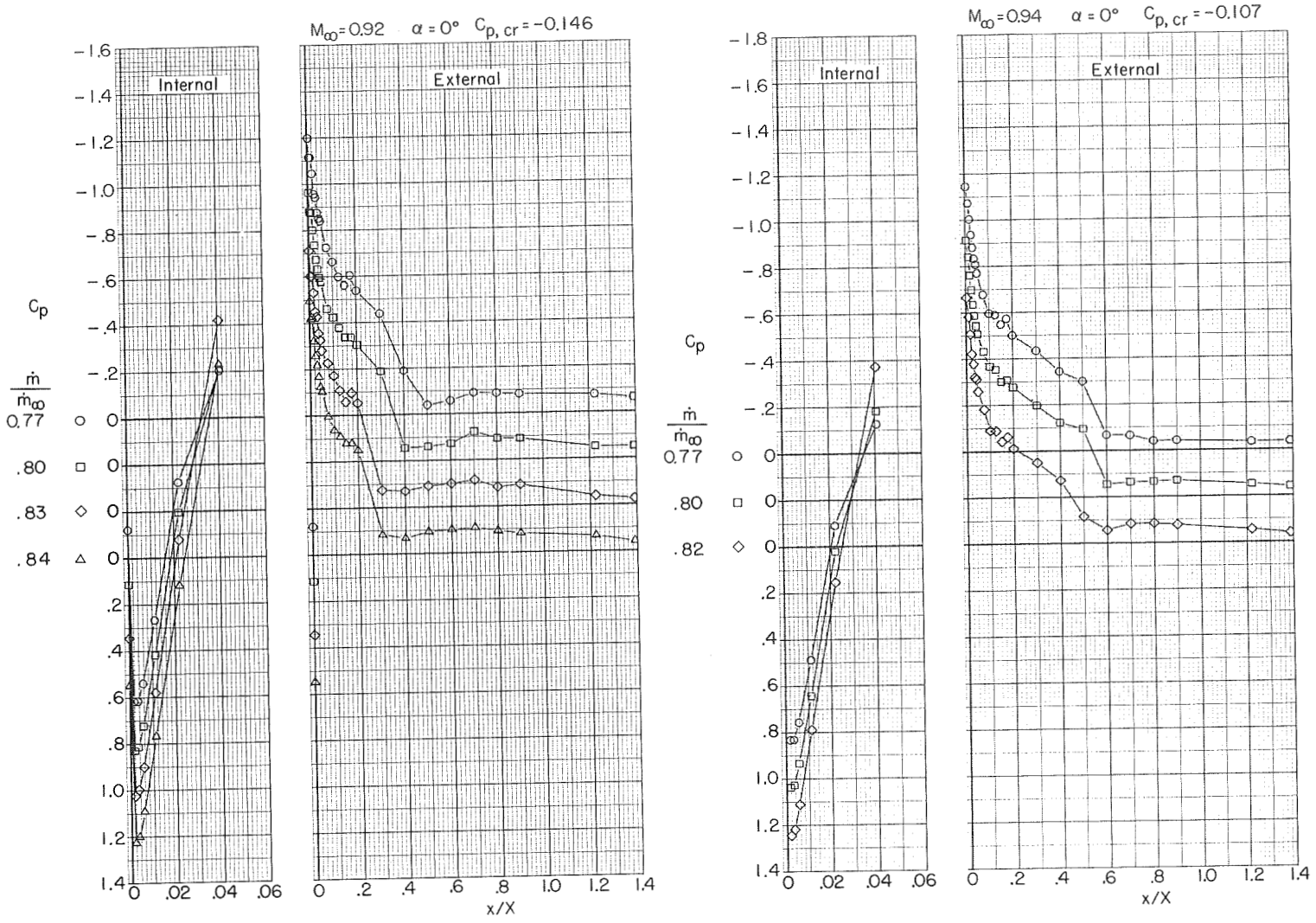

(d) M_∞ = 0.92 and 0.94.

Figure 13.- Continued.

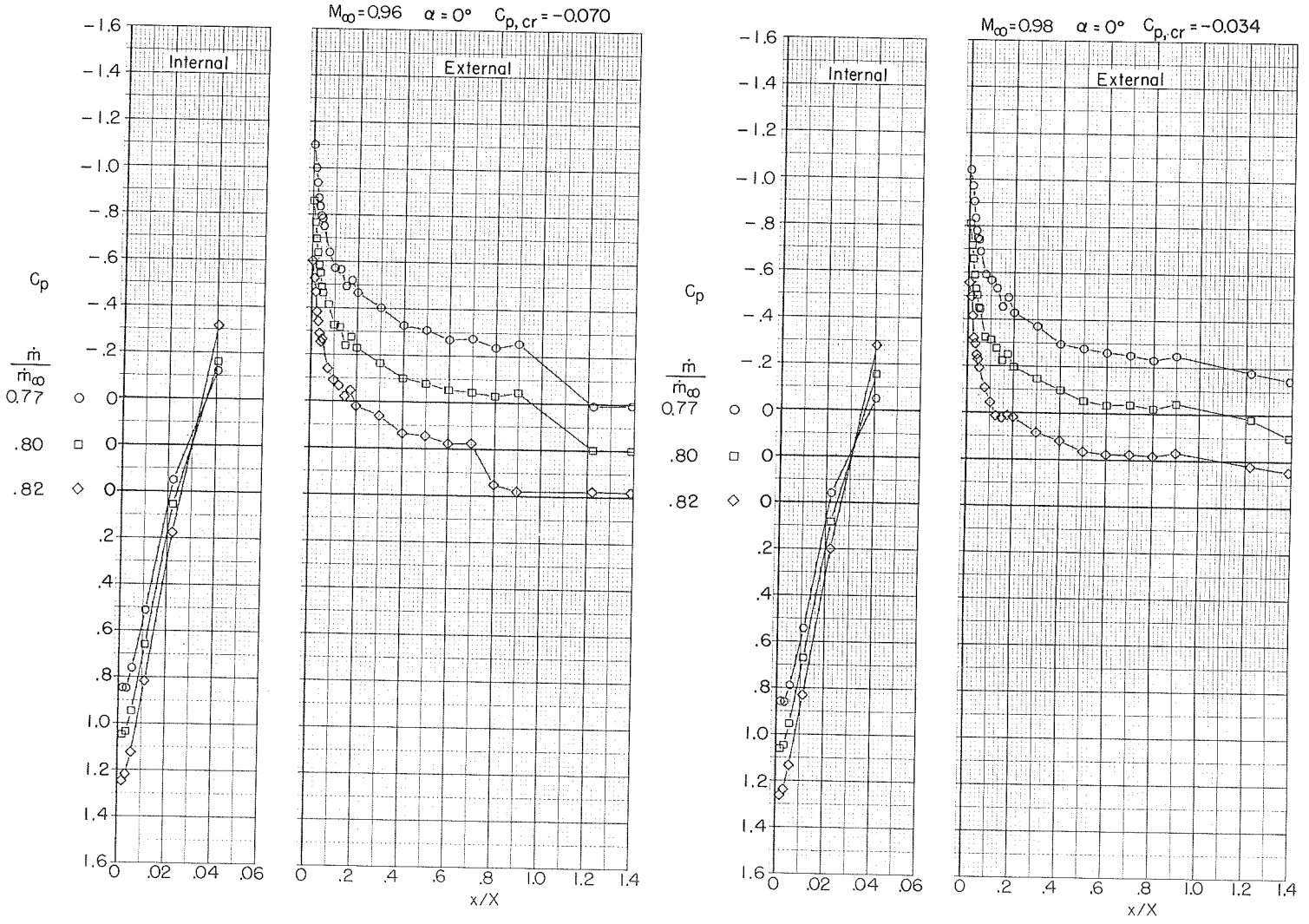

(e) M_∞ = 0.96 and 0.98.

Figure 13.- Continued.

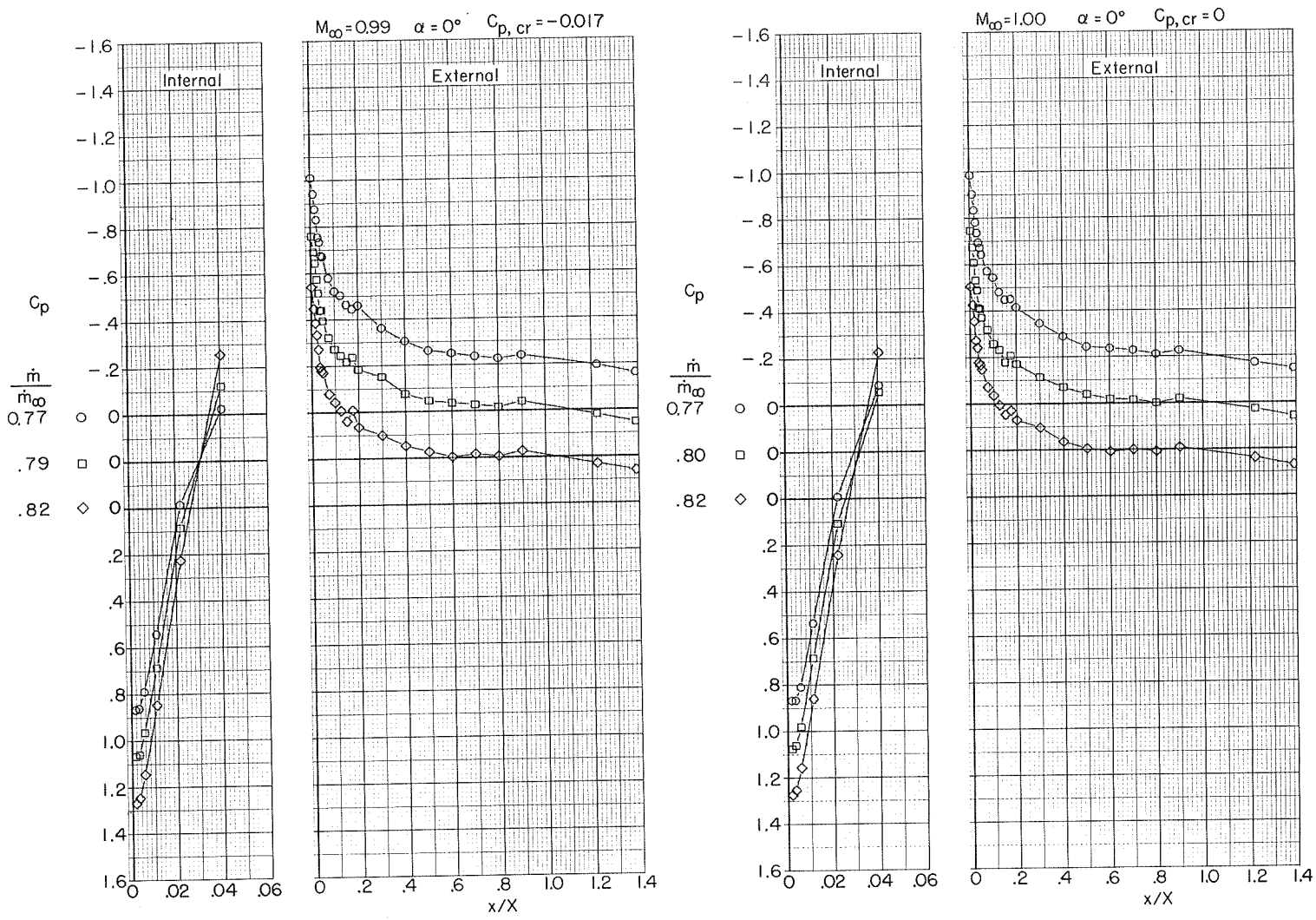

(f) M_∞ = 0.99 and 1.00.

Figure 13.- Continued.

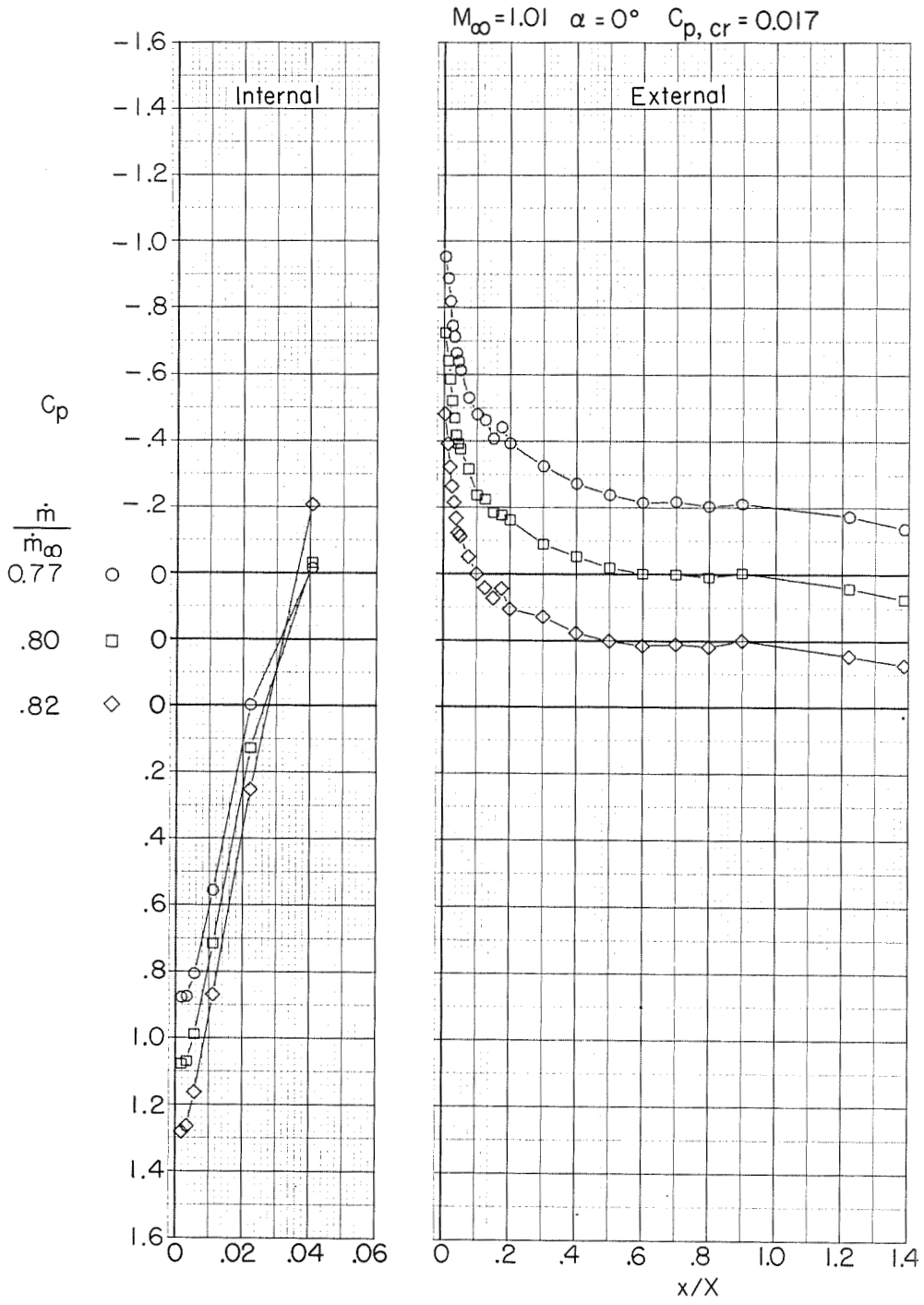

(g) $M_\infty = 1.01$.

Figure 13.- Concluded.

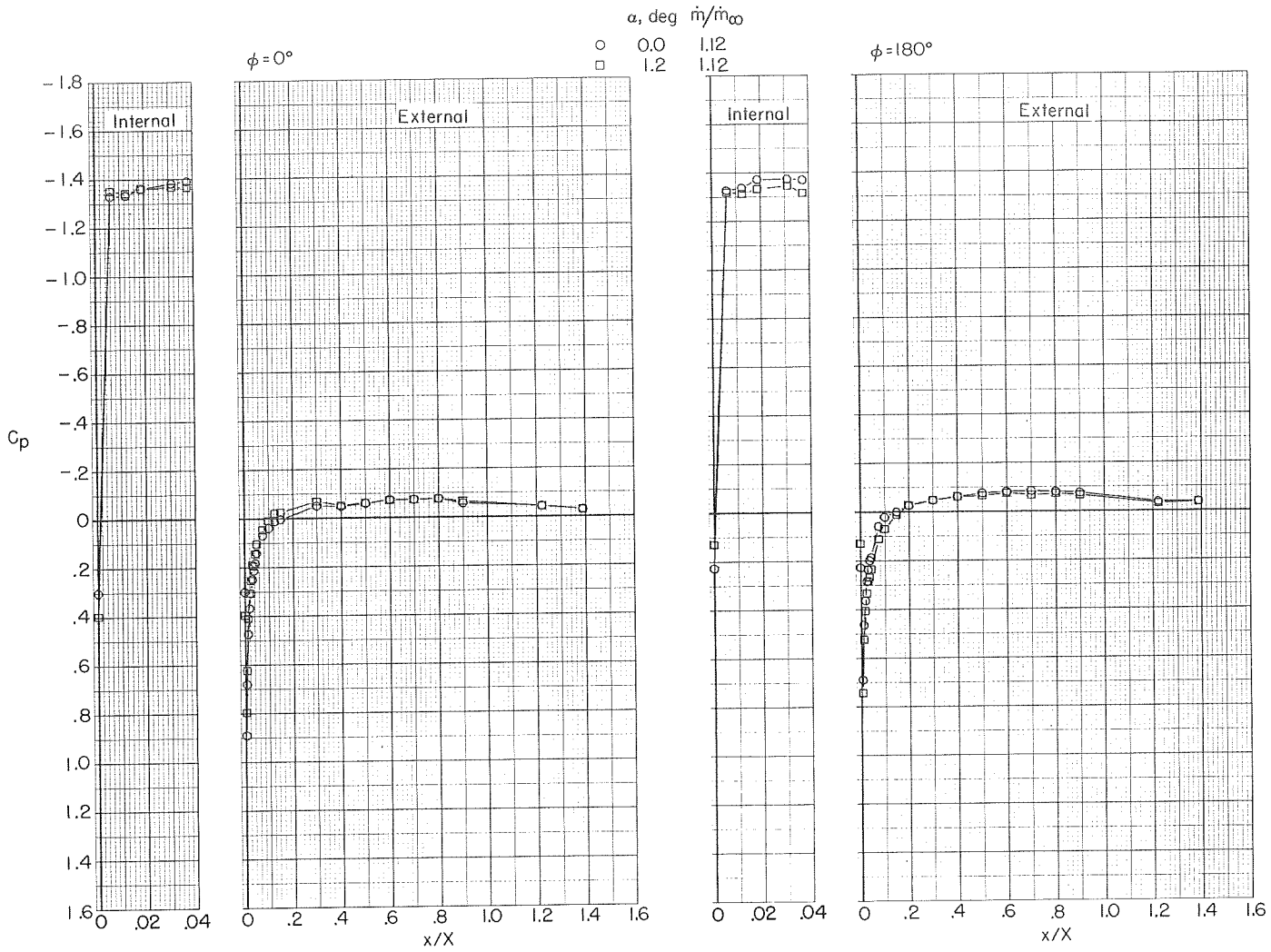

(a) $M_\infty = 0.40$.

Figure 14.- Variation with length of pressure coefficient on top and bottom of NACA 1-85-100 inlet (lip radius 0.084 cm, contraction ratio 1.009) at small angle of attack.

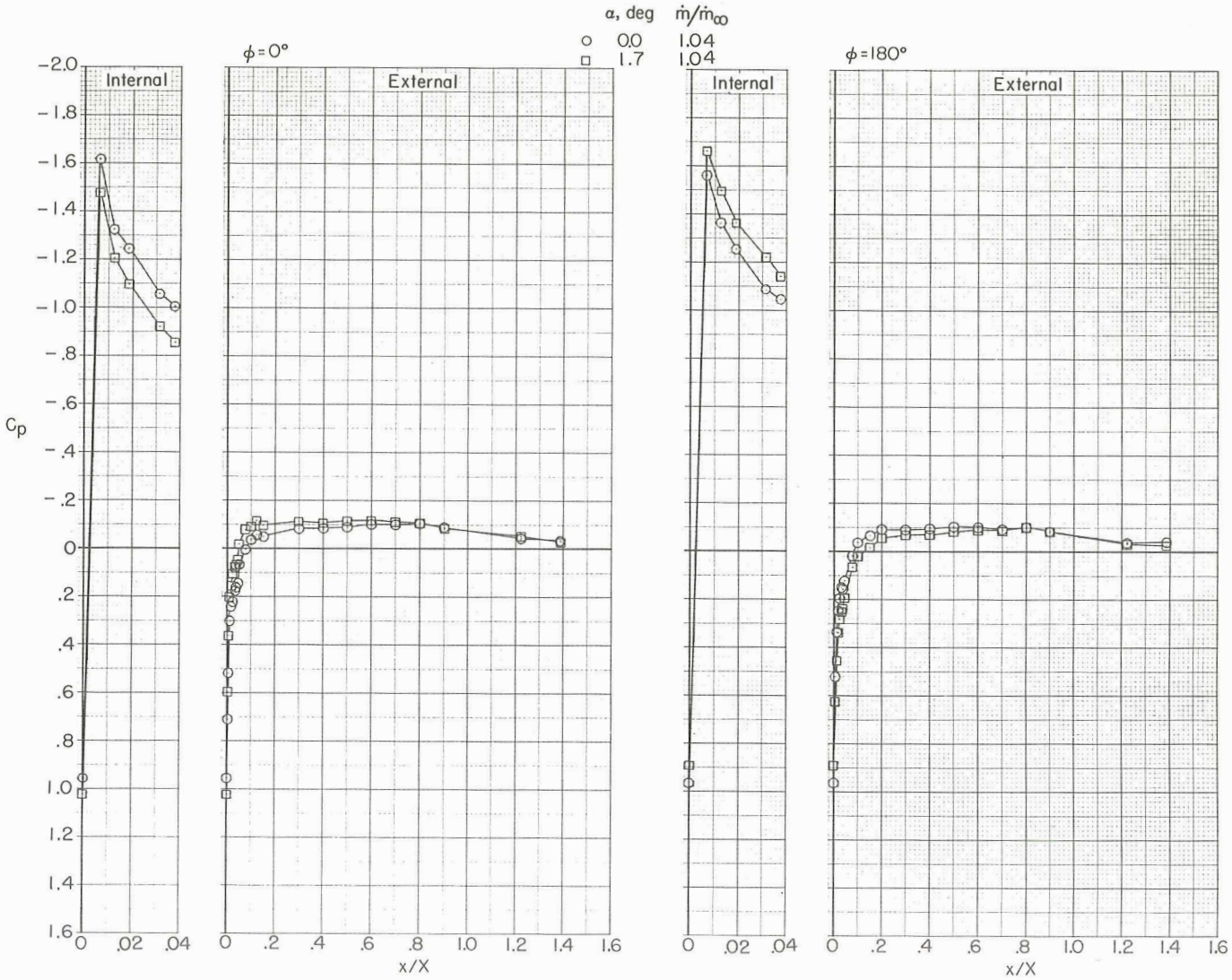

(b) $M_\infty = 0.80$.

Figure 14.- Continued.

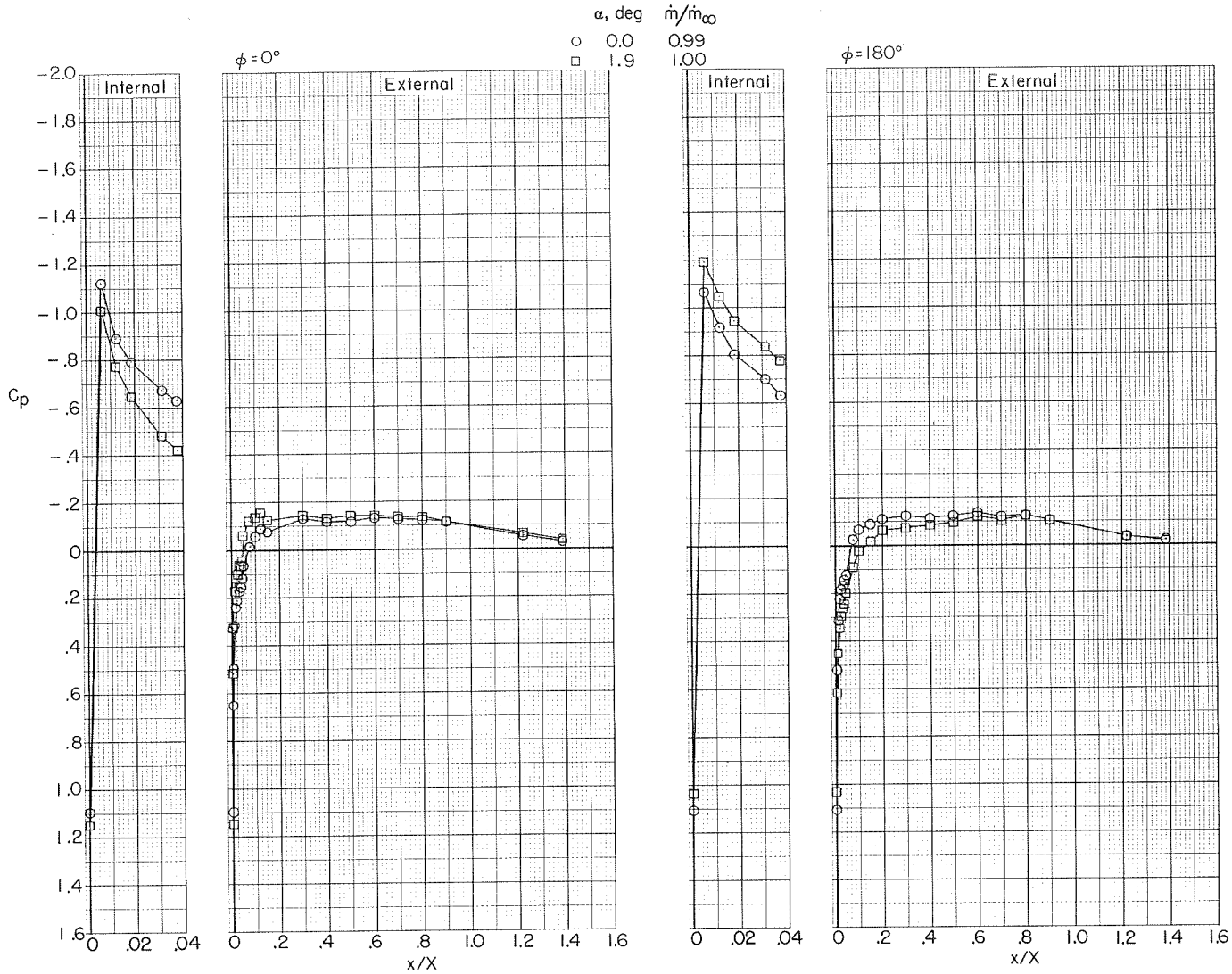

(c) $M_\infty = 0.90$.

Figure 14.- Concluded.

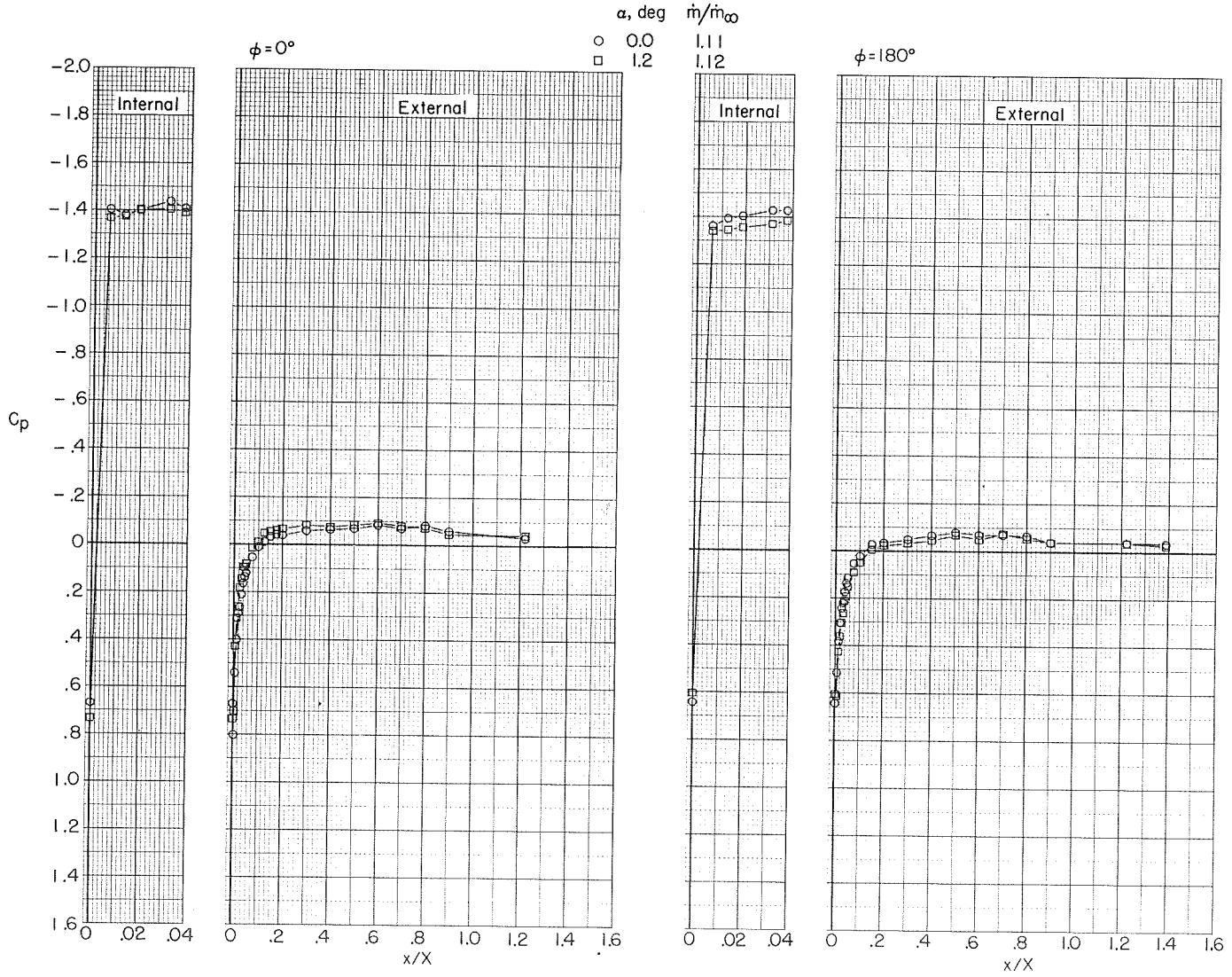

Figure 15.- Variation with length of pressure coefficient on top and bottom of NACA 1-85-100 inlet (lip radius 0.168 cm, contraction ratio 1.017) at Mach number of 0.40 and small angle of attack.

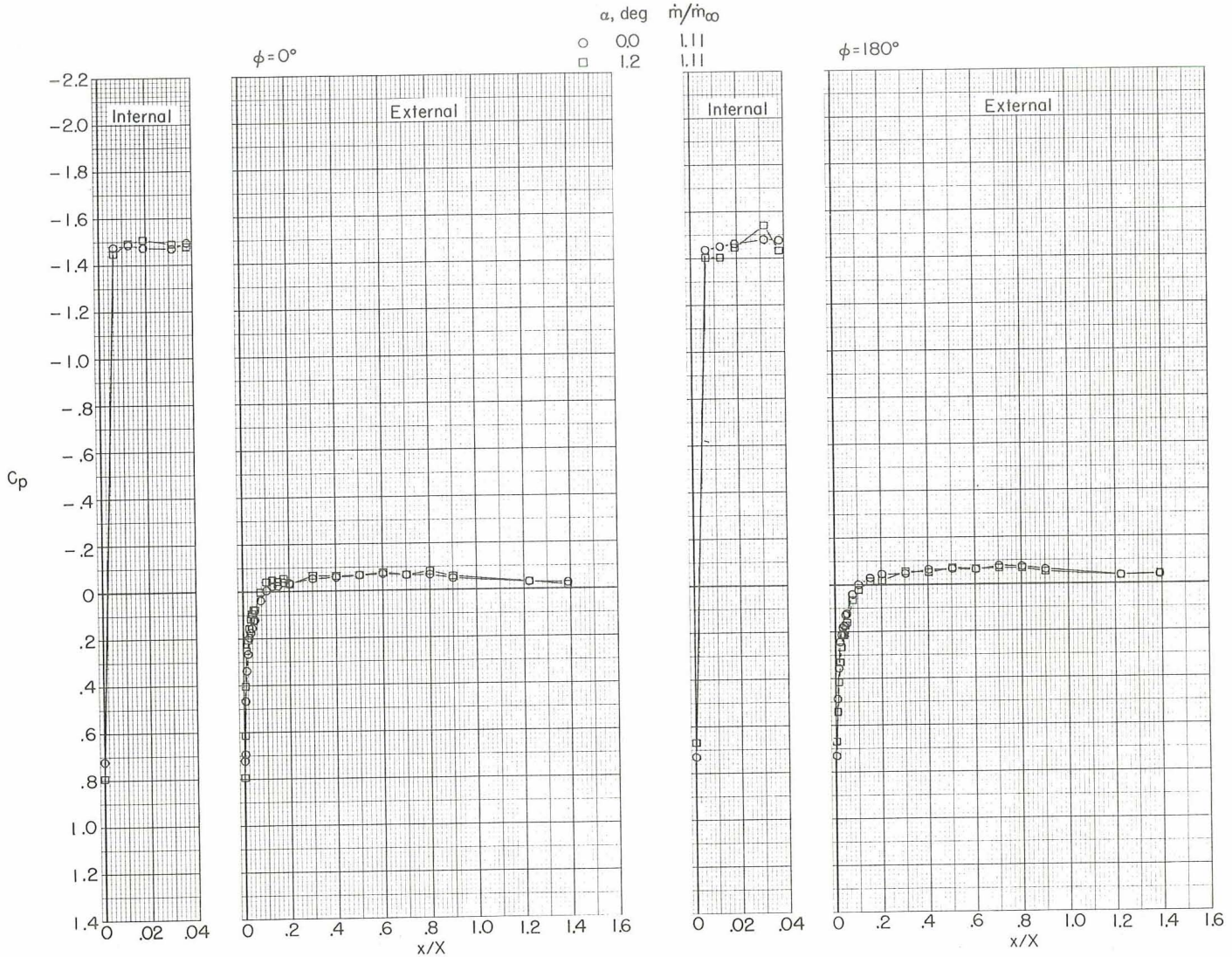

Figure 16.- Variation with length of pressure coefficient on top and bottom of NACA 1-85-100 inlet (lip radius 0.251 cm, contraction ratio 1.026) at Mach number of 0.40 and small angle of attack.

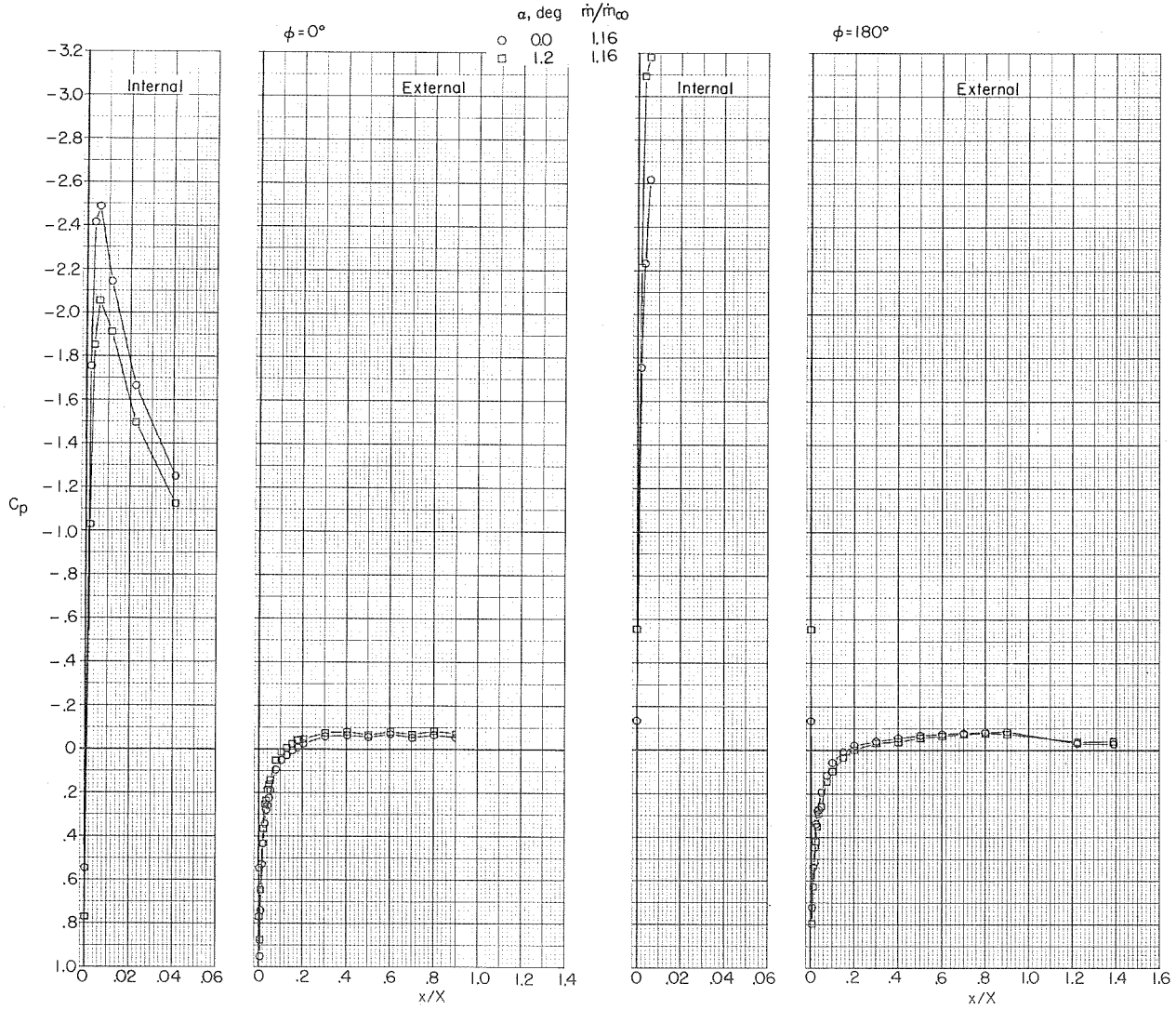

Figure 17.- Variation with length of pressure coefficient on top and bottom of NACA 1-85-100 inlet (lip radius 0.084 cm, contraction ratio 1.046) at Mach number of 0.40 and small angle of attack.

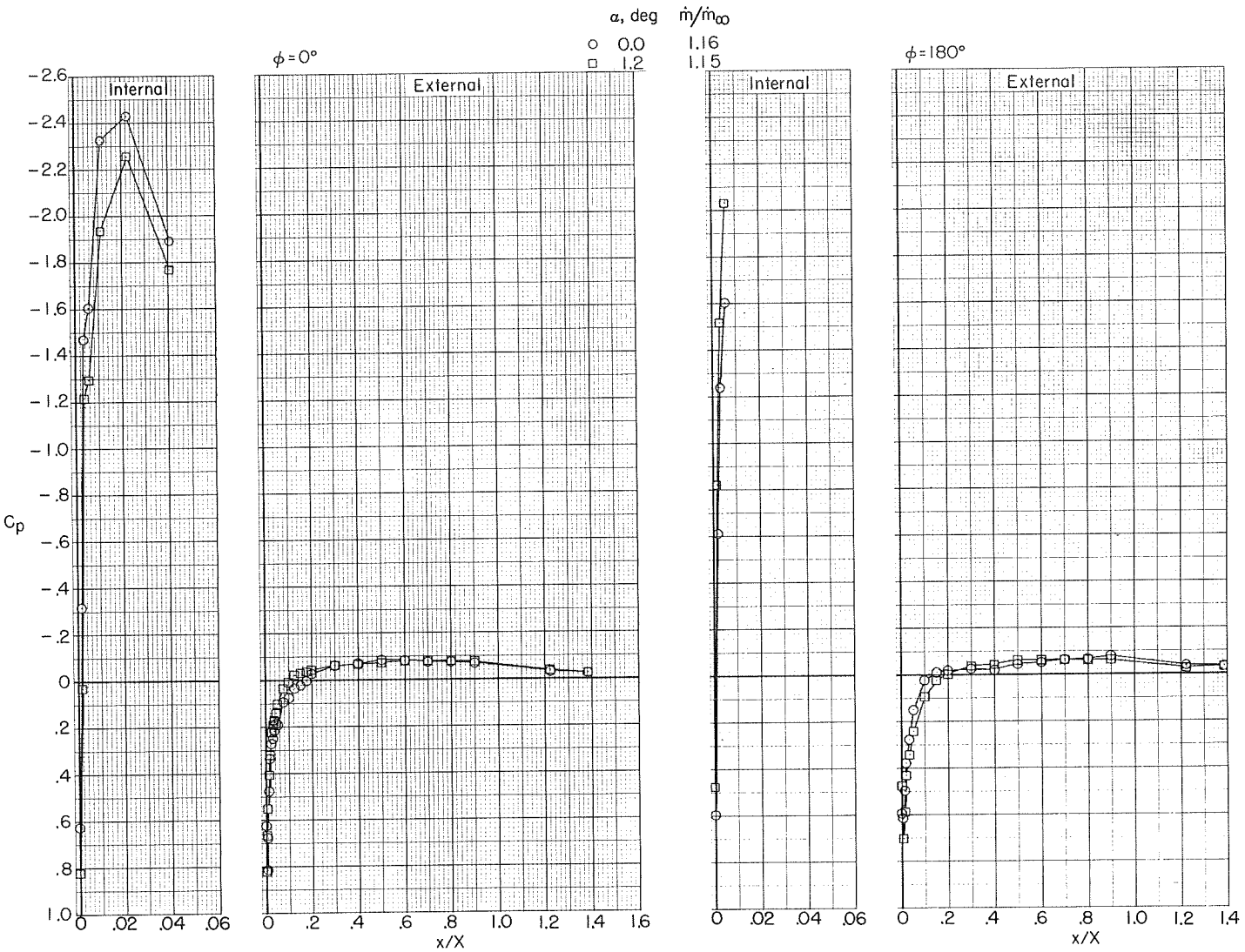

Figure 18.- Variation with length of pressure coefficient on top and bottom of NACA 1-85-100 inlet (lip radius 0.084 cm, contraction ratio 1.093) at Mach number of 0.40 and small angle of attack.

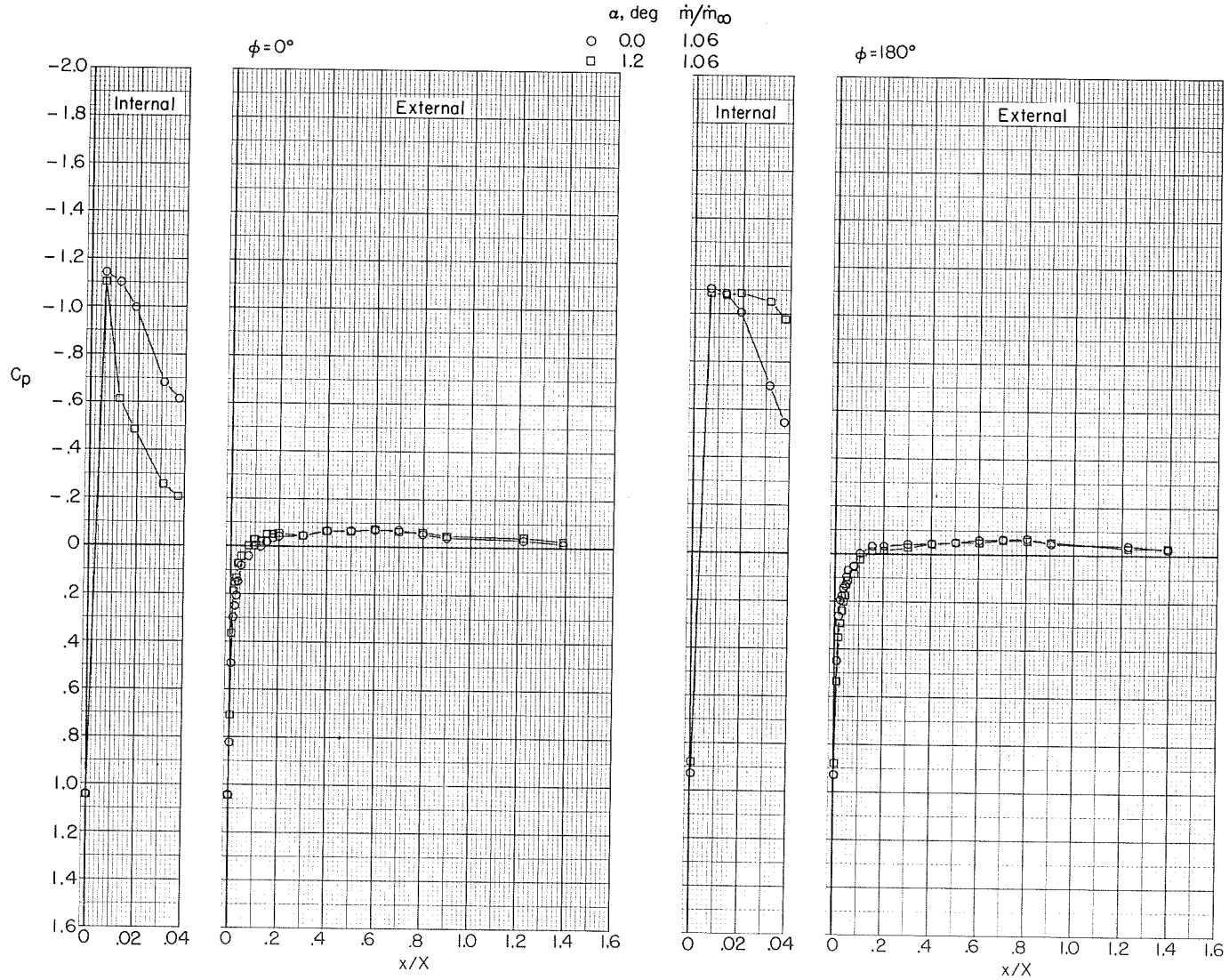

(a) $M_\infty = 0.40$.

Figure 19.- Variation with length of pressure coefficient on top and bottom of NACA 1-85-100 inlet (lip radius 0.061 cm, contraction ratio 1.006) at small angle of attack.

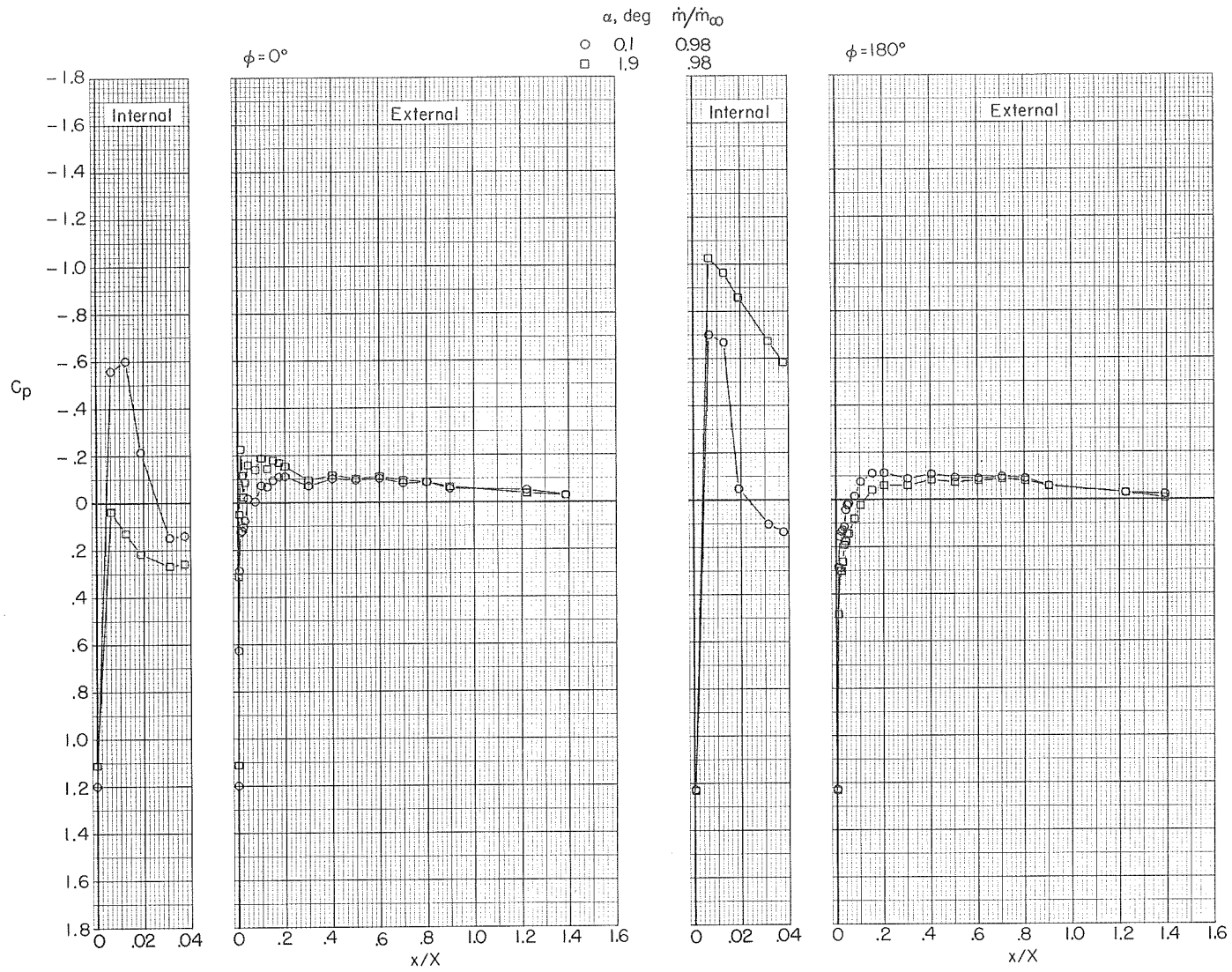

(b) $M_\infty = 0.90$.

Figure 19.- Continued.

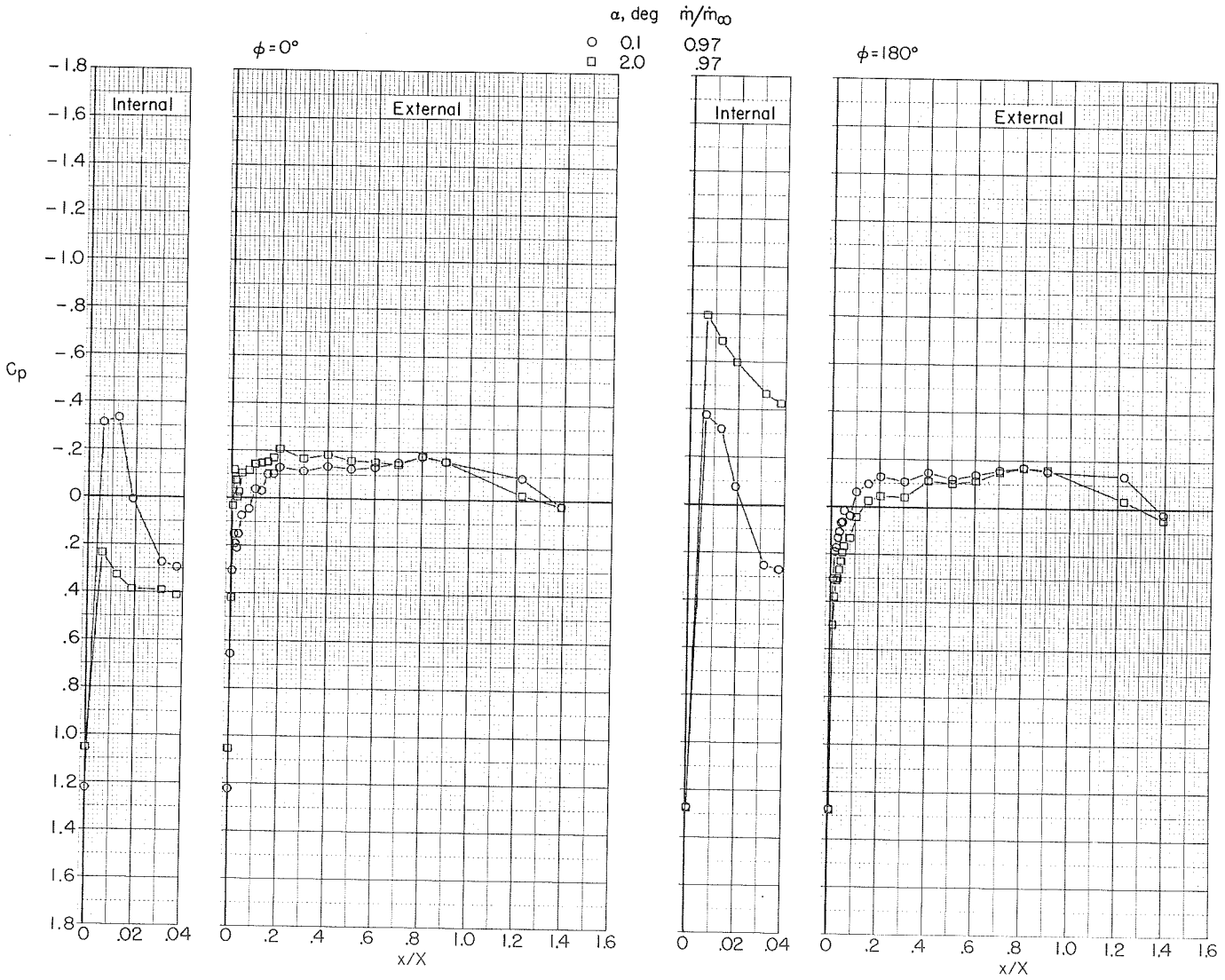

(c) $M_\infty = 0.98$.

Figure 19.- Concluded.

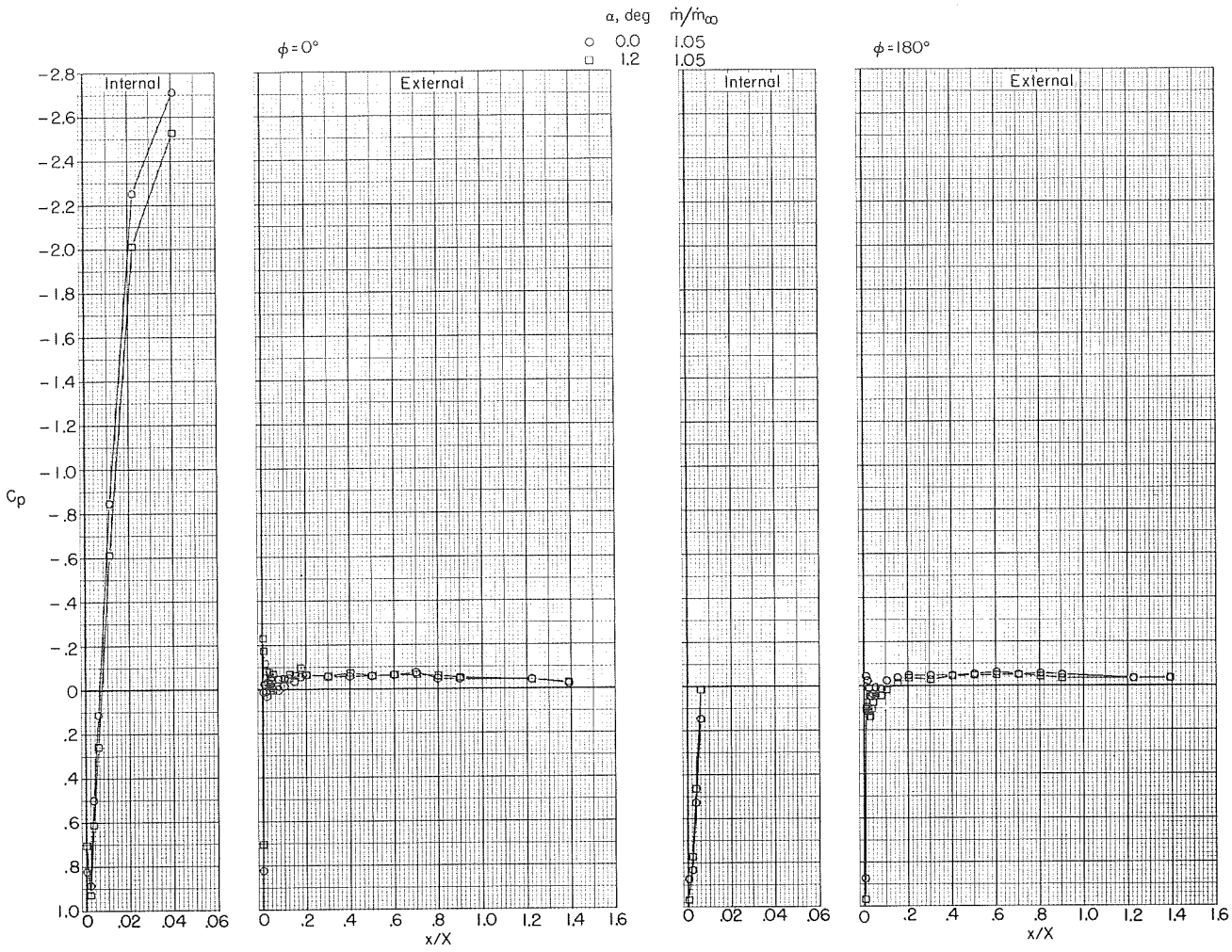

Figure 20.- Variation with length of pressure coefficient on top and bottom of NACA 1-89-100 inlet (lip radius 0.061 cm, contraction ratio 1.195) at Mach number of 0.40 and small angle of attack.

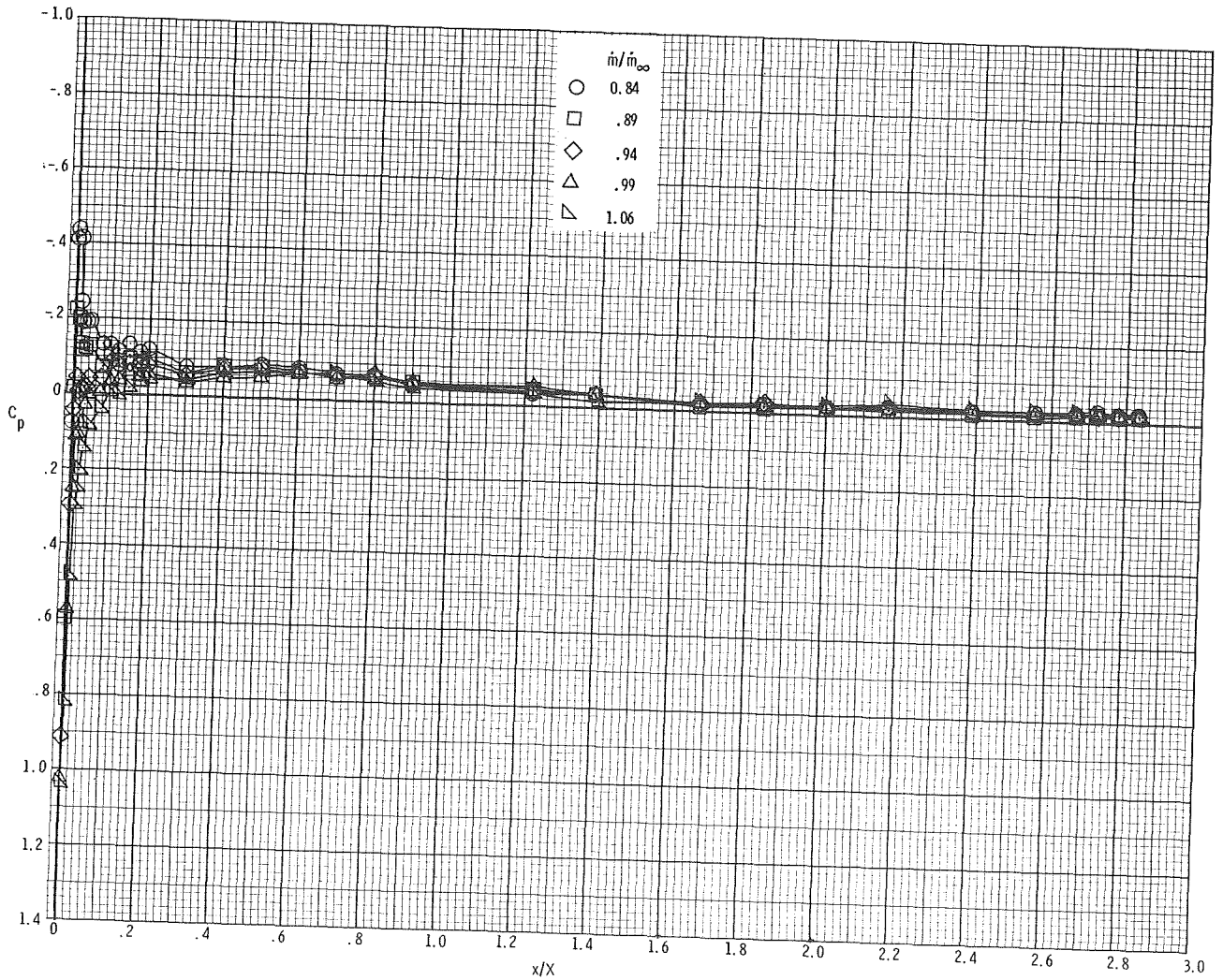

(a) $M_\infty = 0.40$.

Figure 21.- Effect of inlet mass-flow ratio on afterbody pressure-coefficient distribution for NACA 1-89-100 inlet (lip radius 0.061 cm, contraction ratio 1.006) at several Mach numbers ($\alpha = .0^o$).

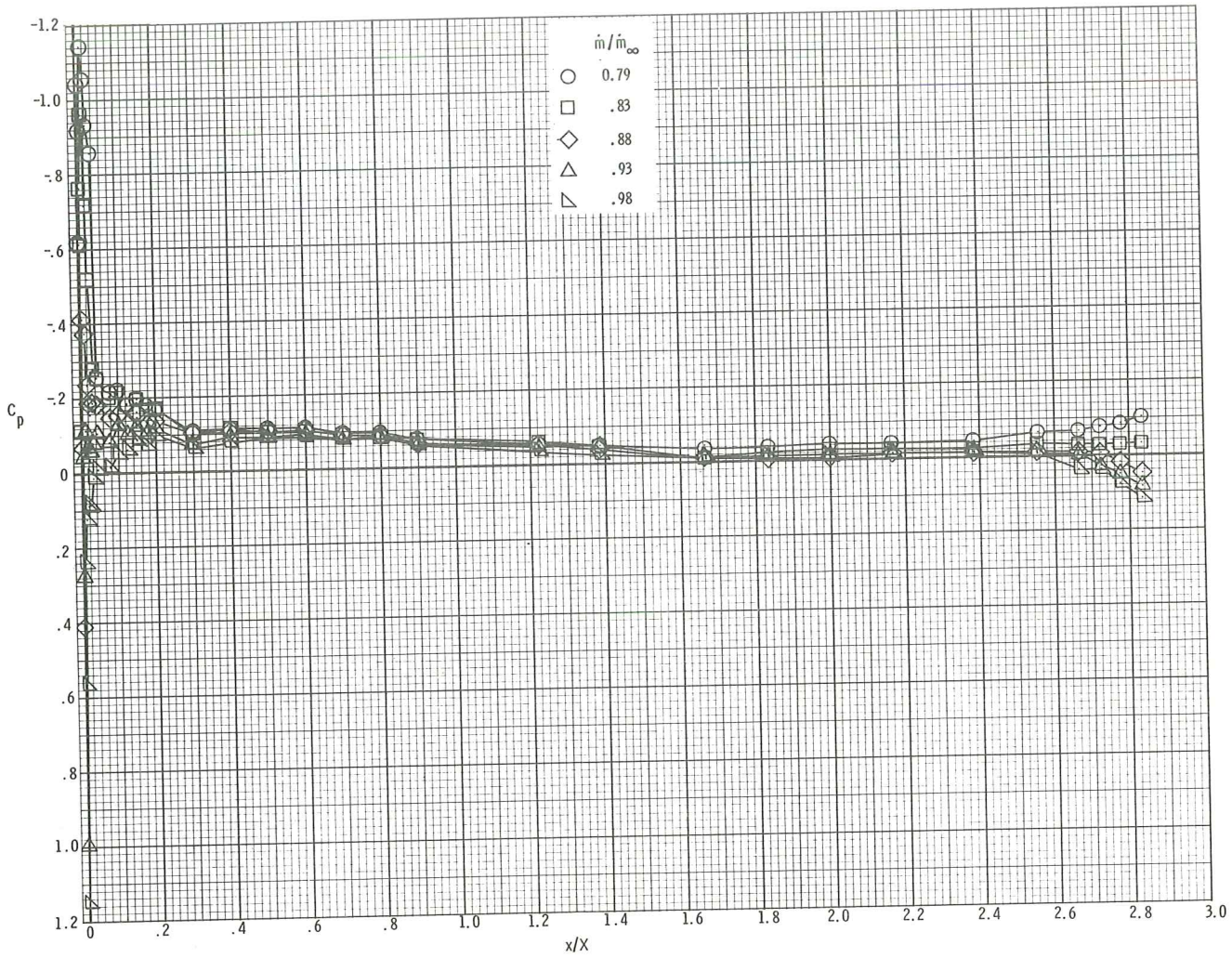

(b) $M_\infty = 0.80$.

Figure 21.- Continued.

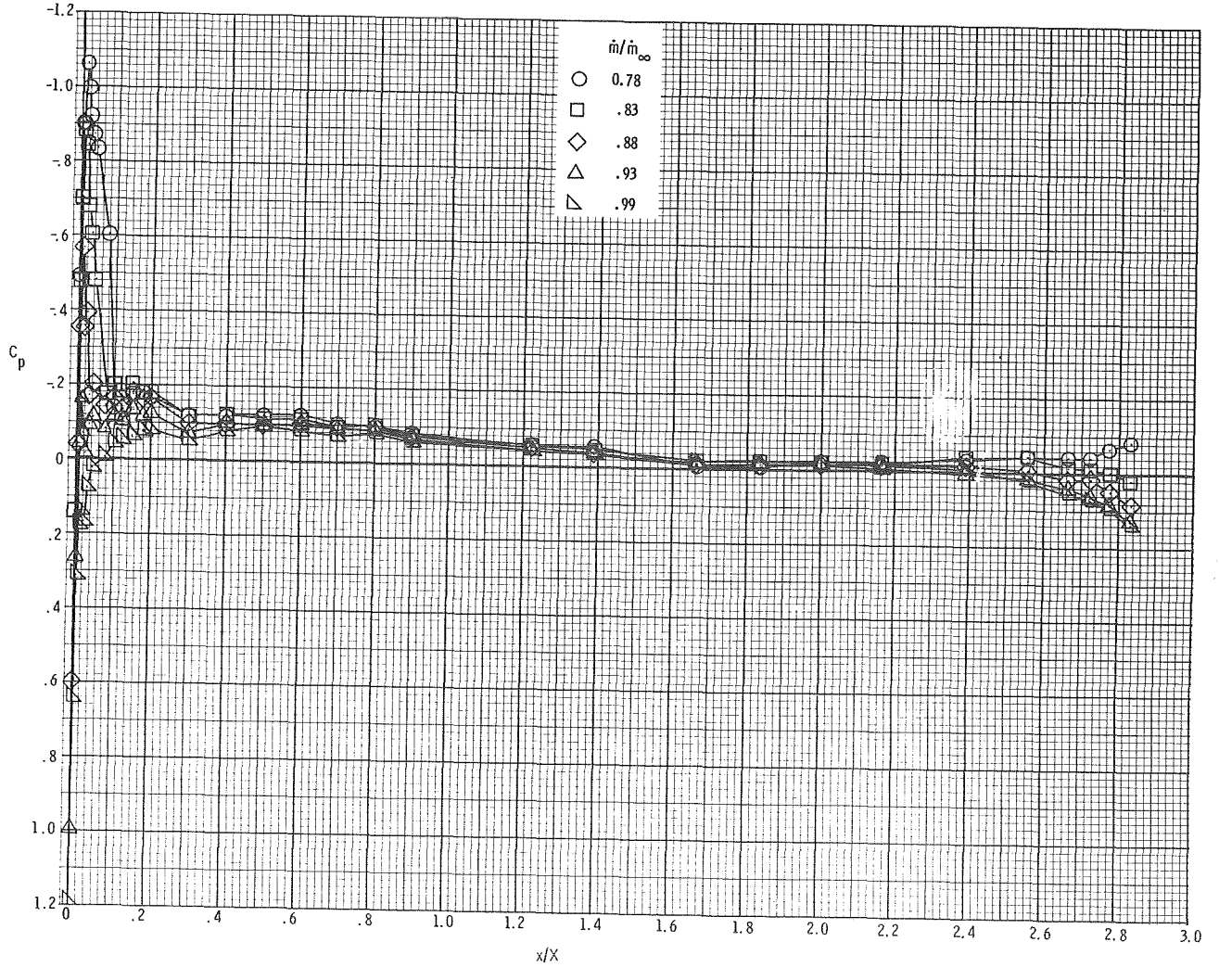

(c) $M_\infty = 0.85$.

Figure 21.- Continued.

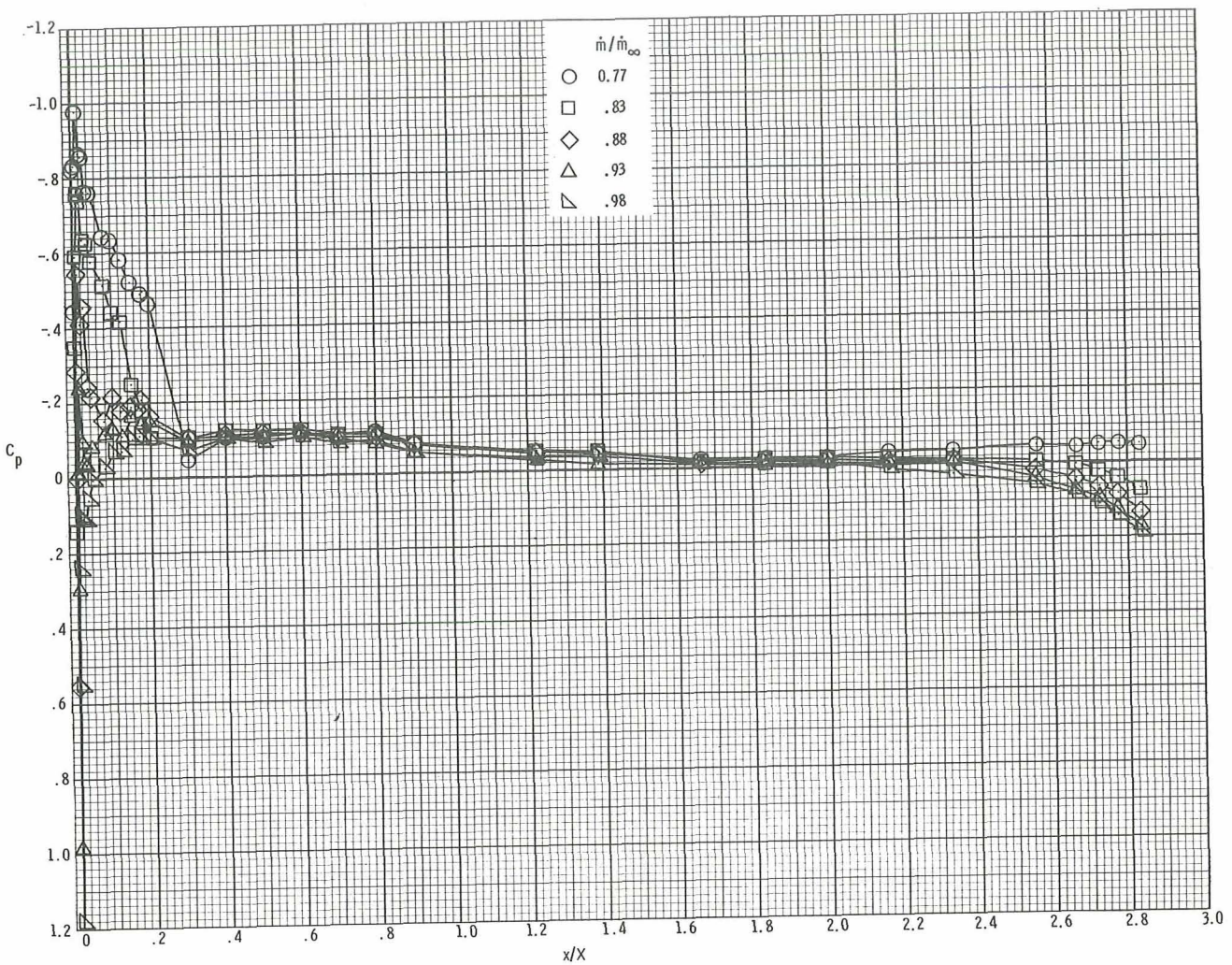

(d) $M_\infty = 0.90$.

Figure 21.- Continued.

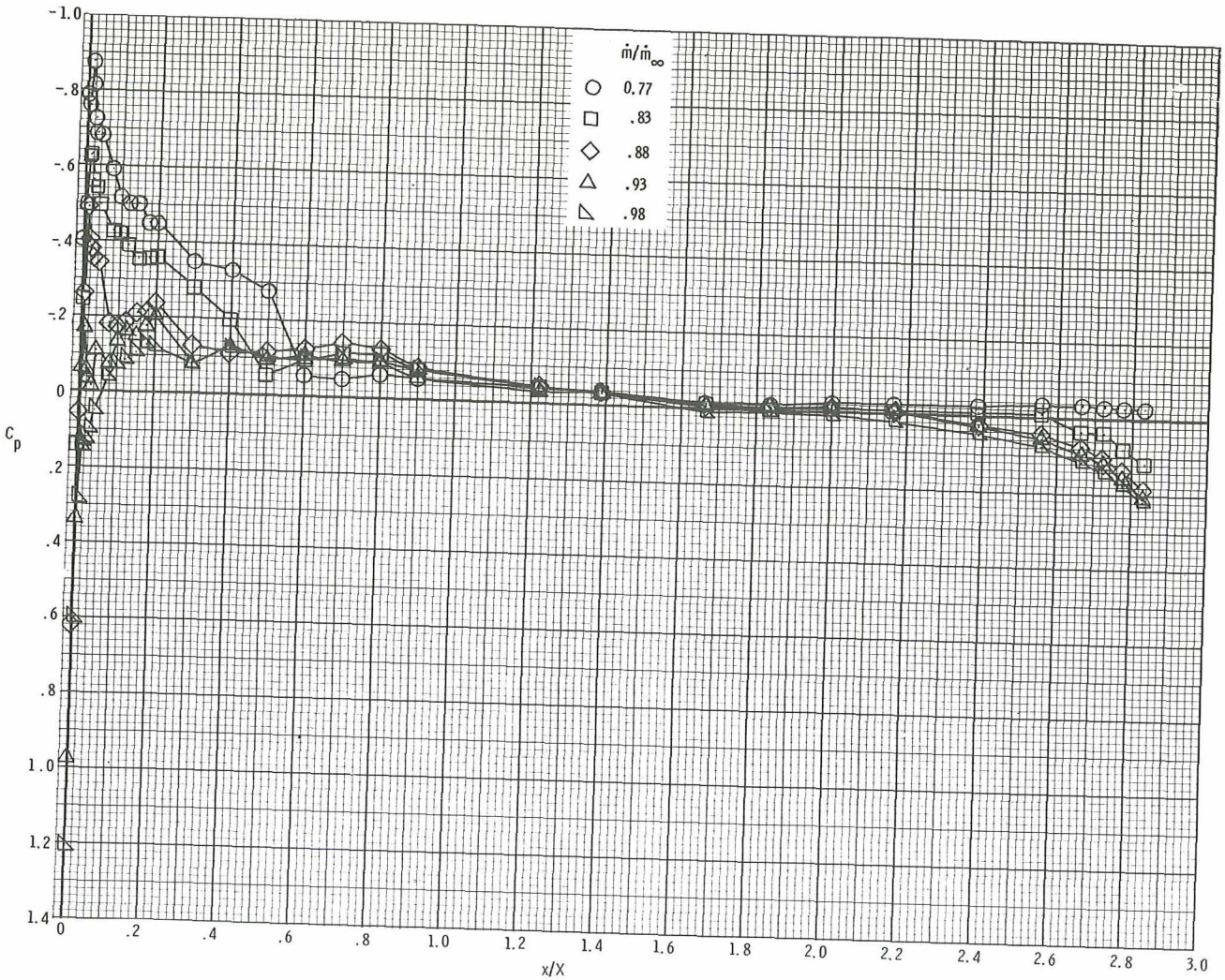

(e) $M_\infty = 0.94$.

Figure 21.- Continued.

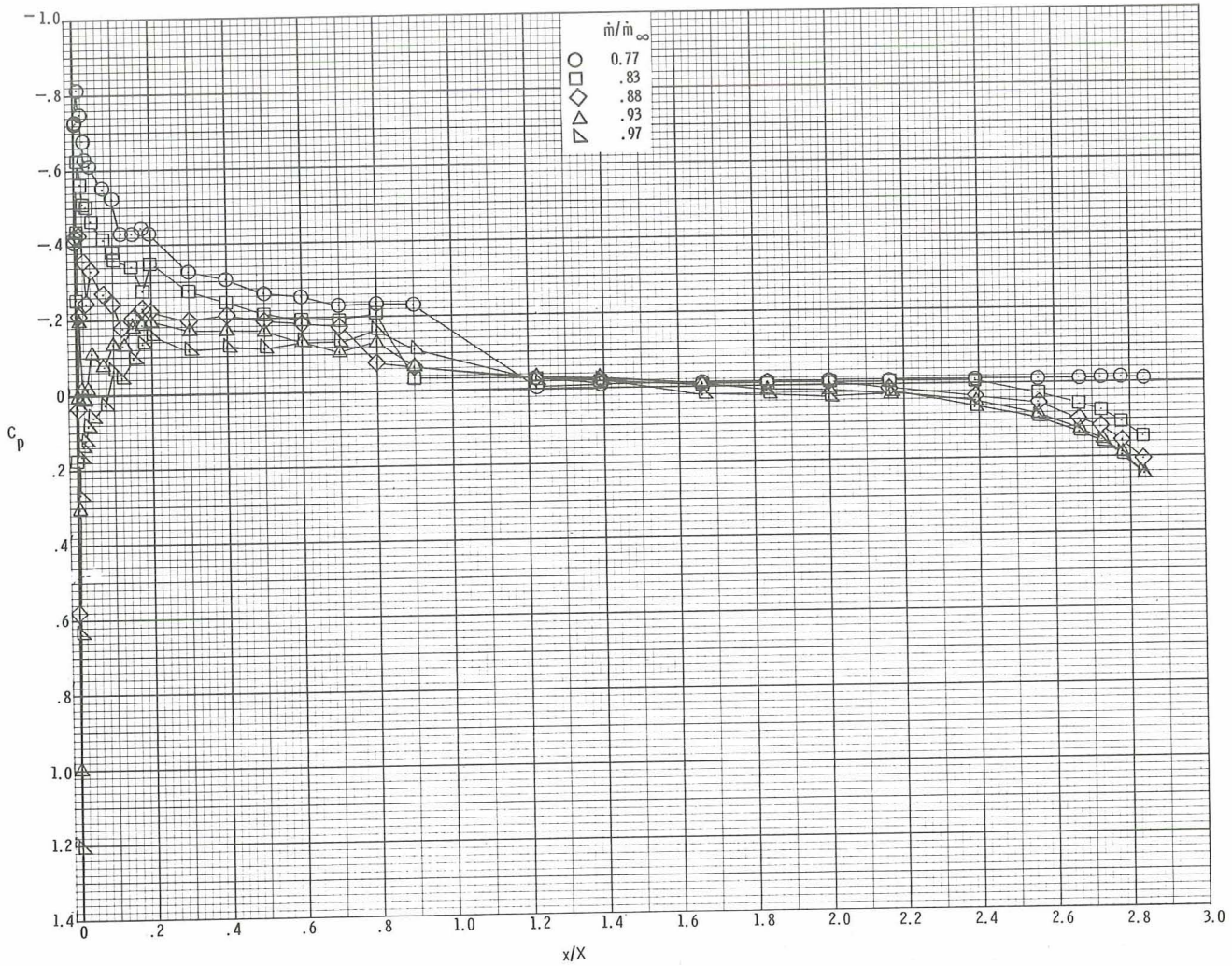

(f) $M_\infty = 0.96$.

Figure 21.- Continued.

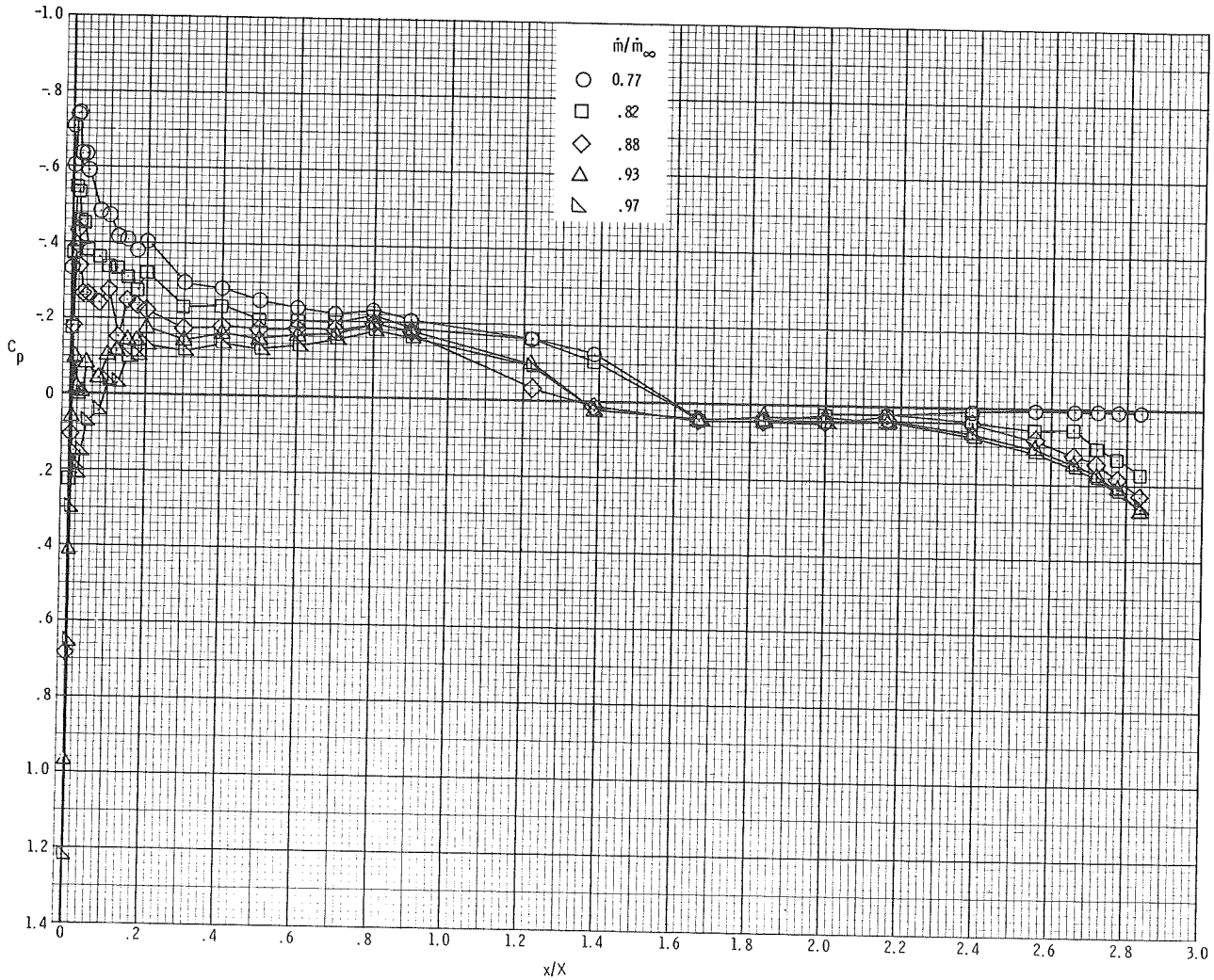

(g) $M_\infty = 0.98$.

Figure 21.- Continued.

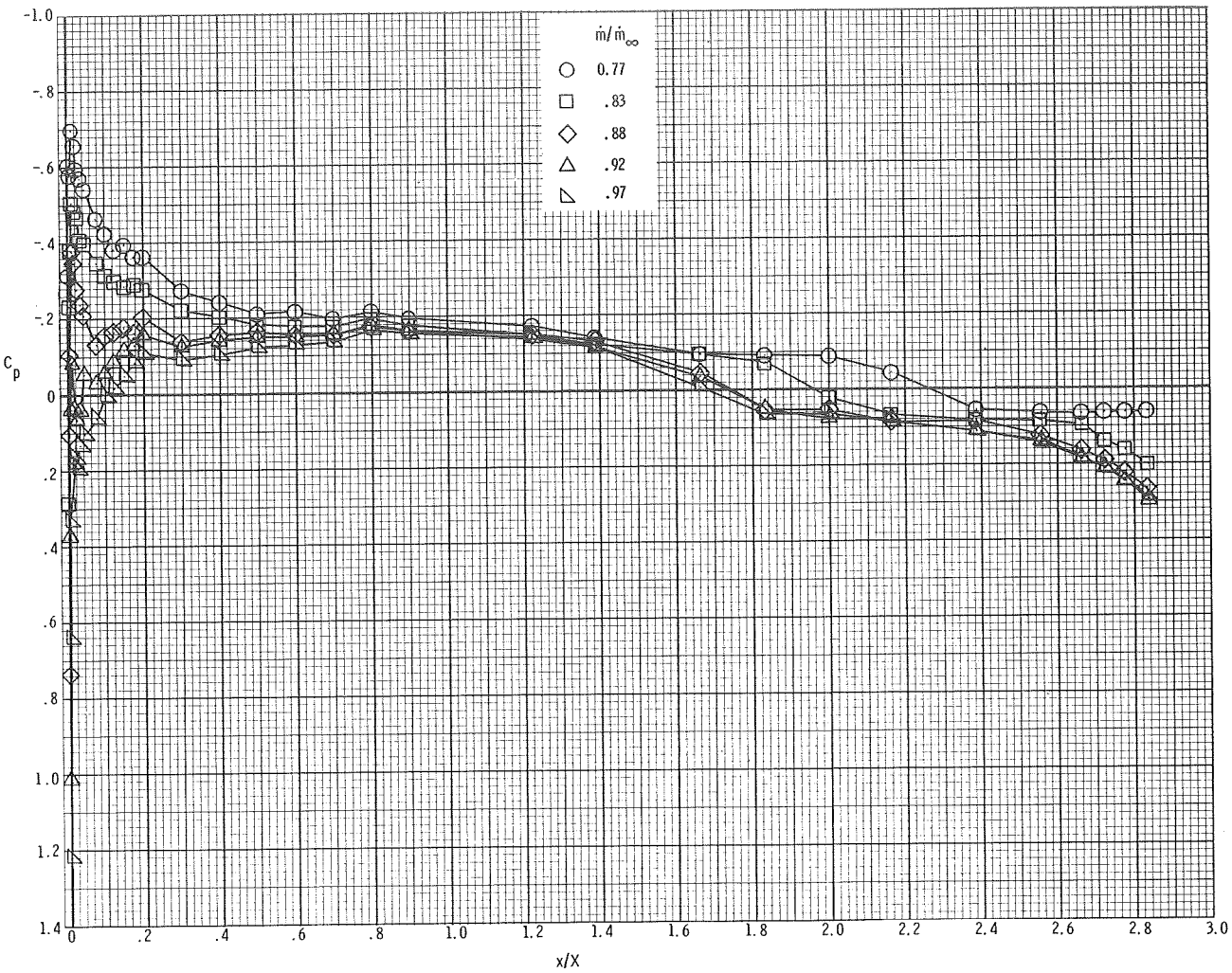

(h) $M_\infty = 1.00$.

Figure 21.- Continued.

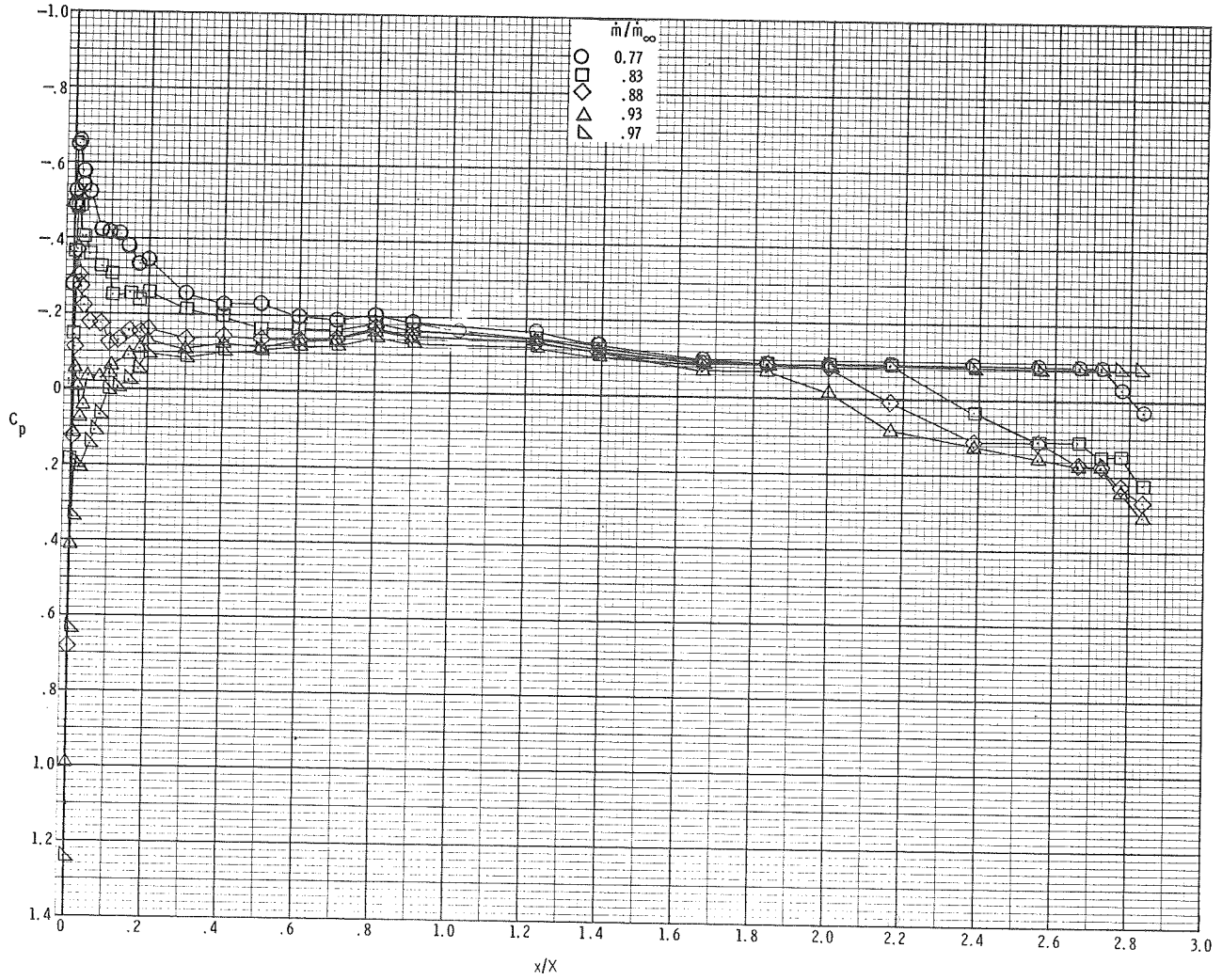

(i) $M_\infty = 1.01$.

Figure 21.- Concluded.

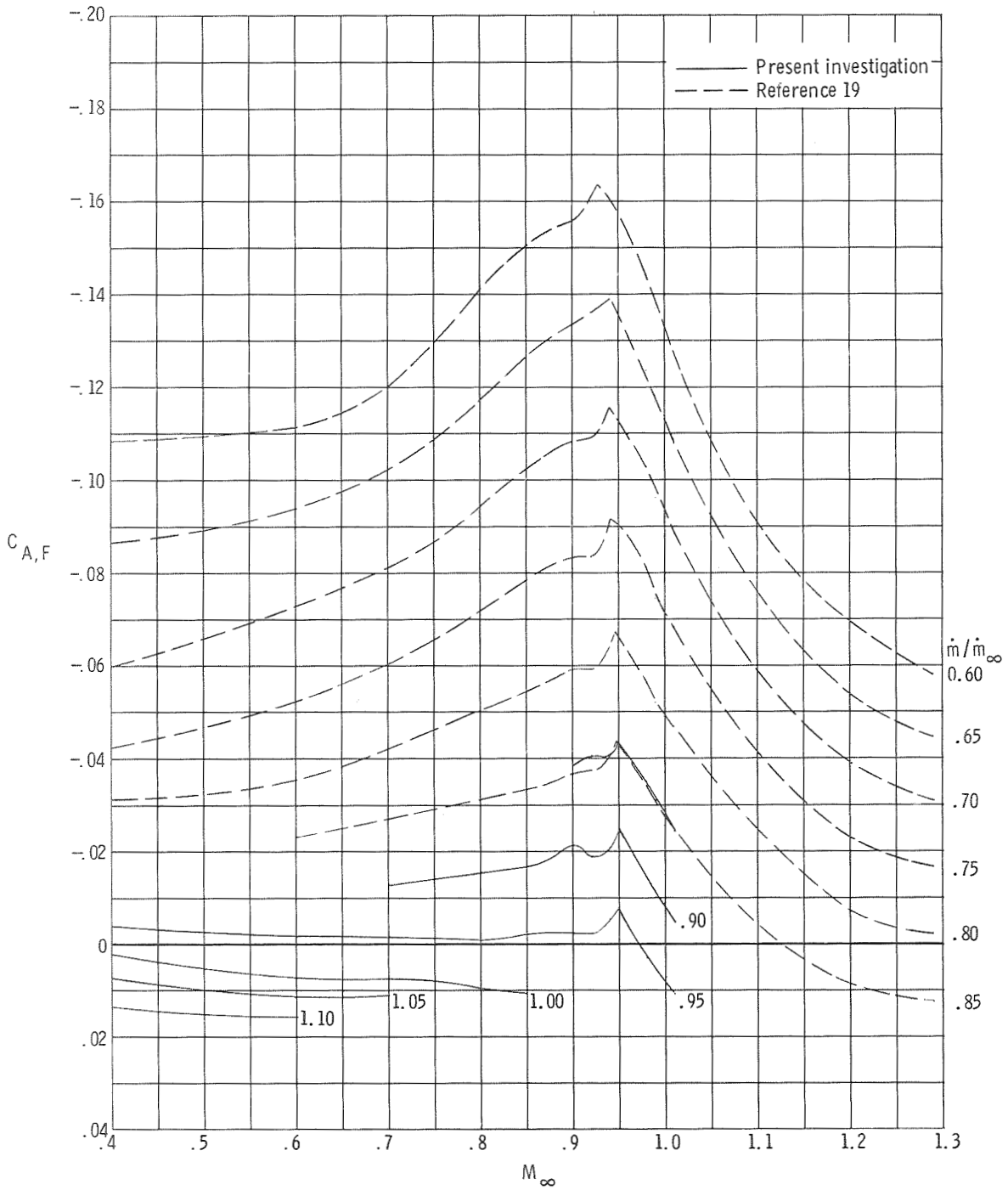

(a) NACA 1-85-100, lip radius 0.084 cm, contraction ratio 1.009.

Figure 22.- Variation with Mach number of forebody axial-force coefficient obtained by integration of inlet pressures in axial direction.

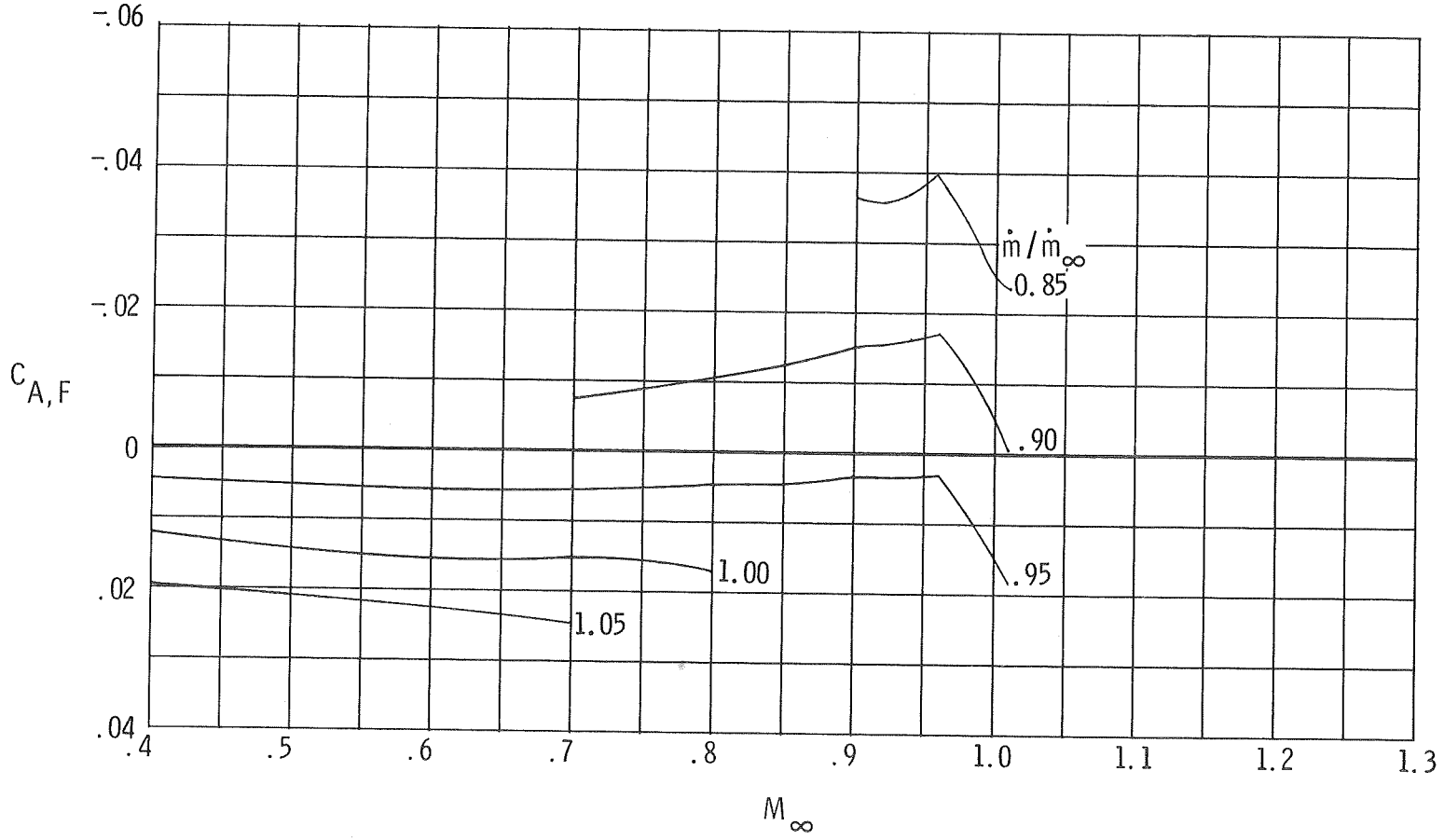

(b) NACA 1-85-100, lip radius 0.168 cm, contraction ratio 1.017.

Figure 22.- Continued.

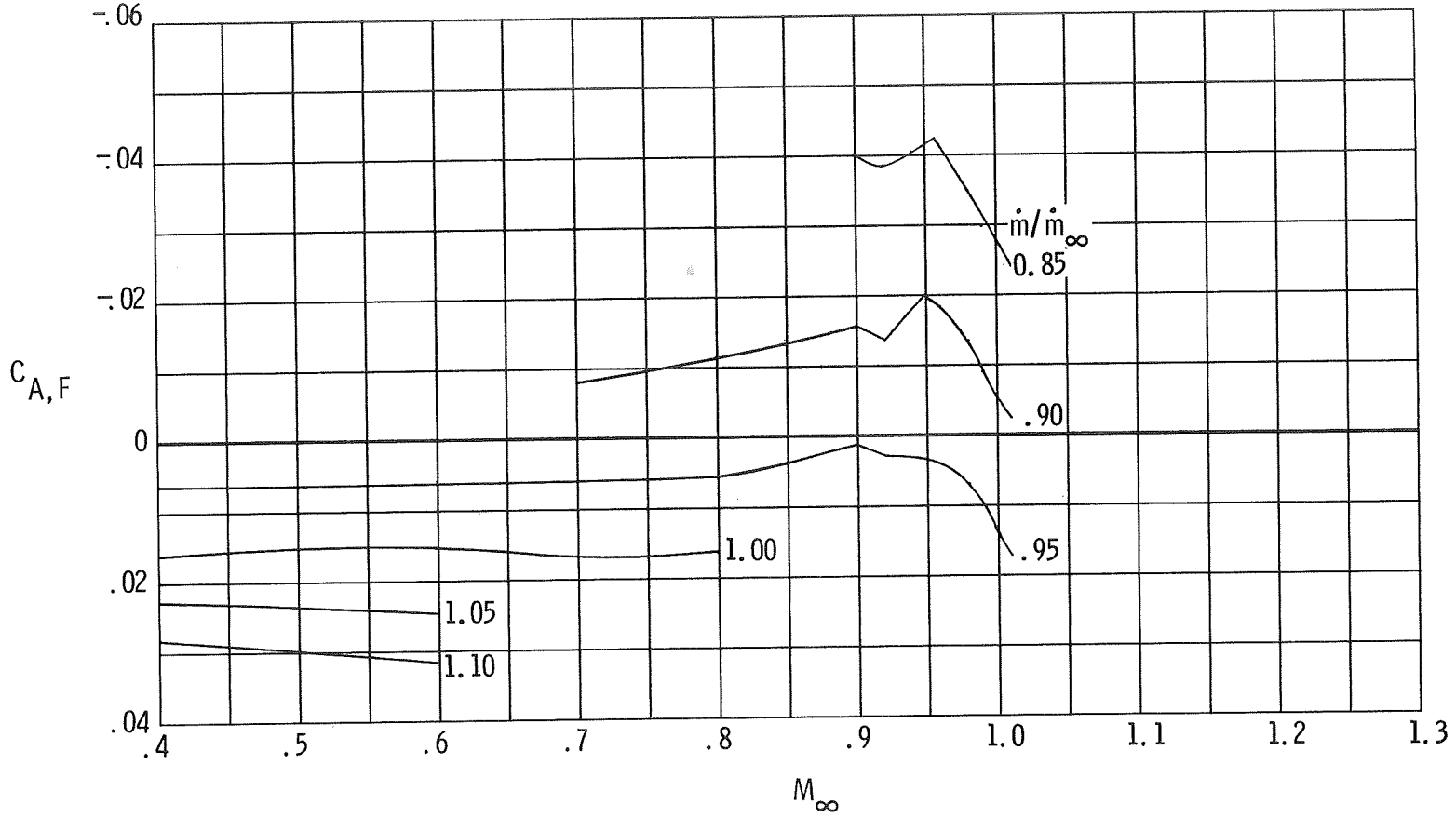

(c) NACA 1-85-100, lip radius 0.251 cm, contraction ratio 1.026.

Figure 22.- Continued.

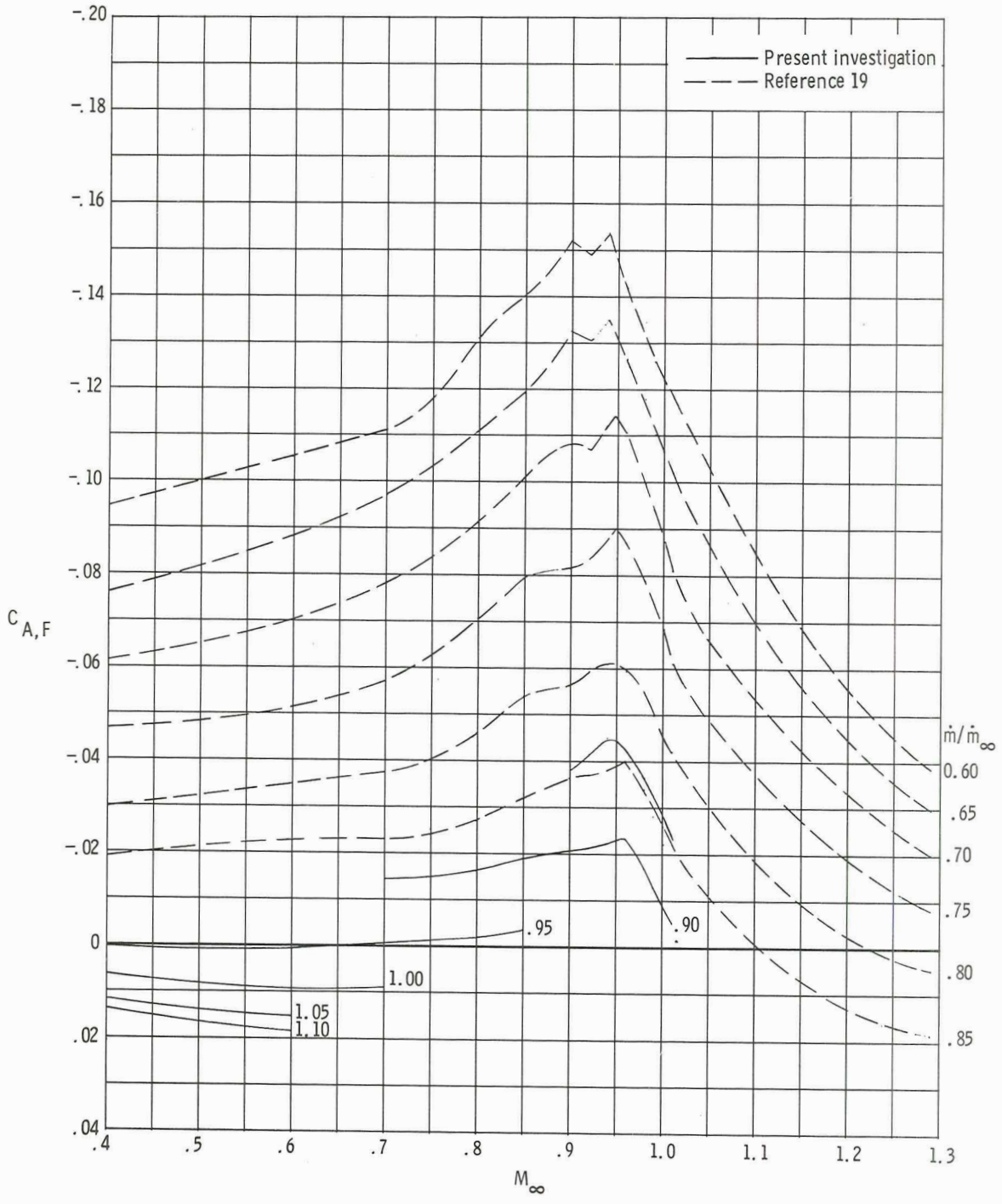

(d) NACA 1-85-100, lip radius 0.084 cm, contraction ratio 1.046.

Figure 22.- Continued.

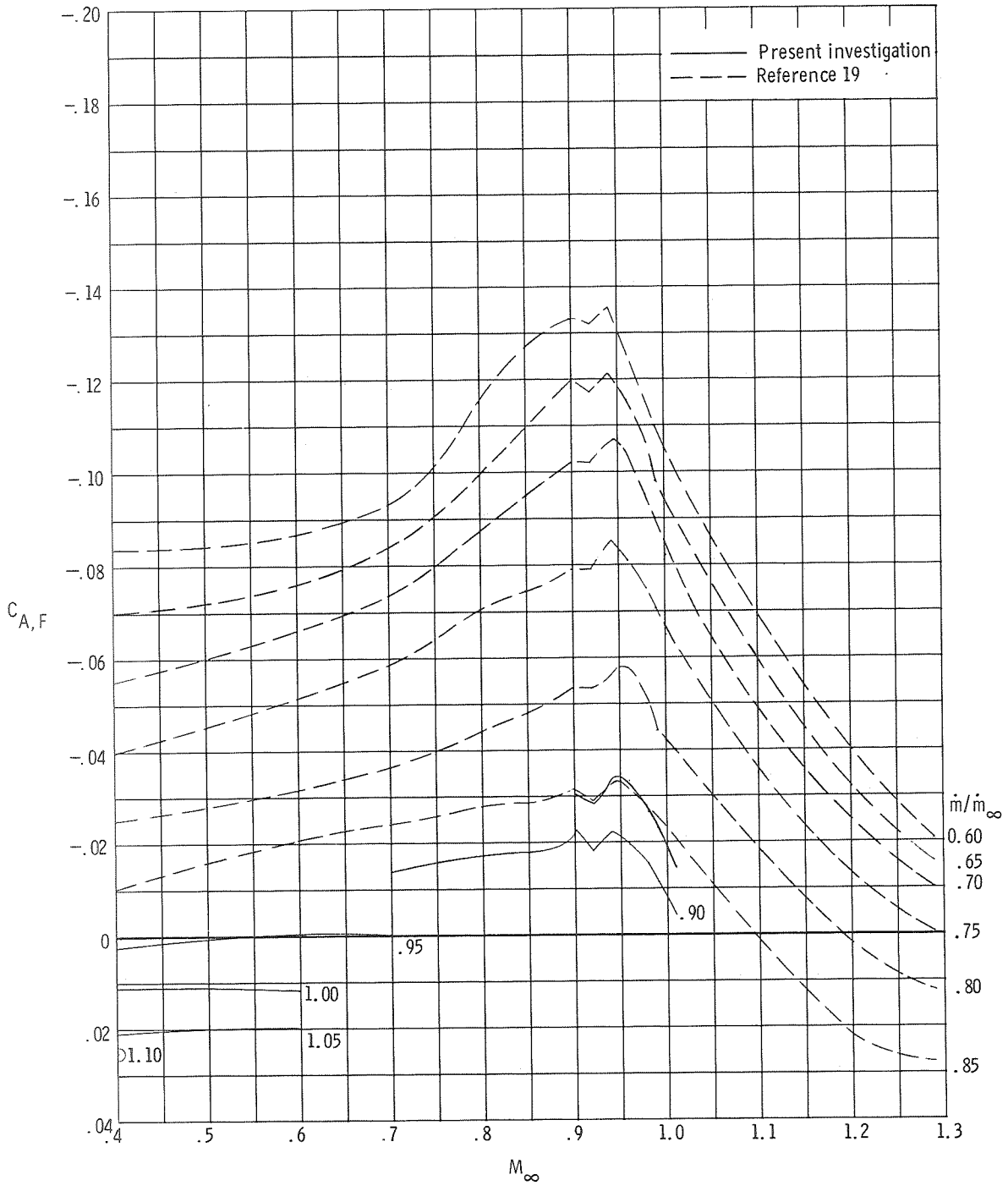

(e) NACA 1-85-100, lip radius 0.084 cm, contraction ratio 1.093.

Figure 22.- Continued.

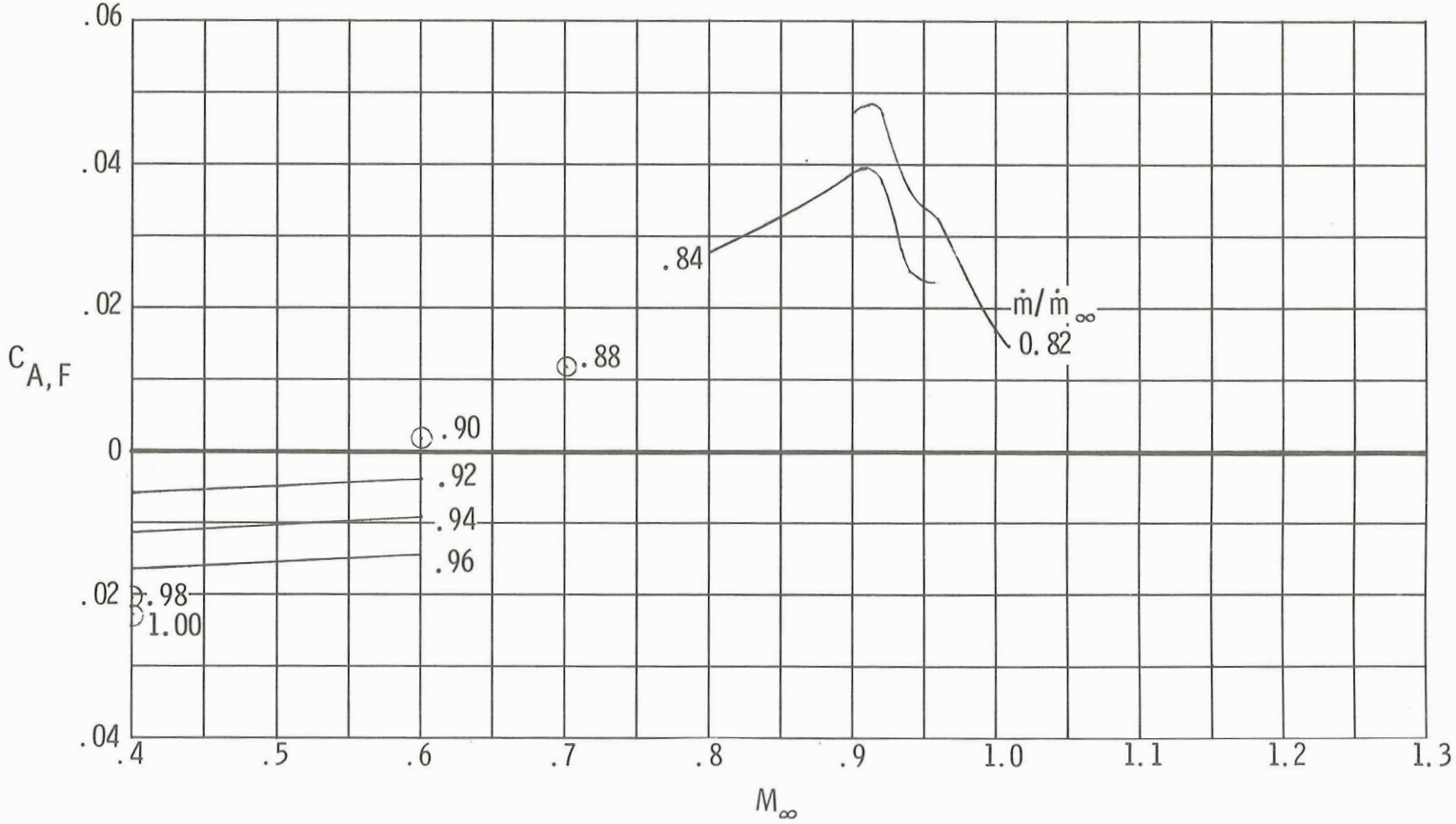

(f) NACA 1-85-100, lip radius 0.084 cm, contraction ratio 1.201.

Figure 22.- Continued.

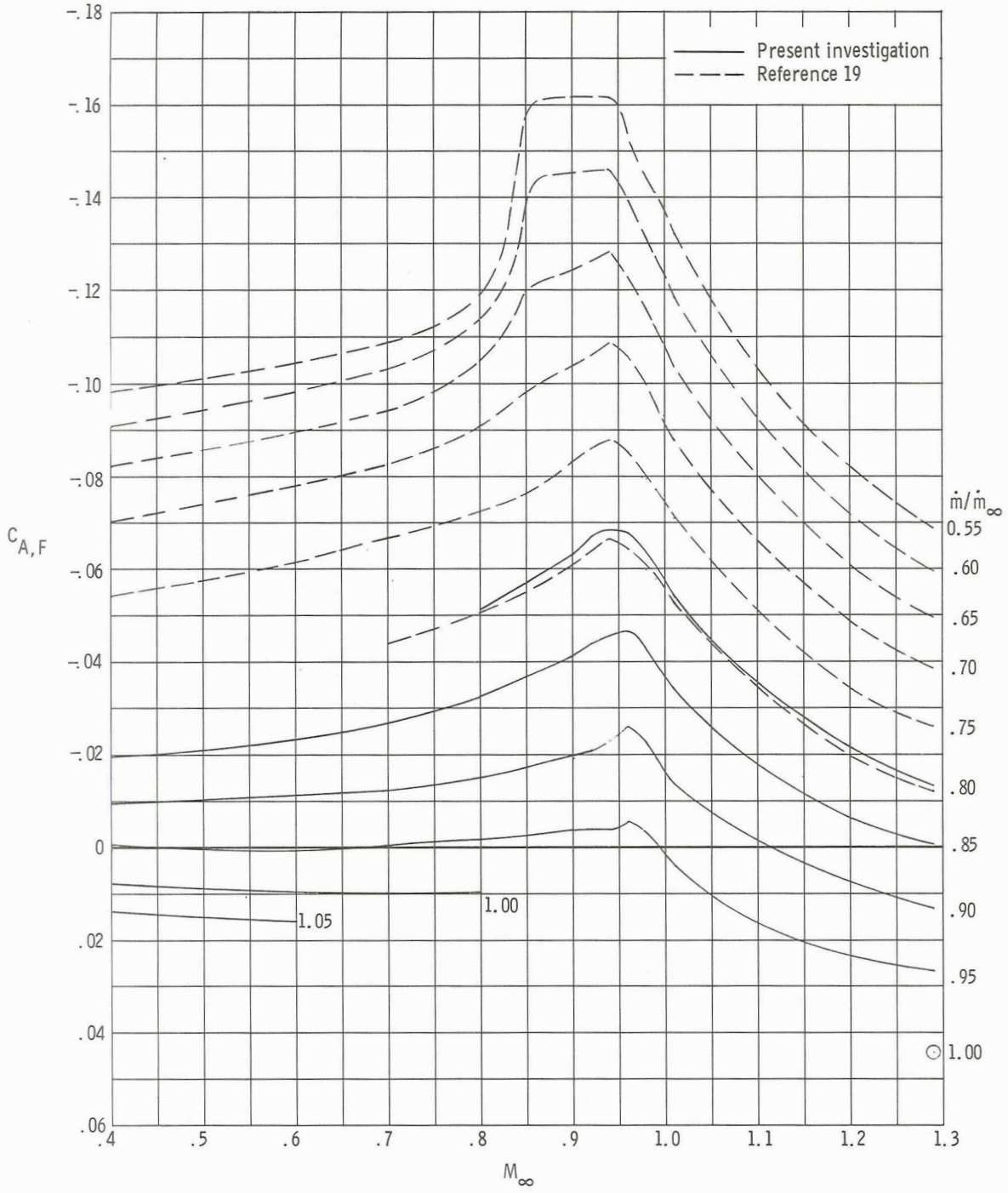

(g) NACA 1-89-100, lip radius 0.061 cm, contraction ratio 1.006.

Figure 22.- Continued.

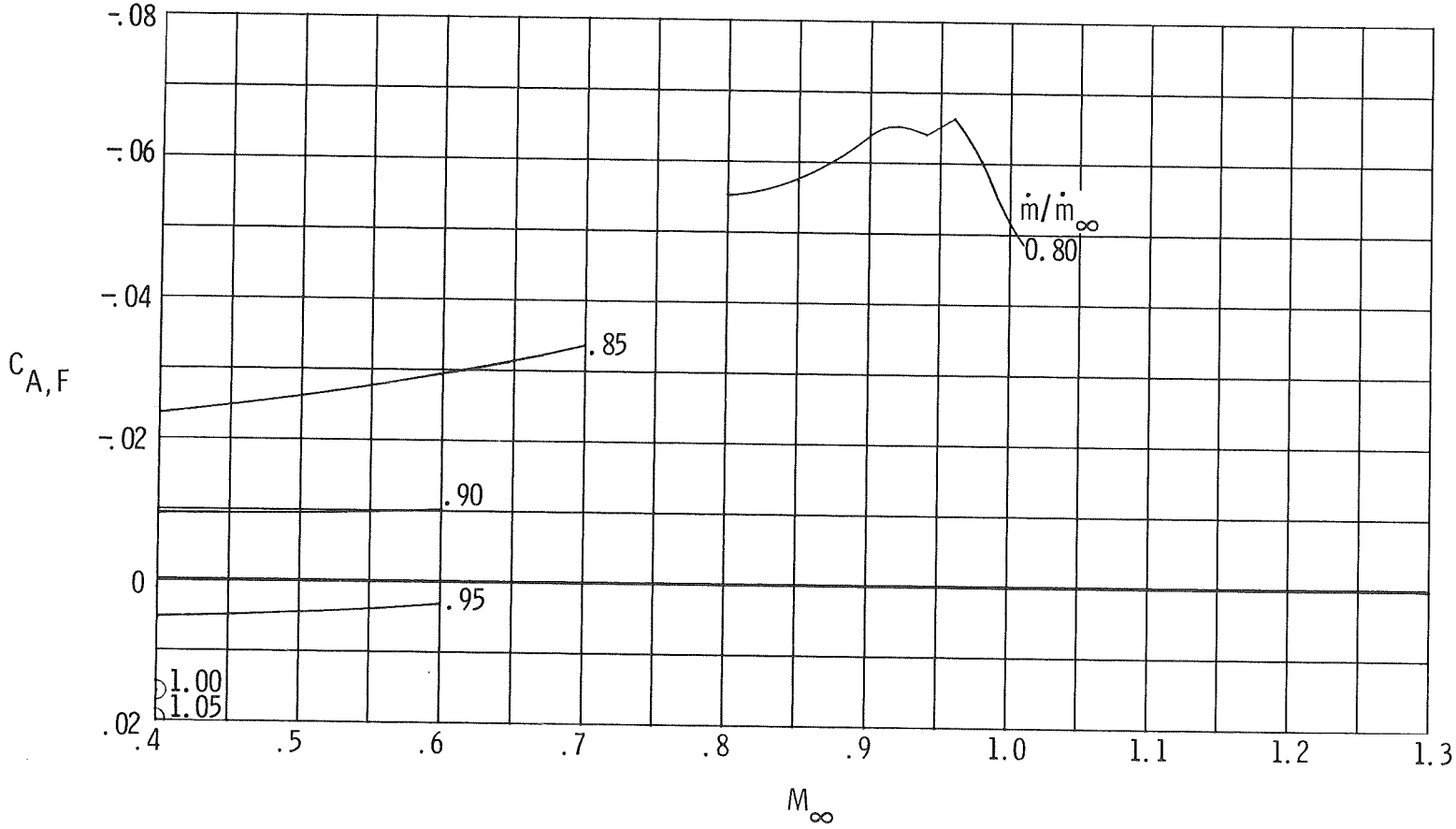

(h) NACA 1-89-100, lip radius 0.061 cm, contraction ratio 1.195.

Figure 22.- Concluded.

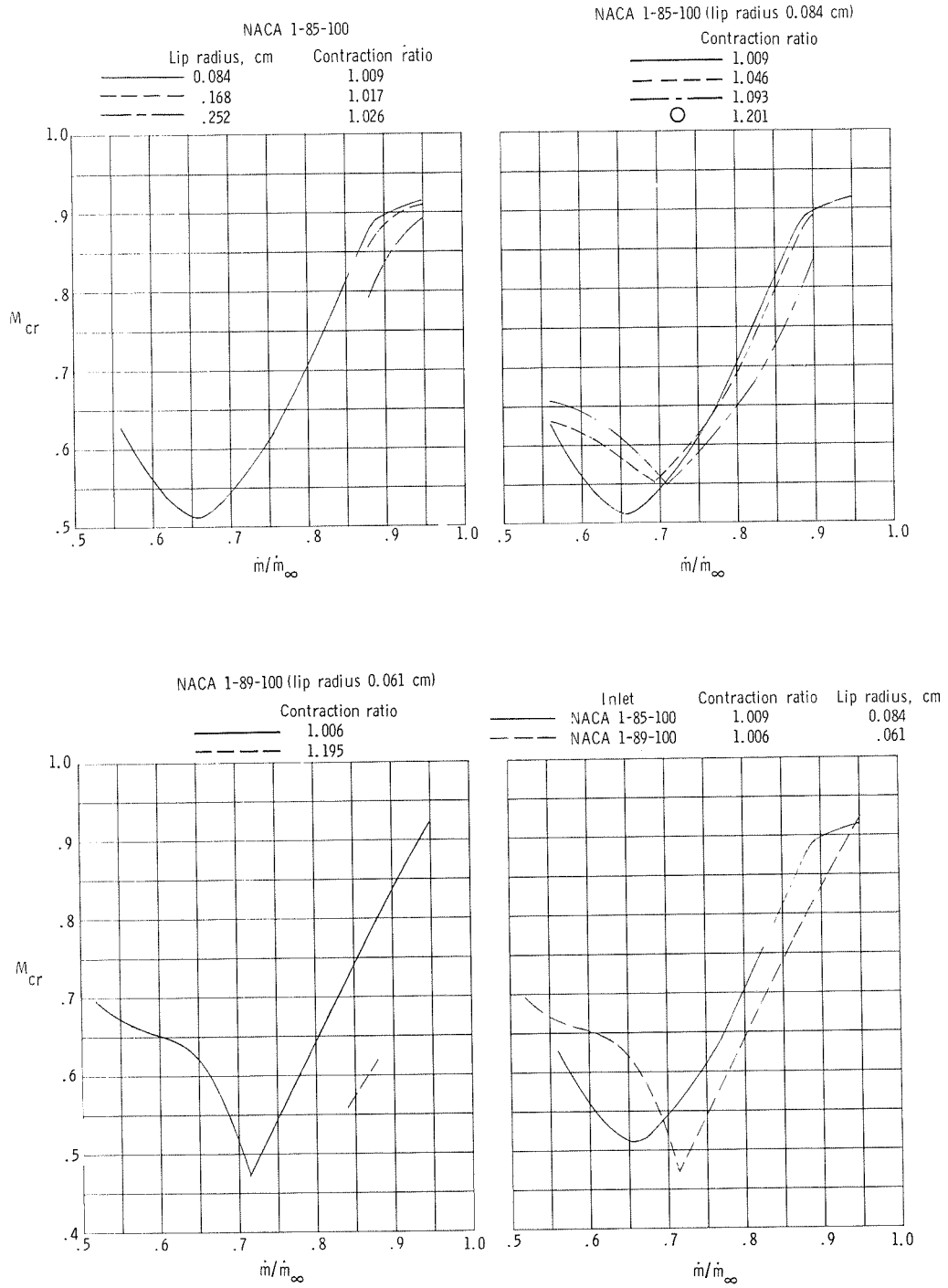

Figure 23.- Comparisons of variation of inlet lower critical Mach number with mass-flow ratio for four geometric variables (lower critical Mach number from experimental pressure-coefficient data of present investigation and that of ref. 19).

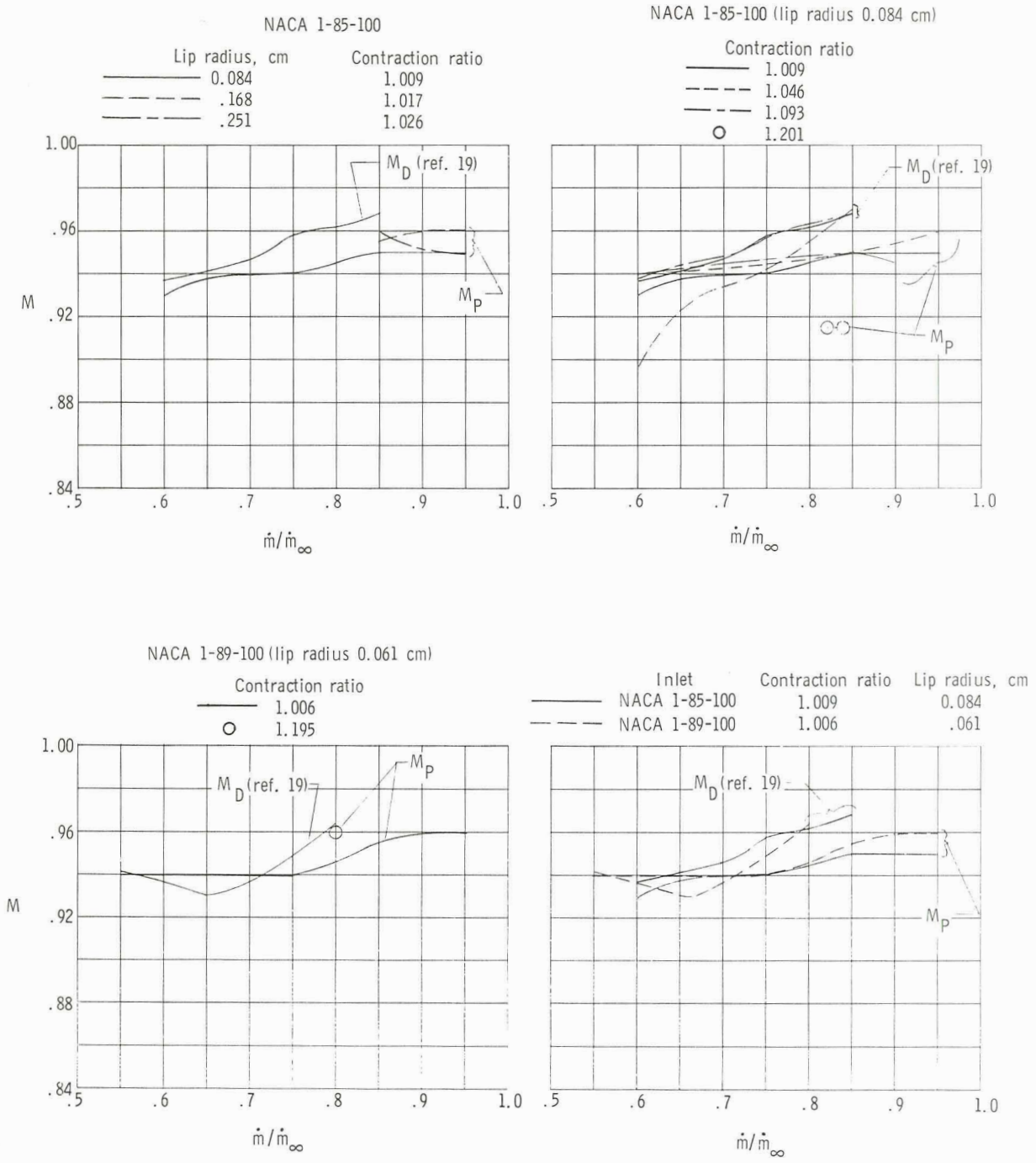

Figure 24.- Comparison of drag-divergence Mach number M_D from reference 19 with Mach number M_P at which peak value of integrated forebody axial-force coefficient $(C_{A,F})$ occurred.

NATIONAL AERONAUTICS AND SPACE ADMINISTRATION
WASHINGTON, D.C. 20546

OFFICIAL BUSINESS
PENALTY FOR PRIVATE USE $300

SPECIAL FOURTH-CLASS RATE
BOOK

POSTAGE AND FEES PAID
NATIONAL AERONAUTICS AND
SPACE ADMINISTRATION
451

U.S.MAIL

POSTMASTER: If Undeliverable (Section 158 Postal Manual) Do Not Return

"The aeronautical and space activities of the United States shall be conducted so as to contribute . . . to the expansion of human knowledge of phenomena in the atmosphere and space. The Administration shall provide for the widest practicable and appropriate dissemination of information concerning its activities and the results thereof."

—NATIONAL AERONAUTICS AND SPACE ACT OF 1958

NASA SCIENTIFIC AND TECHNICAL PUBLICATIONS

TECHNICAL REPORTS: Scientific and technical information considered important, complete, and a lasting contribution to existing knowledge.

TECHNICAL NOTES: Information less broad in scope but nevertheless of importance as a contribution to existing knowledge.

TECHNICAL MEMORANDUMS: Information receiving limited distribution because of preliminary data, security classification, or other reasons. Also includes conference proceedings with either limited or unlimited distribution.

CONTRACTOR REPORTS: Scientific and technical information generated under a NASA contract or grant and considered an important contribution to existing knowledge.

TECHNICAL TRANSLATIONS: Information published in a foreign language considered to merit NASA distribution in English.

SPECIAL PUBLICATIONS: Information derived from or of value to NASA activities. Publications include final reports of major projects, monographs, data compilations, handbooks, sourcebooks, and special bibliographies.

TECHNOLOGY UTILIZATION PUBLICATIONS: Information on technology used by NASA that may be of particular interest in commercial and other non-aerospace applications. Publications include Tech Briefs, Technology Utilization Reports and Technology Surveys.

Details on the availability of these publications may be obtained from:

SCIENTIFIC AND TECHNICAL INFORMATION OFFICE

NATIONAL AERONAUTICS AND SPACE ADMINISTRATION

Washington, D.C. 20546